[American Journal of Science, Vol. 303, November, 2003, P. 753–816]

American Journal of Science

NOVEMBER 2003

FLUID INFILTRATION AND TRANSPORT OF MAJOR, MINOR, AND TRACE ELEMENTS DURING REGIONAL METAMORPHISM OF CARBONATE ROCKS, WEPAWAUG SCHIST, CONNECTICUT, USA

JAY J. AGUE

Department of Geology and Geophysics, Yale University, P.O. Box 208109, New Haven, Connecticut 06520-8109, USA; jay.ague@yale.edu

ABSTRACT. Geochemical alteration of metacarbonate layers due to fluid infiltration during greenschist and amphibolite facies metamorphism was investigated based on 149 whole-rock analyses of the Wepawaug Schist, USA. Ankerite-Albite (Ank-Ab), rare Ankerite-Oligoclase (Ank-Ol), Biotite (Bt), Amphibole (Amp), and Diopside (Di) index mineral zones developed during progressive metamorphism (Acadian Orogeny) and devolatilization (CO_2, H_2O, S loss). Ank-Ab, Ank-Ol, and Bt zone rocks were altered along some lithologic contacts and in reaction selvages around veins. Mass changes included gains of Na, Y and, in many cases, P and Fe. K, Rb, and Ba were typically lost, and Sr was lost except where calcite precipitated in and around calcite-bearing veins. Na gain and K loss reflect muscovite destruction and albite growth in response to infiltration of fluids from surrounding metapelitic and metapsammitic (metaclastic) rocks. At higher metamorphic grades, K, Rb, and Ba were lost when biotite broke down to form amphibole or diopside; these elements were transported out of metacarbonate layers down chemical potential gradients at lithologic contacts and in selvages. Na was lost as plagioclase reacted to form clinozoisite/zoisite (Czo/Zo). Calc-silicates (cm to dm scale thickness) rich in amphibole and Czo/Zo (Amp zones) or diopside and Zo (Di zones) formed at layer margins and in selvages via extreme metasomatism including major: 1) addition of Al, Si, and, in many rocks, Fe, 2) destruction of calcite, and 3) loss of Ca and volatiles. Volatile losses near -90 percent relative to low-grade precursors demonstrate that calc-silicate formation resulting from Al-Si metasomatism is an important source of CO_2 to be considered when assessing regional devolatilization. Al mass gains for calc-silicates indicate that large quartz veins and some lithologic contacts were loci for massive time-integrated fluid fluxes of $\sim 10^5$ m^3 m^{-2}. Heavy rare earth elements (HREE) were gained in the Ank-Ab through the Amp zones, and a Di zone example gained light- and mid-REE including Sm and Nd. The REE gains coincide with gains of Y and, in most cases, P, suggesting that P and Y complexes transport REE. Volume was lost progressively from the unveined interiors of metacarbonate beds, attaining -20 to -30 percent loss in the Di-II zone. Mass addition due to veining reduced volume losses and, in some cases, produced volume gains. Reaction-transport modeling indicates that fluid flow was mostly layer-parallel, was focused along lithologic contacts, fractures, and permeable horizons, and was accompanied by diffusion and/or mechanical dispersion at high angles to the flow directions. The metasomatic fluids infiltrated from surrounding metaclastic and/or syn-metamorphic igneous rocks. Thus, interaction of fluids derived from different rock types must be considered when assessing mass transfer in lithologically diverse mountain belts.

INTRODUCTION

Metacarbonate rocks are valuable monitors of fluid flow and fluid-rock interaction in the crust. Numerous studies have demonstrated that regional fluid flow transporting volatiles including H_2O and CO_2 is an integral part of prograde regional metamorphism. The mobility and geochemical cycling of other elements during metamorphism of carbonate rocks, however, have remained more difficult to determine. Metacarbonate

rocks are commonly out of chemical equilibrium, at least in part, with surrounding lithologies such as metaclastic rocks (metapelites, metapsammites) and pre- and syn-metamorphic igneous rocks. Consequently, fluids that infiltrate metacarbonate layers can drive significant chemical reaction involving volatiles and other elements, particularly at lithologic contacts (for example, Vidale, 1969; Hewitt, 1973; Vidale and Hewitt, 1973; Joesten, 1974; Thompson, 1975; Brady 1977; Palin, ms, 1992; Walther, 1996; Ague, 2000) and in alteration zones or "selvages" around syn-metamorphic veins (Hewitt, 1973; Tracy and others, 1983; Palin, ms, 1992; Ague and Rye, 1999; Ague, 2002).

Mounting evidence strongly suggests that mass transfer of "non-volatile" rock-forming elements was significant during regional metamorphism of metacarbonate rocks in the New England orogenic belt, and elsewhere. For example, K and Na were lost from metacarbonate layers in Maine (Ferry, 1982, 1983a, 1994) and the Scottish Highlands (Tanner and Miller, 1980). In Vermont, Ferry (1992) concluded that K and Na were gained and lost at local scales, and Léger and Ferry (1993) found loss of K and Na at larger scales adjacent to syn-metamorphic intrusions. In southern New England, Ague and van Haren (1996) documented significant losses of K, Rb, Sr, and Ba from metacarbonate layers in the Wepawaug Schist, Connecticut. Furthermore, the formation of strongly metasomatic calc-silicate rocks rich in diopside, hornblende, and zoisite/clinozoisite at lithologic contacts and in vein selvages probably required loss of Ca and alkali metals as well as mobility of Si, Fe, and Mg at many localities in New England (Vidale 1969; Thompson, 1975; Brady, 1977; Tracy and others, 1983; Palin, ms, 1992). The mobility of Al is generally considered limited (Tracy and others, 1983; Widmer and Thompson, 2001; Carlson, 2002). Nonetheless, recent experiments demonstrate considerable solubilities for Al-bearing phases at regional metamorphic pressure-temperature (*P-T*) conditions (Manning, 2001; Shmulovich and others, 2001). However, it remains unclear if regional fluid flow can transport significant Al.

Mass transfer of rock-forming elements to and from metacarbonate rocks in metasedimentary sequences worldwide has been documented, but the potential for element mobility to illuminate processes of crustal fluid-rock interaction remains to be fully explored. Key questions include the following. Can spatial patterns of element redistribution elucidate fluid sources, mechanisms of mass transfer, and pathways and directions of fluid motion? How does element mobility vary as a function of metamorphic grade? Is Al mobile during metamorphism of metacarbonate layers and, if so, how does the mobility influence prograde mineral reactions and volatile loss? Both gains and losses of alkali metals are apparently possible, but what reactions and gradients in fluid composition drive the mobility? How are trace elements, including the rare earths (REE), affected by metamorphic fluid-rock interaction? Does calc-silicate formation require large losses of mass and volume from metacarbonate layers (compare Tracy and others, 1983)?

In an effort to address these questions, a geochemical and mineralogical mass balance study of metacarbonate rocks of the Wepawaug Schist, Connecticut, USA was done based on 149 whole-rock chemical analyses. Many of these analyses were done on samples collected along high spatial resolution traverses across lithologic contacts and vein selvages (figs. 1 and 2). The Wepawaug Schist is a logical field target because prior work on volatile, elemental, and isotopic mass transfer provides a firm basis for study (Hewitt, 1973; Tracy and others, 1983; Palin, ms, 1992; Ague, 1994a, 1994b, 2002; van Haren and others, 1996; Ague and van Haren, 1996). The results of this research are general, however, and should be widely applicable to common types of metasedimentary sequences containing metacarbonate rocks intercalated with metaclastic and syn-metamorphic igneous rocks.

Analytical and fluid speciation methods are presented in appendix A; modes, balancing of fluid-rock reactions, and estimation of bulk volatile losses are discussed in appendices B, C, and D; and whole-rock chemical analyses are presented in appendix E. Mineral chemistry is given by Ague (2002).

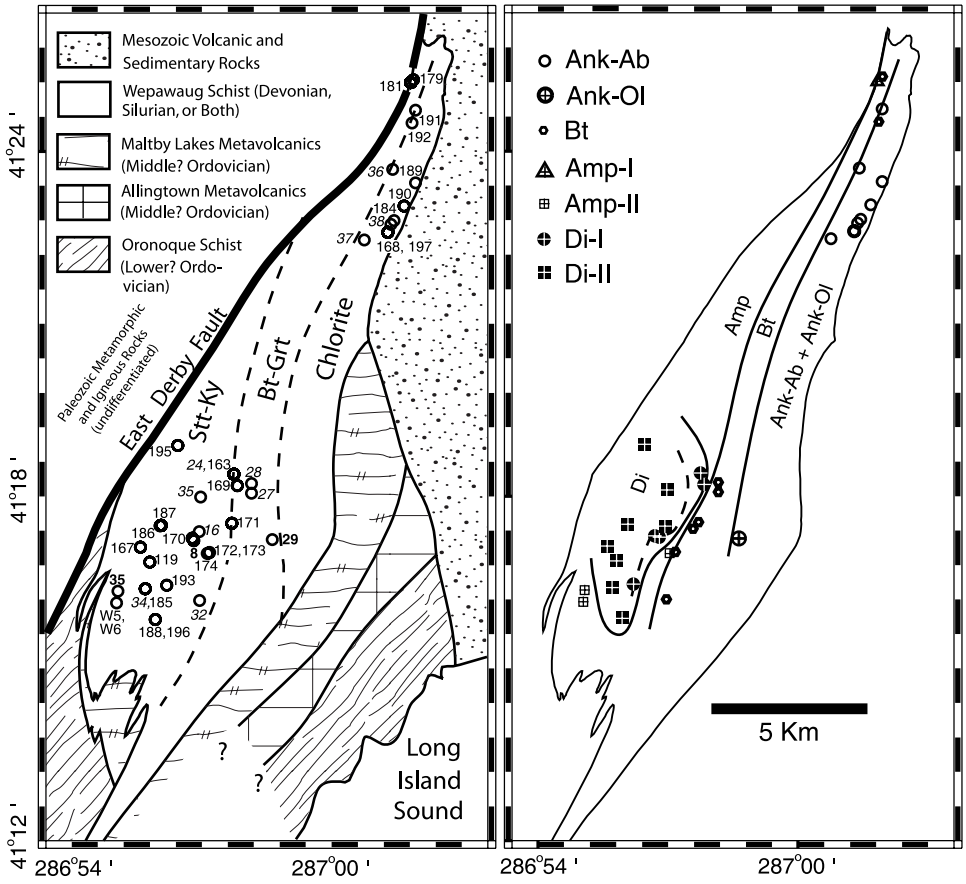

Fig. 1. Geology of study area (Fritts, 1963, 1965a, 1965b; Ague 1994b, 2002). Index mineral zones for Wepawaug Schist based on mapping or sampling at 206 localities. *Left panel:* Metapelitic Chlorite (Chl), Biotite-Garnet (Bt-Grt), and Staurolite-Kyanite (Stt-Ky) zones after Ague (1994a, 2002). Sample numbers begin with prefix JAW except: 1) samples W5 and W6 (from Wep-16 locality of Hewitt, 1973), 2) JvH-W samples from Ague and van Haren (1996) (italic type), 3) Wep samples from Hewitt (1973) (bold face type). *Right panel:* Index mineral zones for metacarbonate layers modified after Ague (2002): Ankerite-Albite (Ank-Ab), Ankerite-Oligoclase (Ank-Ol), Biotite (Bt), Amphibole-I (Amp-I), Amphibole-II (Amp-II), Diopside-I (Di-I), and Diopside-II (Di-II).

GEOLOGIC SETTING

The Wepawaug Schist is composed mostly of metapelitic rocks, but also contains metapsammite layers, metacarbonate layers, and pre- and syn-metamorphic felsic igneous rocks (Fritts, 1963, 1965a, 1965b). The regional proportion of metacarbonate rocks is difficult to assess due to exposure limitations, but is between 1 and 10 volume percent. The thickness of the metacarbonate layers ranges from a few millimeters to ~10 meters, most are several decimeters (dm) to ~1 meter (m) thick. Prograde Barrovian-style metamorphism occurred during the Acadian orogeny (~410 - 380 Ma; Lanzirotti and Hanson, 1996). Metamorphic grade increases from chlorite zone (420° - 430°C, 6-7 kb) in the east to staurolite-kyanite zone (610° - 620°C, 9 - 10 kb) in the west (Fritts, 1963, 1965a, 1965b; Ague, 2002) (fig. 1). Abbreviations and terms are defined in table 1; rock types and rock type symbols are defined in table 2; and modes are given in table 3.

Mineral assemblages in metacarbonate rocks change systematically with increasing metamorphic grade (Fritts, 1963, 1965a; Hewitt, 1973; Palin, ms, 1992; Ague,

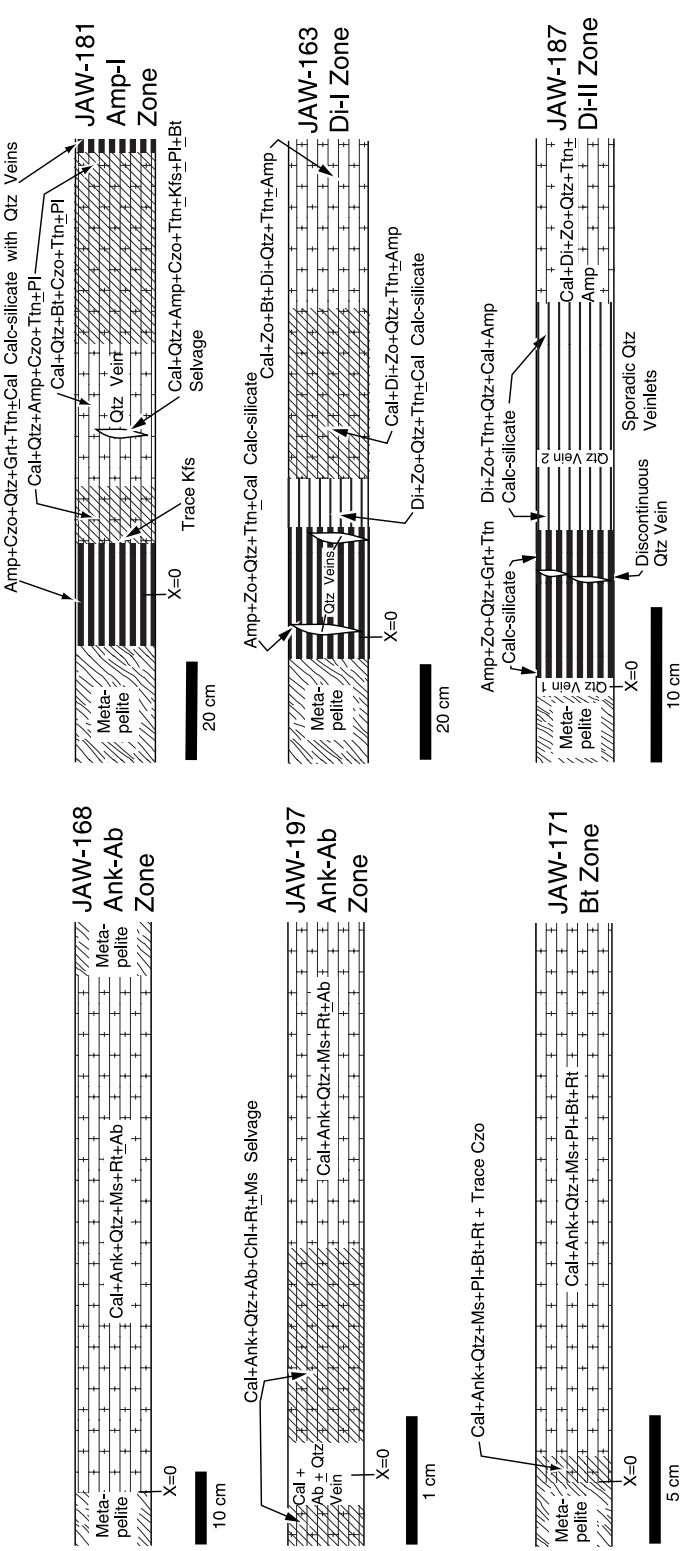

Fig. 2. Spatial distribution of mineral assemblages across metacarbonate layers for detailed geochemical profiles discussed herein; shown perpendicular to lithologic contacts with metaclastic layers or veins. Note differing scale bars between figures.

TABLE 1

Abbreviations and terms used to describe minerals and rocks

Mineral Name Abbreviations

Ab	Albite	Grt	Garnet
Amp	Calcic Amphibole	Hbl	Hornblende
Ank	Ankerite	Ky	Kyanite
An	Anorthite	Ms	Muscovite
Ap	Apatite	Ol	Oligoclase
Bt	Biotite	Pg	Paragonite
Cal	Calcite	Pl	Plagioclase
Chl	Chlorite	Po	Pyrrhotite
Crn	Corundum	Py	Pyrite
Czo/Zo	Clinozoisite/Zoisite	Qtz	Quartz
Di	Diopside	Rt	Rutile
Grs	Grossular	Ttn	Titanite

Mineral Abbreviations follow Kretz (1983) except for Amp and Ol.

Rock Terms

Metacarbonate Rock	Derived from impure limestones; contained Cal + Ank + Qtz + Ms + Rt ± Ab ± Py under low-grade, Ank-Ab zone metamorphic conditions.
Metaclastic Rock	Metapelitic or metapsammitic rocks.
Protolith or Precursor	An earlier stage in a given rock's history. The terms "protolith" and "precursor" are used interchangeably herein.
Calc-silicate (mc)	Rock derived from metacarbonate protolith; contains abundant Ca-rich silicates (for example Hbl, Di, Czo/Zo, Grt) but little or no Cal or Ank.
Calc-silicate (s)	Similar to calc-silicate (mc), but derived from schistose metaclastic protolith.
Calc-silicate	If the (mc) or (s) designation is omitted, the calc-silicate under discussion was derived from a metacarbonate protolith.

Regional Index Mineral Zones for Metacarbonate Rocks

Ank-Ab	Ankerite-Albite Zone
Ank-Ol	Ankerite-Oligoclase Zone
Bt	Biotite Zone
Amp-I, Amp-II	Amphibole-I Zone, Amphibole-II Zone
Di-I, Di-II	Diopside-I Zone, Diopside-II Zone

2002). Regional mineral assemblage zones can be defined and mapped (Ague, 2002) that are similar to those recognized by Ferry (1992, 1994) in northern New England. If reaction progress varies across individual layers, it is greatest at lithologic contacts with surrounding metaclastic schists or in reaction selvages around syn-metamorphic veins (Hewitt, 1973) (fig. 2). In the lowest grade "Ankerite-Albite" (Ank-Ab) zone, layers consist mostly of calcite, ankerite, quartz, muscovite, albite, pyrite, and rutile (fig. 2). Chlorite is present in reaction selvages around some syn-metamorphic veins (fig. 2). At slightly higher grades in northern New England, Ferry (1992) mapped an "Ankerite-

TABLE 2

Rock types and prograde silicate and oxide mineral assemblages

Rock Type Code	Symbol	Description
1	○	Ankerite-Albite and Ankerite-Oligoclase Zone Metacarbonate; Cal + Ank + Ms + Qtz + Rt ± Ab ± Pg ± Chl ± Ol
2	◯	Ankerite-Albite Zone Vein Selvage; Cal + Ank + Ab + Qtz + Rt ± Ms ± Chl
3	□	Biotite Zone Metacarbonate; Cal + Ank + Ms + Bt + Pl + Qtz ± Rt ± Ttn ± Czo ± Chl
4	◇	Biotite-bearing Metacarbonate; Cal + Bt + Qtz ± Pl ± Czo/Zo ± Rt ± Ttn ± Chl
5	△	Amphibole + Biotite-bearing Metacarbonate; Cal + Amp + Bt + Qtz + Ttn ± Pl ± Czo/Zo ± Kfs ± Chl (+Grt in 173A and W5)
6	▽	Amphibole-bearing Metacarbonate; Cal + Amp + Qtz + Ttn ± Pl ± Czo/Zo ± Kfs ± Chl (+ Grt in W6i)
7	●	Diopside + Biotite-bearing Metacarbonate; Cal + Di + Zo + Qtz + Bt + Ttn ± Amp ± Kfs
8	■	Diopside-bearing Metacarbonate; Cal + Di + Zo + Qtz + Ttn ± Amp ± Bt ± Kfs
9	▲	Dioside-Zoisite Calc-silicate; Di + Zo + Ttn + Qtz ± Cal ± Grt ± Amp ± Bt
10	▼	Amphibolite Calc-silicate (Metacarbonate Protolith); Amp + Czo/Zo + Qtz + Ttn ± Grt ± Chl
11	◆	Amphibolite Calc-silicate (Metapelite/psammite Protolith); Czo/Zo + Amp + Qtz + Grt + Ttn ± Bt ± Chl
12	⬢	Amphibolite at Contact Between Metacarbonate and Metapelite/psammite
13	☆	Czo/Zo-rich Metapelite at Contact with Calc-silicate or in Vein Selvage; Czo/Zo + Bt + Grt + Qtz + Ttn ± Amp
14	+	Metapelitic or Metapsammitic Schist

Oligoclase" (Ank-Ol) zone in which calcite and paragonite reacted to form plagioclase via the model reaction: Pg + Cal + 2 Qtz = Ab + An + CO_2 + H_2O. Paragonite has not been recognized in the Wepawaug Schist, but one sample probably contained it originally (Wep-29a; app. B). With increasing grade, muscovite was consumed by reactions that formed biotite in the "Biotite" (Bt) zone (Hewitt, 1973; Ferry, 1992) (fig. 2). In the higher-grade parts of the Bt zone, plagioclase began to break down to form clinozoisite in some rocks, and rutile reacted to form titanite (model reactions: Cal + 3 An + H_2O = 2 Czo + CO_2, and Rt + Qtz + Cal = Ttn + CO_2; Hewitt, 1973; Ague, 2002). Chlorite crystals are rare in the Bt zone and at higher grades, and it is usually difficult to ascertain whether they are prograde or retrograde.

At still higher metamorphic grades, calcic amphibole (hornblende) formed and mineral assemblage zonation across layers or in vein selvages is pronounced (fig. 2). In the "Amphibole-I" (Amp-I) zone, biotite-bearing, amphibole-free assemblages are

TABLE 3

Modes (moles kg^{-1}) used to balance fluid-rock reactions

Sample	Zone	TS	Rxn	Cal	Qtz	Ank	Ms	Chl	Pl	Bt	Czo/Zo	Di	Kfs	Amp	Grt	Ap	Rt	Ttn	Py	Po
197B-2	Ank-Ab	A-2	R.1	4.112	3.022	0.973	0.471		0.062							0.005	0.031		0.094	
197Ai	Ank-Ab	A-3	R.1	4.533	1.874	0.921	0.052	0.055	0.772							0.005	0.032		0.015	
171D	Bt	A	R.2	6.224	1.279	0.583	0.350		0.052	0.083						0.008	0.026		0.020	0.038
171A	Bt	A	R.2	5.568	1.504	0.750	0.137		0.325	0.130	0.002(C)					0.005	0.027		0.016	0.030
181DDiia	Amp-I	FF-2	R.3	6.063	2.598			0.072	0.029	0.202	0.167(C)					0.007		0.020	0.039	
181DDia	Amp-I	FF-2	R.3	5.999	1.929			0.047		0.027	0.221(C)			0.145		0.008		0.030		
181DDiia	Amp-I	FF-2	R.4	6.063	2.598			0.072	0.029	0.202	0.167(C)					0.007		0.020	0.039	
181DDiv-v	Amp-I	FF-2	R.4	1.023	4.578						0.843(C)		0.050	0.215		0.039		0.024		
W5	Amp-II	W5	R.5	5.817	1.708				0.107	0.318	0.001(C)			0.148	0.051	0.011		0.001		
W6i	Amp-II	W6A	R.5	5.349	0.999				0.137	0.071	0.011(C)			0.311	0.101	0.012		0.020		
163IVAii	Di-I	IVA	R.6	4.607	0.017					0.180	0.178(Z)			0.436		0.010		0.027		
163IVAi	Di-I	IVA	R.6	3.117	0.271						0.340(Z)	1.416		0.215		0.007		0.038		
170A	Di-I	A	R.7	4.637	0.007				0.237	0.267	0.066(Z)		0.332	0.245		0.004		0.038		
170C	Di-I	C	R.7	2.709	0.255						0.573(Z)	1.389		0.137		0.004		0.045		
Wep-8a	Di-I	8a	R.8	5.108	1.956				0.439	0.462				0.038		0.005		0.024	0.141	
Wep-8b	Di-I	8b	R.8	0.195	0.942						0.984(Z)	1.323		0.159		0.011		0.059		
187Mi	Di-II	M-1	R.9	2.847	0.017						0.506(Z)	1.784		0.058		0.013		0.066		
187Biv	Di-II	A-2	R.9	0.010	0.786						0.945(Z)	1.952		0.058		0.015		0.051		

General Notes: All sample numbers begin with prefix JAW unless noted otherwise. *Rxn:* reaction number in text; *TS:* thin section number for mineral analyses from Ague (2002); *(C):* clinozoisite; *(Z):* zoisite. For each pair of modes, the first sample listed is the protolith/precursor. Mineral compositions across the JAW-181 layer vary little; representative compositions from thin section 181FF-2 were used (Ague, 2002) with the exception of the chlorite composition determined in the present study: $K_{0.003}Mg_{2.891}Fe_{1.668}Al_{2.628}Ti_{0.005}Si_{2.731}(F_{0.103},OH_{7.897})$ (88.30 total wt %). Inferred retrograde chlorite normalized out of 181DDiv-v mode (app. B). Representative samples 187Mi and 187Biv were chosen for reaction (R.9); other samples give nearly identical results.

present in the central parts of metacarbonate layers and far-removed from cross-cutting veins. Closer to lithologic contacts or veins, amphibole formed as ankerite and/or biotite broke down (Hewitt, 1973; Ferry, 1992). Directly at contacts with surrounding schists or veins, centimeter to decimeter wide bands of amphibolite calc-silicate rocks are found containing amphibole + clinozoisite/zoisite + titanite + quartz ± garnet ± quartz veins, but that are poor in calcite (fig. 2). At higher grades in the "Amphibole-II" (Amp-II) zone, amphibole is present throughout the interiors of the metacarbonate beds.

Diopside formed via reactions that destroyed amphibole or biotite (Hewitt, 1973; Ferry, 1992). In the "Diopside-I" (Di-I) zone, the central parts of metacarbonate layers and areas far-removed from veins retain biotite and/or amphibole-bearing assemblages (fig. 2). As contacts and veins are approached, amphibole and biotite abundances drop sharply in favor of diopside and zoisite (clinozoisite is rare). Still closer to contacts and veins, centimeter to decimeter wide bands of calc-silicate are found that commonly contain quartz veins, are poor in calcite, and are rich in diopside, zoisite, and titanite. Finally, contacts and vein margins are occupied by calc-silicates comprising amphibole + zoisite + titanite + quartz ± garnet ± quartz veins. These calc-silicates strongly resemble the amphibolite calc-silicates found in the Amp-I and Amp-II zones, and almost certainly pre-date the growth of diopside because amphibole crystals can be found that are overprinted and replaced by diopside. The "Diopside-II" (Di-II) zone is similar to the Di-I zone, except that diopside is abundant throughout the interiors of the metacarbonate layers and little or no amphibole or biotite are present (fig. 2). Note that the distinction between the Di-I and Di-II zones is based on typical meter scale layers. Some thin layers ($<\sim$10 cm thick) in the Di-I zone are completely reacted to the Di-II zone pattern of mineral assemblages, presumably because buffer capacity decreases as layer thickness decreases (Ague, 2000).

It could be argued that the calc-silicates at layer margins reflect some protolith bedding heterogeneity that resulted from increased deposition of aluminous minerals like clays relative to carbonate minerals in the original sediments near contacts. This closed system hypothesis can be definitively rejected because the same patterns of calc-silicate formation are observed in alteration selvages adjacent to veins that cross-cut the homogeneous interiors of the layers at high angles to bedding. Furthermore, the geochemical systematics of the metacarbonate layers vary as functions of metamorphic grade and the intensity of fluid-rock interaction, inconsistent with the sedimentary hypothesis.

MASS BALANCE RELATIONSHIPS

Basic Equations

The overall change in rock mass is given by (see Ague, 1994a; Ague and van Haren, 1996, and references therein for detailed discussions):

$$T_{i\cdot} = \frac{C^{o}_{i\cdot}}{C'_{i\cdot}} - 1, \tag{1}$$

in which $C_{i\cdot}$ is the concentration of an immobile reference species i• and the superscripts $'$ and ^{o} refer to the altered and protolith states, respectively. The terms *protolith* and *precursor* are used in a general way to denote some earlier stage in an altered rock's history. The concentrations of the reference elements provide a "geochemical reference frame" for assessing changes in mass and volume. $T_{i\cdot}$ is the fractional mass change which is <0 if the rock lost mass and >0 if mass was gained (multiplication by 100 yields percentage mass changes). The reference species ratio proves useful for other calculations, so the quantities r and r_{inv} are defined as:

$$r \equiv \frac{C_{i\cdot}^{o}}{C_{i\cdot}'}, \quad \text{and} \quad r_{inv} \equiv \frac{C_{i\cdot}'}{C_{i\cdot}^{o}}. \tag{2}$$

Thus, equation (1) can also be written as:

$$T_{i\cdot} = \frac{1}{r_{inv}} - 1. \tag{3}$$

In many cases, the best estimate for r or r_{inv} is obtained using more than one element (Ague and van Haren, 1996). The mass change of any individual mobile constituent j is:

$$\tau^{j} = r\left(\frac{C_j'}{C_j^{o}}\right) - 1, \tag{4}$$

in which C_j denotes the concentration of j and τ^j is the fractional mass change for j. The volume change ε (volume strain) resulting from reaction and alteration is given by:

$$\varepsilon = r\left(\frac{\rho_g^{o}}{\rho_g'}\right)\left(\frac{1-\phi^{o}}{1-\phi'}\right) - 1, \tag{5}$$

in which ϕ is porosity and ρ_g is the rock density on a porosity-free basis. Loss of rock mass, loss of porosity, and increases in mineral densities all contribute to volume loss, and vice versa. Volume changes were calculated using rock density and mass changes only ($\varepsilon_{\rho m}$), setting the porosity ratio term to unity. Thus, $\varepsilon_{\rho m}$ estimates accurately volume changes for the rocks in their post-metamorphic, low-porosity state. The porosity ratios during metamorphism are uncertain and likely varied with time; they would have been near unity if ϕ^{o} and ϕ' were small, or if ϕ^{o} and ϕ' had similar values (Ague, 1994a).

Concentration Ratio Diagrams

Concentration ratio diagrams compare quantitatively the compositions of altered rocks to their protoliths without the arbitrary scaling factors employed with some other methods (including isocon diagrams; Grant, 1986). The concentration of each analyzed element or oxide in the altered state relative to a precursor state is plotted on the *y*-axis, and the elements are arranged in any convenient order along *x*. If the protolith was homogeneous in composition and the chemical analyses are error-free, then all perfectly immobile constituents will have exactly the same concentration ratio r_{inv}. Mobile elements that have ratios $> r_{inv}$ have been added to the rock, and those with ratios $< r_{inv}$ have been lost. The magnitude of r_{inv} is important to appreciate. For example, $r_{inv} > 1$ indicates overall rock mass loss due to removal of mobile constituents; this has the effect of increasing the concentrations of the immobile reference constituents ("residual enrichment"; Ague, 1994a). Conversely, $r_{inv} < 1$ indicates overall rock mass gain. In practice, precursors are heterogeneous to varying degrees, chemical analyses have errors, and few if any elements are perfectly immobile. Consequently, there is always some scatter in r_{inv} values. The "best" value was evaluated graphically unless very accurate estimates of mass changes were required. Ague and van Haren (1996) discuss geochemical reference frame selection; note that for statistical analysis they plotted precursor/altered concentration ratios in their figure 3, not the altered/precursor ratios used herein.

LITHOLOGIC CONTACTS

To assess the directions and magnitudes of mass transfer between rock types, the positions of original lithologic contacts must be determined. This task has proved difficult in many previous studies owing to strong metasomatism that obfuscates

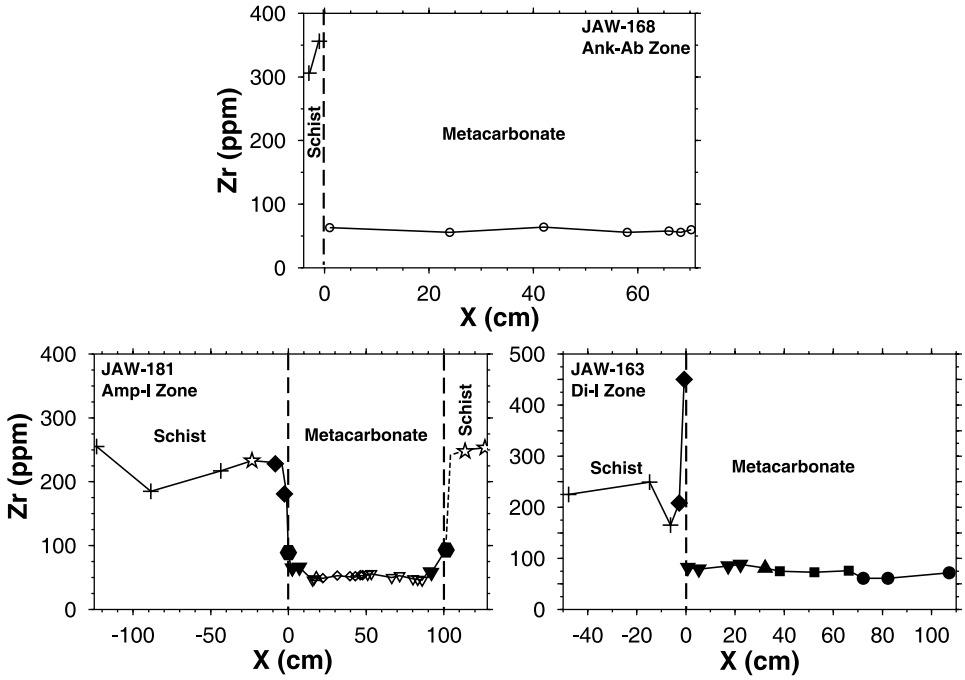

Fig. 3. Representative Zr profiles across metacarbonate layers and adjacent metaclastic schists. Original lithologic contacts (denoted by vertical dashed lines) marked by sharp increases in Zr content from metacarbonate to schist. Rock type symbols defined in table 2.

contacts. An inert chemical marker is required whose concentration in metacarbonate rocks differs greatly from that in metaclastic rocks. Zr fulfils these requirements. The solubility of zircon, the primary host of Zr, is extremely low in typical metamorphic fluids (Ayers and Watson, 1991; Carson and others, 2002). The concentration of Zr in the metacarbonate layers is typically around 40 to 80 ppm, but is factors of ~2 to over 10 greater in schists (app. E; Ague, 1994a). Notably, the concentration of Zr across a given metacarbonate layer varies little (fig. 3), attesting to the pre-metamorphic chemical homogeneity of the rocks first recognized by Hewitt (1973). The steep gradients in Zr content, from values characteristic of metacarbonate rocks to those of metaclastic rocks, clearly mark the positions of original lithologic contacts (fig. 3).

GEOCHEMISTRY OF ALTERATION

Ankerite-Albite Zone

Chemical profiles across layers are strikingly uniform for many elements (fig. 4). Near lithologic contacts, however, a distinct pattern of alteration is observed in some layers involving mass gain of Na, Y, heavy REE (HREE), and loss of K and Sr (fig. 4). P is commonly gained and Rb and Ba lost (not shown). Carbonaceous organic material was partially destroyed along some contacts and vein selvages, resulting in a "bleached", light gray field appearance.

Veins make up a few volume percent of the rocks in the low-grade parts of the Wepawaug Schist (Ague, 1994b). They are found running along lithologic contacts and, more rarely, cutting across the metacarbonate layers. A cross-cutting calcite-albite-quartz vein surrounded by a chloritic selvage is described in figures 2, 5, and 6A. The vein is metamorphic because it cross-cuts the pervasive metamorphic foliation defined by muscovite, but yields a calcite-dolomite equilibration T of ~440°C—consistent with the peak T

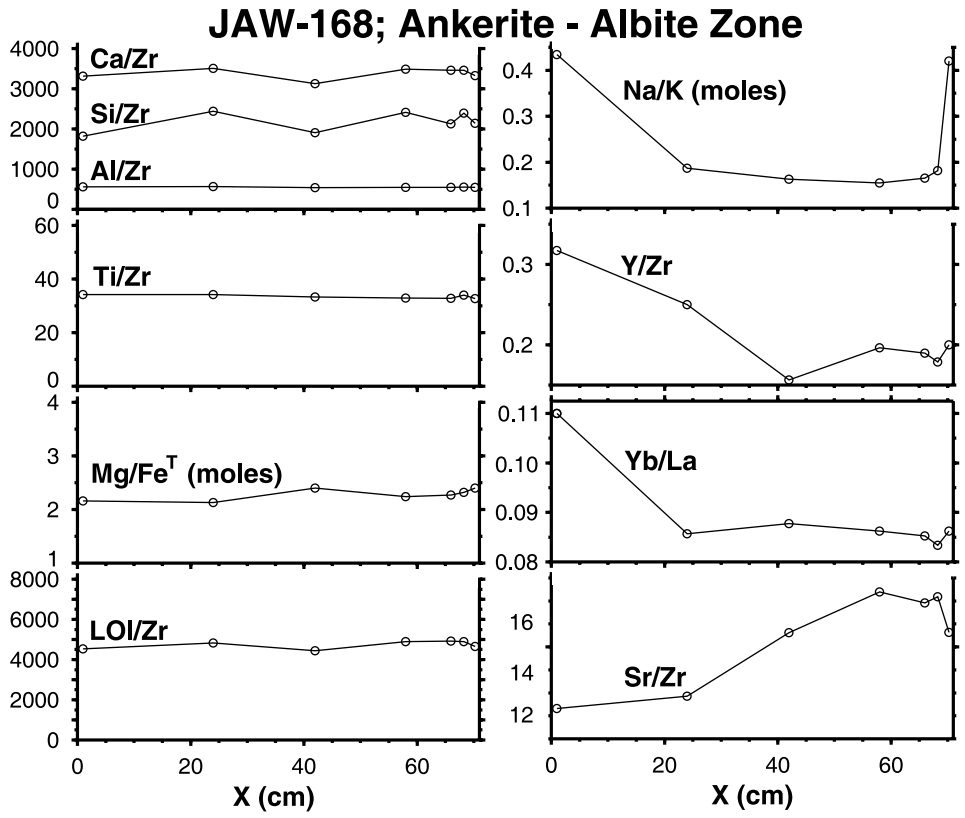

Fig. 4. Geochemical profiles across JAW-168 layer, Ankerite-Albite zone. Contacts with metapelitic schists at 0 cm and 71 cm. Some relatively immobile constituents illustrated on left panels. Right panels illustrate increase in Na/K due to Na gain and K loss, increase in Y, increase in heavy rare earth (HREE) Yb relative to light rare earth La, and decrease in Sr near contacts. Metasomatic changes tend to be most pronounced near "left" contact at 0 cm. All ratios for these and subsequent geochemical profiles are on a mass basis (kg per kg) unless otherwise noted.

conditions recorded in the Ank-Ab zone (Ague, 2002). The pattern of chemical alteration, involving mass addition of Na, HREE, Y, and P and loss of K, Rb, and Ba, is similar to that recorded at contacts, but is generally more pronounced and also includes gains of Si, Ca, Fe, Mg, Mn, Sr, and volatiles (figs. 5 and 6A). The gain of Sr probably resulted from the precipitation of carbonate minerals. The vein and selvage-forming reaction produced calcite, albite, chlorite, and ankerite at the expense of quartz, muscovite, and pyrite (table 3; app. B):

$$0.586\ \mathrm{Qtz} + 0.403\ \mathrm{Ms} + 0.074\ \mathrm{Py} + 1.957\ \mathrm{CaCl_2} + 1.138\ \mathrm{Si(OH)_4} + 0.876\ \mathrm{NaCl} +$$
$$0.162\ \mathrm{FeCl_2} + 0.272\ \mathrm{MgCl_2} + 0.042\ \mathrm{MnCl_2} + 0.096\ \mathrm{Al(OH)_3} +$$
$$0.009\ \mathrm{H_3PO_4} + 2.231\ \mathrm{CO_2} + 0.319\ \mathrm{H_2O} =$$

$$1.781\ \mathrm{Cal} + 0.941\ \mathrm{Ab} + 0.225\ \mathrm{Ank} + 0.071\ \mathrm{Chl} + 0.011\ \mathrm{Rt} + 0.002\ \mathrm{Ap} + 5.409\ \mathrm{HCl} +$$
$$0.331\ \mathrm{KCl} + 0.149\ \mathrm{H_2S} + 0.017\ \mathrm{HF}. \qquad \text{(R.1)}$$

The reaction indicates addition of CO_2 and H_2O and release of S. The r_{inv} ratio for reference species, based on Ti, Zr, and light REE (LREE) indicates an overall mass gain

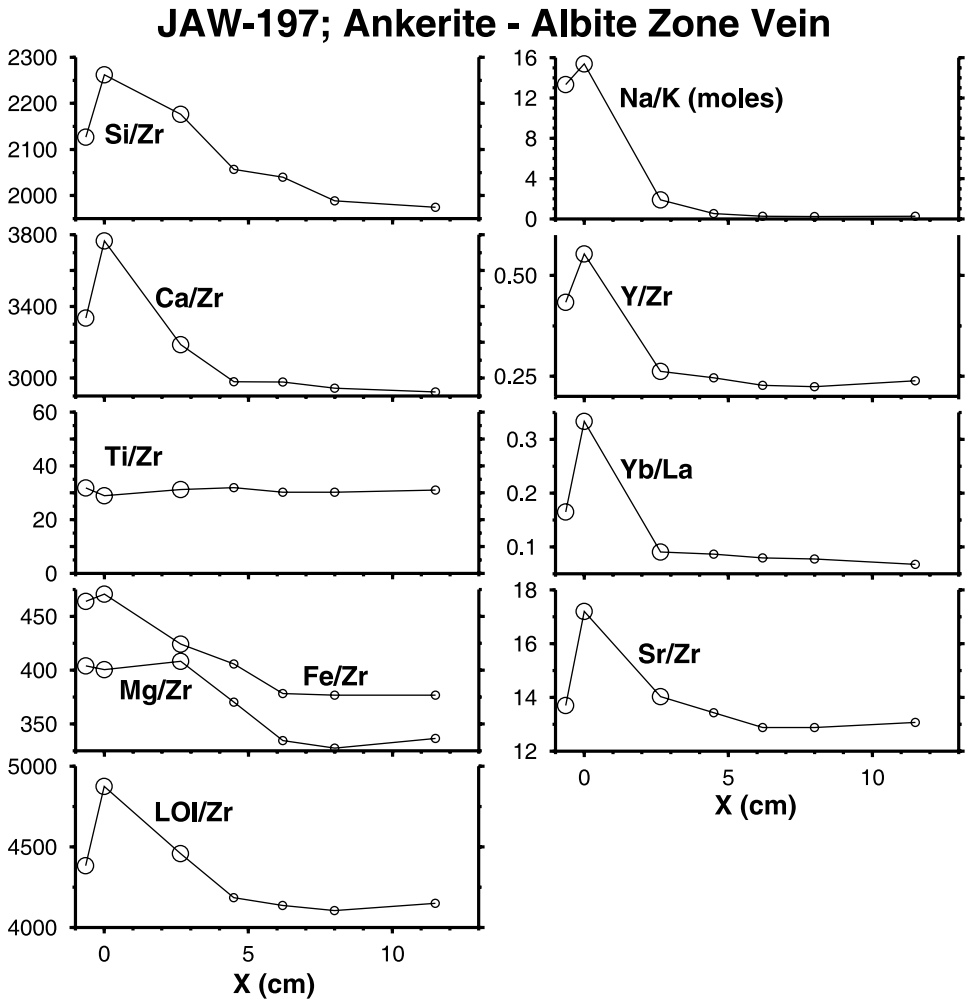

Fig. 5. Geochemical profiles for JAW-197 vein and wallrock, Ankerite-Albite zone. Vein center at 0 cm. Significant elemental mobility is evident in vicinity of vein, with exception of Zr and Ti. Rock type symbols defined in table 2.

of about +20 percent for the bulk vein + selvage relative to "unaltered" rock beyond the selvage margins (eq 3; fig. 6A).

The second example is for a vein selvage only, and indicates input of Na, P, and Y, and loss of K, Rb, Ba, and Sr (fig. 6B); the adjacent quartz + calcite vein material is not included in the analysis. The losses of Si, Ca, and volatiles (dominantly CO_2) are interpreted to reflect local (cm scale) transfer of quartz and calcite from the selvage to the vein, resulting in a mass loss of -28 percent from the selvage (fig. 6B). The vein may have also hosted open system transport of Si, Ca, and volatiles, but it was not analyzed so the amount of any such transport is indeterminate. What is clear is that open system transport along the vein added Na, P, and Y, and removed K, Rb, Ba, and Sr from the selvage.

Biotite Zone

Here, lithologic contacts are still discernable in the field. Mass transfer at the lithologic contact in the Bt zone profile included significant gains of Na, Y, and HREE

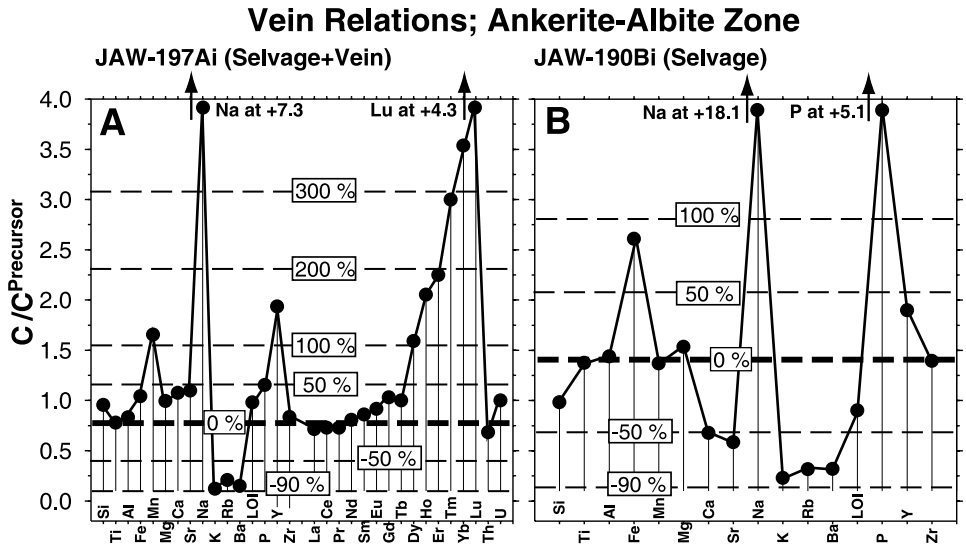

Fig. 6. Concentration ratio diagrams illustrating vein relations for Ankerite-Albite zone. Estimate of concentration ratio for immobile elements (r_{imv}) indicated by thick horizontal dashed line marked 0 % mass change. Elements plotting above this line were gained, those plotting below were lost. Contours of mass gain or loss denoted by thin horizontal dashed lines. Nb determinations have large relative uncertainties and are not plotted on these or subsequent diagrams. Filled circles on this and following concentration ratio diagrams simply denote ratio values and do not correspond to the rock type codes in table 2. (A) 197Ai selvage and vein relative to 197B-2 precursor. Concentration ratio estimate for immobile elements is 0.83, indicating an overall mass gain for vein + selvage of +20 % (eq 3). Many elements were mobile; note in particular pronounced gains of Na, Y, and HREE, and losses of K, Rb, and Ba (compare with fig. 5). (B) 190Bi vein selvage relative to 190H precursor. Concentration ratio estimate for immobile elements is 1.4, indicating overall mass loss for selvage of -28 % (eq 3). Significant percentage losses of Si, Ca, and LOI (proxy for volatiles) reflect local (cm scale) transfer of quartz and calcite to adjacent vein and produced overall mass change of -28 %. Gains of Na, P, and Y, and losses of K, Rb, and Ba, reflect infiltration of external fluids along vein. REE, U, Th not analyzed.

and losses of K and Sr (figs. 2, 7 and 8A). The mass transfer resembles that found in the Ank-Ab zone, with the exception of the loss of P (fig. 8A). Biotite formed at the contact according to:

$$0.656\ \mathrm{Cal} + 0.213\ \mathrm{Ms} + 0.008\ \mathrm{Po} + 0.004\ \mathrm{Py} + 0.004\ \mathrm{Ap} + 0.370\ \mathrm{Si(OH)_4} + 0.283\ \mathrm{HCl} + 0.121\ \mathrm{MgCl_2} + 0.113\ \mathrm{NaCl} + 0.038\ \mathrm{FeCl_2} =$$

$$0.273\ \mathrm{Pl} + 0.225\ \mathrm{Qtz} + 0.167\ \mathrm{Ank} + 0.047\ \mathrm{Bt} + 0.002\ \mathrm{Czo} + 0.002\ \mathrm{Rt} + 0.284\ \mathrm{CaCl_2} + 0.140\ \mathrm{KCl} + 0.073\ \mathrm{Al(OH)_3} + 0.003\ \mathrm{HF} + 0.003\ \mathrm{MnCl_2} + 0.014\ \mathrm{H_3PO_4} + 0.017\ \mathrm{H_2S} + 0.322\ \mathrm{CO_2} + 0.899\ \mathrm{H_2O}. \quad \text{(R.2)}$$

The second Bt zone example compares a 5 to 10 centimeter wide selvage bordering a 30 centimeter wide quartz + calcite + plagioclase + titanite + rutile + rare biotite vein, to rock far-removed (70 cm) from the vein margin. The selvage lost Si, Ca, Na, Ti, Mn, Sr, and volatiles (dominantly CO_2) (fig. 8B). Because the vein contains all of these constituents, they were probably transferred locally from the selvage to the vein while the vein formed, most likely by diffusional processes (compare Ague, 1994b, 1997b). This led to local mass losses in the selvage of roughly –30 percent. Note that Ti was mobile and lost from the selvage, at least over the length scales needed to form this "segregation" vein. The selvage also gained P, Rb, and, possibly, Al.

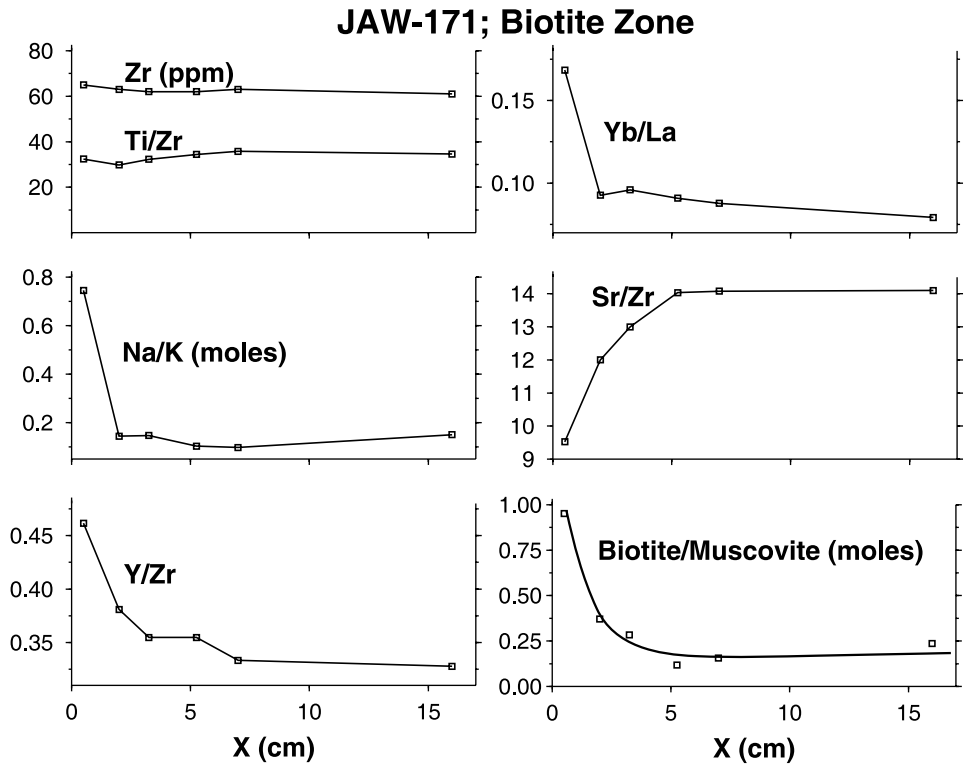

Fig. 7. Geochemical profiles across JAW-171 layer, metacarbonate Biotite zone. Lithologic contact with adjacent metapelitic schist at 0 cm. Zr and Ti were immobile, but Na/K increased due to Na gain and K loss, Y and Yb (an HREE) were added, and Sr was lost near contact. Note molar biotite/muscovite ratio increases markedly by a factor of ~4.5 near contact.

Amphibole-I Zone

Amphibole and clinozoisite/zoisite-rich calc-silicate rocks first become abundant in the Amp-I zone. They are found at lithologic contacts, often together with abundant quartz-rich veins, and in veins and vein selvages that cross-cut the interiors of metacarbonate layers. On the metacarbonate side of lithologic contacts, calc-silicates have low Zr contents consistent with metacarbonate protoliths, whereas calc-silicate rocks on the schist side have much higher Zr contents consistent with metaclastic protoliths (fig. 3). In the latter case, the rock matrix consists largely of massive clinozoisite/zoisite that is pseudomorphous after the original micaceous foliations, and relic garnets that preserve inclusion trails indicative of growth over these earlier foliations prior to the Ca influx that produced the clinozoisite/zoisite. Thus, mass transfer in and around lithologic contacts produced calc-silicate rocks in both metacarbonate and schistose protoliths. The terms calc-silicate (mc) and calc-silicate (s) denote metacarbonate and schistose protoliths, respectively. The example Amp-I traverse (fig. 2) includes some sedimentary heterogeneities such as varying fractions of carbonate and silicate minerals through the metacarbonate bed, and intercalated metapelitic and metapsammitic rocks in the metaclastic schists. Retrogression of some amphibole and clinozoisite crystals to calcite + chlorite ± K-feldspar was avoided as much as possible.

The Al/Zr ratio is constant across most of the sequence, but increases strongly in the calc-silicate (mc) rocks near lithologic contacts (fig. 9A). Increases in Si/Zr indicate major silica enrichment in these same areas (fig. 9B). Losses of Al or Si are not

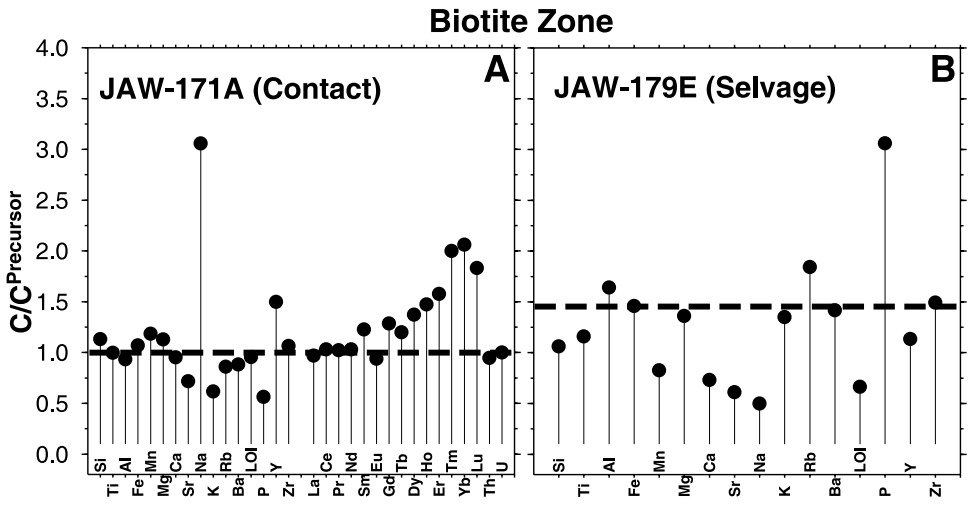

Fig. 8. Concentration ratio diagrams for metacarbonate Biotite zone. Estimate of concentration ratio for immobile elements (r_{inv}) denoted by heavy horizontal dashed lines. (A) Sample 171A at lithologic contact relative to 171D from interior of metacarbonate layer. Note marked Na, Y, and HREE mass gains, and K, P, and Sr losses. (B) 179E selvage relative to 179B precursor. Concentration ratio estimate for immobile elements is 1.45, indicating overall mass loss for selvage of about -30 % (eq 3). Significant percentage losses of Si, Ca, Na, Ti, Mn, and LOI (proxy for volatiles) reflect local (cm scale) transfer of quartz, calcite, plagioclase, titanite, and rutile to adjacent vein. P, Rb and, possibly, some Al were gained, and Y may have been lost. REE, U, Th not analyzed.

detectable in the adjacent metaclastic rocks, so the Al and Si added to form the calc-silicates (mc) must have been derived from external fluids flowing parallel to the contacts. P/Zr and Y/Zr increase in the metacarbonate layer at ~10 to 20 centimeters, and have elevated values in the calc-silicate (mc) at both lithologic contacts (fig. 9C and D). Small values of P/Zr are also observed in the calc-silicate (mc) near ~0 centimeters, and P/Zr decreases in the schists toward ~0 centimeters, suggesting some redistribution of P both within the calc-silicate and from the schists to the calc-silicate. For the representative HREE Yb, Yb/Zr increases near the contacts, reaching peak values in the calc-silicate (mc) (fig. 9E).

Ca decreases sharply in the calc-silicate (mc) rocks, but increases in the adjacent calc-silicate (s) rocks, suggesting some coupled Ca loss from calc-silicates (mc) and gain in schists across lithologic contacts (fig. 9F). The variations in Si/Zr and Ca/Zr in the calcite-rich part of the layer (~15 - 90 cm) reflect modal variations in quartz and calcite that are inferred to be relic sedimentary heterogeneities. Sr/Zr decreases from the interior of the metacarbonate layer outward toward the lithologic contacts, and increases in the schists toward the contact at X ~ 0 cm (fig. 9G). Thus, at least some of the Sr lost from the metacarbonate rocks may have been redeposited in the surrounding schists.

The central part of the metacarbonate layer contains biotite-bearing assemblages, which give way to amphibole-bearing ones toward lithologic contacts (fig. 9H). K/Zr drops steeply at the biotite → amphibole transitions due to the near complete absence of any biotite or other K-rich phase coexisting with amphibole (fig. 9H). Rb/Zr and Ba/Zr behave similarly (not shown). K-feldspar is rare and found pseudomorphous after biotite at X ~ 15 - 20 cm along the profile, and in a few tiny, millimeter scale cross-cutting veinlets (fig. 9H). The calc-silicate (s) rocks also have very low K/Zr, due mainly to the replacement of micas by clinozoisite. In the micaceous schists beyond the calc-silicates, no clear loss or gain of K is evident.

Metasomatic changes in and around cross-cutting quartz veins mirror those at lithologic contacts. The concentration ratio diagram for the biotite → amphibole

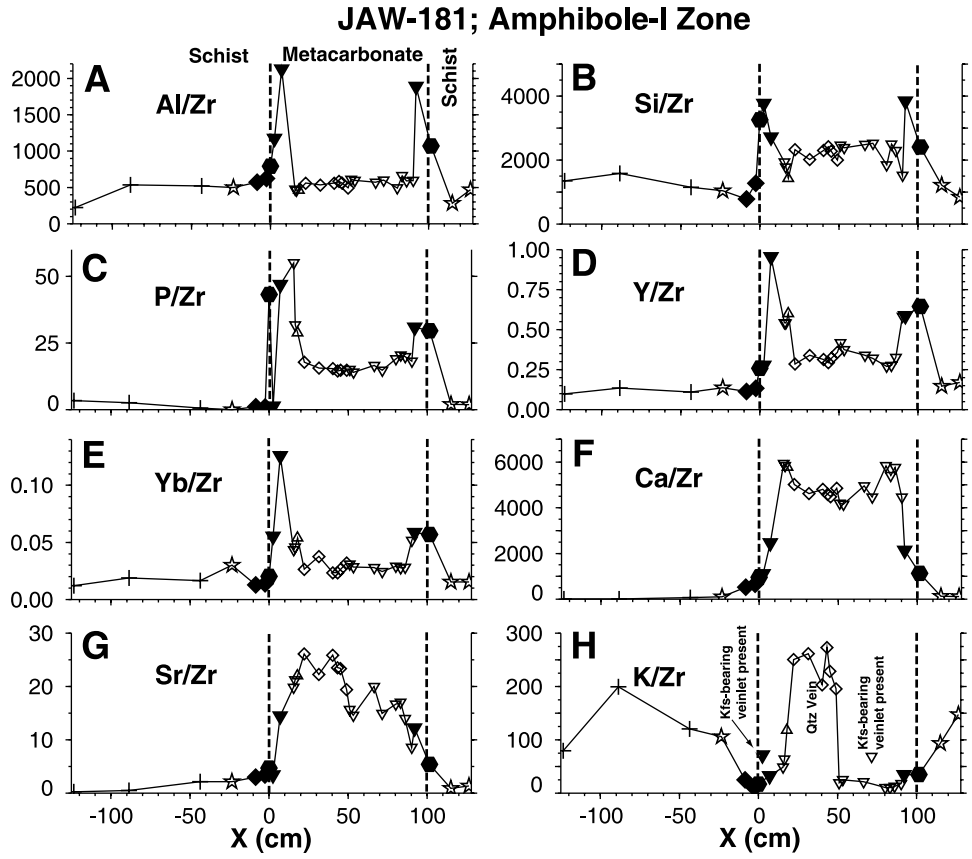

Fig. 9. Geochemical profiles across metacarbonate layer and adjacent metapsammitic and metapelitic schists, JAW-181 locality, Amphibole-I zone. Original lithologic contacts denoted by vertical dashed lines. Rock type symbols given in table 2. Detailed discussion in text, but note strong increases in Al/Zr, indicative of major Al gain, for calc-silicate rocks derived from metacarbonate precursors at lithologic contacts in part (A) of figure.

reaction in metacarbonate rock adjacent to cross-cutting, highly veined calc-silicate indicates extreme depletion of K, Rb, and Ba, some loss of Si, volatiles, and Sr, and probable slight REE mobility (fig. 10A). The major reactants quartz, calcite, and biotite broke down to form amphibole and clinozoisite:

$$0.764\ \mathrm{Qtz} + 0.359\ \mathrm{Cal} + 0.177\ \mathrm{Bt} + 0.039\ \mathrm{Py} + 0.029\ \mathrm{Pl} + 0.029\ \mathrm{Pl} + 0.027\ \mathrm{Chl} + 0.151\ \mathrm{HCl} + 0.003\ \mathrm{MnCl_2} + 0.003\ \mathrm{H_3PO_4} + 0.587\ \mathrm{H_2O} =$$

$$0.137\ \mathrm{Amp} + 0.077\ \mathrm{Ttn} + 0.044\ \mathrm{Czo} + 0.001\ \mathrm{Ap} + 0.335\ \mathrm{Si(OH)_4} + 0.141\ \mathrm{KCl} + 0.014\ \mathrm{Al(OH)_3} + 0.011\ \mathrm{HF} + 0.006\ \mathrm{FeCl_2} + 0.002\ \mathrm{MnCl_2} + 0.358\ \mathrm{CO_2} + 0.078\ \mathrm{H_2S}. \quad \text{(R.3)}$$

The Si lost was almost certainly transported locally into the adjacent veined calc-silicate.

Relative to the biotite-bearing starting material, the veined calc-silicate (mc) rock lost Ca, Mn, Sr, K, Rb, Ba, and volatiles, and gained silica, Al, Fe, P, Y, HREE, and U (fig. 10B). The 150 percent Al mass gain is particularly noteworthy, second in

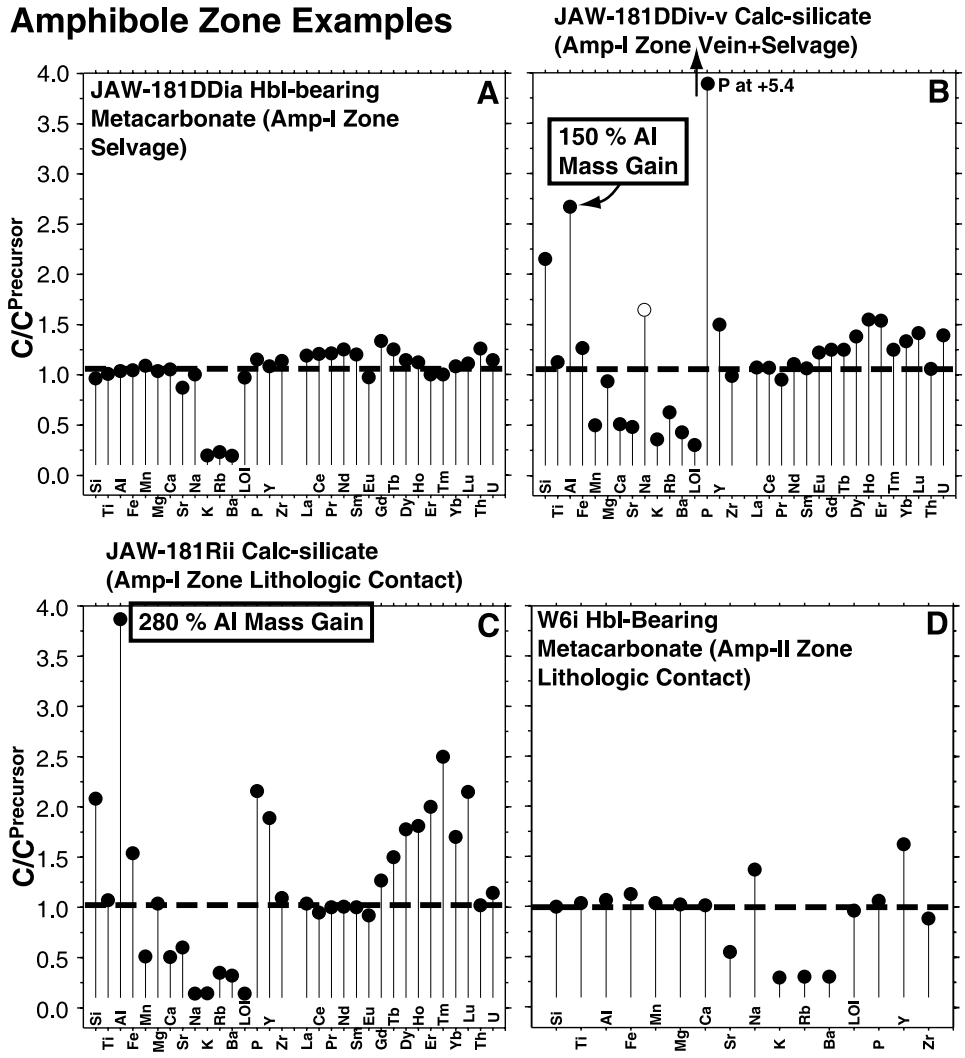

Fig. 10. Concentration ratio diagrams for Amphibole zones. Estimate of concentration ratio for immobile elements (r_{inv}) denoted by heavy horizontal dashed lines. (A) Hornblende-bearing metacarbonate rock in vein selvage (181DDia) relative to biotite-bearing precursor (181DDiia), Amphibole-I zone. Note extreme depletion of K, Rb, and Ba. (B) Amphibolite calc-silicate cut by quartz veins (181DDiv-v) relative to biotite-bearing metacarbonate precursor (181DDiia), Amphibole-I zone. Note extreme metasomatism, including large gains of Al. The precursor contained little Na, so small gains of Na resulted in large apparent Na increases (open circle); the calc-silicate (mc) actually contains only 0.05 wt percent Na_2O more than the precusor. (C) Amphibolite calc-silicate at lithologic contact (181Rii) relative to representative biotite-bearing metacarbonate precursor (181FF), Amphibole-I zone. Extreme metasomatism, including large gains of Al, is similar to fig. 10B. (D) Hornblende-bearing, biotite free metacarbonate rock (W6i) at lithologic contact relative to precursor containing both biotite and hornblende from interior of layer (W5), Amphibole-II zone.

magnitude only to the P gain. The protolith contained very little Na to begin with, so small gains of Na resulted in discernable Na increases on figure 10B. However, the difference in Na_2O between calc-silicate (mc) and precursor is only 0.05 weight percent. The calc-silicate (mc) was produced from the biotite-bearing precursor (fig. 10B) according to the overall mineralogical transformation:

$$5.104\ \text{Cal} + 0.202\ \text{Bt} + 0.072\ \text{Chl} + 0.039\ \text{Py} + 0.029\ \text{Pl} + 6.400\ \text{HCl} + 4.242\ \text{Si(OH)}_4 +$$
$$1.527\ \text{Al(OH)}_3 + 0.124\ \text{FeCl}_2 + 0.119\ \text{H}_3\text{PO}_4 + 0.019\ \text{HF} + 0.033\ \text{NaCl} =$$

$$1.690\ \text{Qtz} + 0.623\ \text{Czo} + 0.201\ \text{Amp} + 0.048\ \text{Kfs} + 0.030\ \text{Ap} +$$
$$0.002\ \text{Ttn} + 3.175\ \text{CaCl}_2 + 0.111\ \text{KCl} + 0.089\ \text{MgCl}_2 +$$
$$0.020\ \text{MnCl}_2 + 5.104\ \text{CO}_2 + 14.062\ \text{H}_2\text{O} + 0.078\ \text{H}_2\text{S}. \qquad \text{(R.4)}$$

Large amounts of calcite were destroyed, releasing Ca and CO_2. The added Si and Al were sequestered mainly in product quartz, clinozoisite, and amphibole. K was lost as biotite broke down. As noted above, K-feldspar may post-date the metamorphic peak.

Calc-silicate metasomatism in vein selvages is similar to that found at lithologic contacts. The concentration ratio diagram for the veined calc-silicate (mc) relative to biotite-bearing metacarbonate beyond the limits of vein alteration (fig. 10A) strongly resembles the diagram for representative calc-silicate (mc) at a lithologic contact compared to biotite-bearing metacarbonate rock within the layer (fig. 10C). For both settings, r_{inv} is near one, indicating that little overall bulk rock mass change accompanied calc-silicate formation even though the chemical compositions of the rocks were dramatically changed. In other words, 1 kilogram of reactant was converted to ~1 kilogram of product, but the reactant's composition was strongly altered to produce the product.

Amphibole-II Zone

The Amp-II zone samples were taken from the Wep-16 layer of Hewitt (1973). A thin calc-silicate layer at the lithologic contact is not considered further here (Ague, 2002). The interior of the layer contains calcic amphibole and biotite, but the layer margin near contacts with metapelite contains little or no biotite—that which is present being typically found as relicts within amphibole. The margins lost K, Rb, and Ba due to biotite breakdown; lost Sr; and gained Y and, probably, Fe (fig. 10D). The Na gain is small on an absolute mass basis and corresponds to an increase in Na_2O between margins and interior of only 0.06 weight percent. The amphibole was produced via:

$$0.719\ \text{Qtz} + 0.522\ \text{Cal} + 0.248\ \text{Bt} + 0.093\ \text{FeCl}_2 + 0.061\ \text{Al(OH)}_3 + 0.023\ \text{CaCl}_2 +$$
$$0.018\ \text{NaCl} + 0.010\ \text{MgCl}_2 + 0.006\ \text{MnCl}_2 + 0.002\ \text{H}_3\text{PO}_4 =$$

$$0.159\ \text{Amp} + 0.050\ \text{Grt} + 0.029\ \text{Pl} + 0.019\ \text{Ttn} + 0.010\ \text{Czo} + 0.001\ \text{Ap} + 0.212\ \text{KCl} +$$
$$0.071\ \text{HCl} + 0.038\ \text{Si(OH)}_4 + 0.014\ \text{HF} + 0.522\ \text{CO}_2 + 0.054\ \text{H}_2\text{O}. \qquad \text{(R.5)}$$

Quartz, calcite, and biotite were the major reactants. Growth of amphibole, garnet, and lesser amounts of plagioclase, titanite, and clinozoisite released K, CO_2, and some H_2O.

Elsewhere in the Amp-II zone, calc-silicate bands can be quite extensive, reaching decimeter to even meter scale thickness. Reaction was commonly so thorough that little or no calcite-rich metacarbonate rock remains. These highly reacted calc-silicates strongly resemble the "thin layer amphibolites" from other localities inferred by Orville (1969) to have metacarbonate, as opposed to metabasic, protoliths.

Diopside-I Zone

Here, for typical meter scale layers, biotite and/or amphibole remain abundant in layer interiors, but diopside-rich metacarbonate and calc-silicate rocks are present toward layer margins (fig. 2). The first example is a profile across a metacarbonate

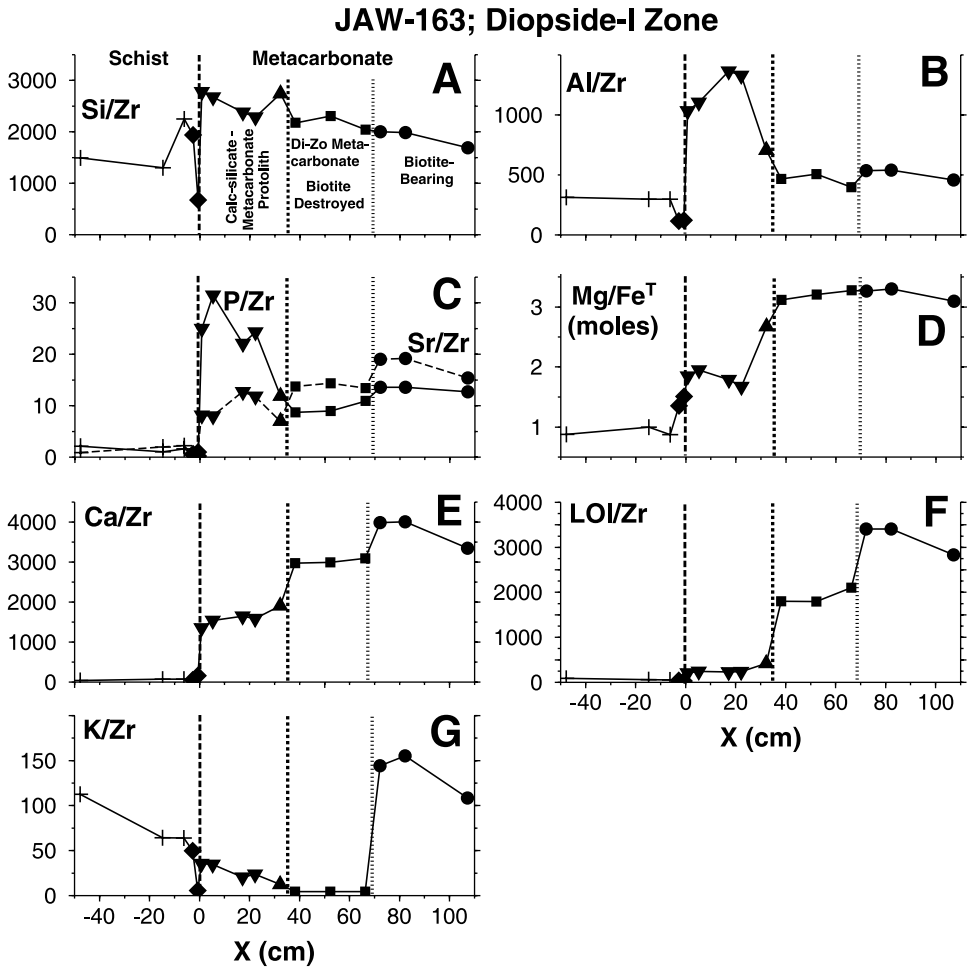

Fig. 11. Geochemical profiles across metacarbonate layer and adjacent metapsammitic and metapelitic schists, JAW-163 locality, Diopside-I zone. Peak in Al/Zr near ~20 cm coincides with position of quartz vein (fig. 2). See text for additional discussion and table 2 for symbol definitions.

layer and the adjacent metapsammitic and metapelitic schists. Si/Zr increases in a fairly regular way through the metacarbonate and calc-silicate (mc) rocks, then drops sharply across the contact (X = 0 cm) before returning to typical metaclastic values (fig. 11A). The Al/Zr ratio is large for the calc-silicate (mc) rocks, reaching peak values in the amphibolite calc-silicate (mc) adjacent to the lithologic contact (fig. 11B). Al/Zr then drops sharply across the contact, to its lowest values, in the calc-silicate (s) rock, and then increases to values characteristic for the metaclastic rocks. P/Zr also increases in the calc-silicate (mc) rocks near the contact (fig. 10C).

Sr/Zr and molar Mg/Fe drop in the calc-silicate (mc) rocks toward the contact (fig. 10C and D). Ca/Zr varies somewhat in the metacarbonate rocks due either to mass transfer or protolith heterogeneity, but then clearly decreases in the calc-silicate (mc) rocks (X ~ 35 cm; fig. 10E). LOI/Zr drops through the successive metacarbonate and calc-silicate (mc) zones, reflecting increasing devolatilization toward the contact (fig. 10F).

The K/Zr ratio drops precipitously at the transition from biotite + amphibole + zoisite ± diopside metacarbonate rock to diopside + zoisite ± amphibole metacarbon-

ate rock at X ~ 70 cm (fig. 10G). Rb/Zr and Ba/Zr behave similarly (not shown). The loss of K is tied to reaction which produced diopside, quartz, and zoisite from reactant calcite, amphibole, and biotite:

$$1.381\ \text{Cal} + 0.214\ \text{Amp} + 0.180\ \text{Bt} + 0.003\ \text{Ap} + 1.658\ \text{Si(OH)}_4 + 0.206\ \text{HCl} + 0.041\ \text{CaCl}_2 + 0.054\ \text{Al(OH)}_3 + 0.003\ \text{MnCl}_2 =$$

$$1.465\ \text{Di} + 0.264\ \text{Qtz} + 0.174\ \text{Zo} + 0.012\ \text{Ttn} + 0.177\ \text{KCl} + 0.125\ \text{HF} + 0.038\ \text{FeCl}_2 + 0.027\ \text{NaCl} + 0.013\ \text{H}_3\text{PO}_4 + 0.007\ \text{MgCl}_2 + 1.381\ \text{CO}_2 + 3.676\ \text{H}_2\text{O} \qquad \text{(R.6)}$$

Aqueous silica, necessary to form the diopside, was added, and significant alkalis, CO_2, and H_2O were lost. The reactant biotite and amphibole contain substantial F (Ague, 2002), so F was lost to the fluid.

Closer to the contact K/Zr increases slightly in the amphibolite calc-silicate (mc) rocks due to the presence of K in amphibole, but never comes near the high K/Zr in biotite-bearing rocks far-removed from the contact (fig. 10G).

Geochemical systematics in vein selvages mirror those at lithologic contacts (fig. 12). Mass changes for the transition from biotite + amphibole + zoisite ± diopside metacarbonate rock to diopside + zoisite ± amphibole metacarbonate rock for a vein selvage (fig. 12B), the geochemical profile across the contact discussed above (fig. 12A), and a sample near another lithologic contact from the same outcrop (fig. 12A), are remarkably similar, and demonstrate gains of Si and, in one case, Al, and clear loss of K, Rb, Ba, and volatiles.

A comparison of diopside-zoisite calc-silicate (mc) rocks in selvages and near contacts to their biotite + amphibole + zoisite ± diopside metacarbonate rock protoliths reveals large mass gains of Si and Al, and losses of K, Rb, Ba, Ca, Sr, and volatiles (fig. 10C and D). Fe and Mg were probably added to the contact example (fig. 10C). For the contact and selvage examples, r_{inv} is ~1, indicating only small overall mass changes (fig. 10C and D). Comparison of amphibolite calc-silicates (mc) along the contact (fig. 10E) and in the selvage (fig. 10F) to their biotite + amphibole + zoisite ± diopside protoliths also indicates gains of Si and Al and losses of volatiles and the alkali and alkaline earth metals. For the contact, Fe and P were gained. Concentration ratios for Na appear large in figure 10C, E, and F because the precursor rocks had little Na (<0.14 wt percent Na_2O). Actual mass additions were small and reflect minor Na uptake by amphibole or diopside. REE mobility was limited, but the amphibolite calc-silicate (mc) at the contact (fig. 10E) shows some HREE enrichment resembling that observed at lower grades.

These patterns of geochemical alteration are repeated elsewhere in the Di-I zone (fig. 13). Production of the diopside-zoisite metacarbonate rocks clearly involved loss of K, Rb, Ba, and volatiles (fig. 13A and B). Gains of Si and losses of Na and Sr were common, Al was added to some rocks, and overall bulk rock mass changes were small. An example reaction is:

$$2.022\ \text{Cal} + 0.332\ \text{Kfs} + 0.267\ \text{Bt} + 0.237\ \text{Pl} + 0.113\ \text{Amp} + 0.057\ \text{Po} + 1.137\ \text{Si(OH)}_4 + 0.588\ \text{HCl} + 0.337\ \text{Al(OH)}_3 + 0.112\ \text{FeCl}_2 + 0.017\ \text{MnCl}_2 =$$

$$1.340\ \text{Di} + 0.487\ \text{Zo} + 0.239\ \text{Qtz} + 0.006\ \text{Ttn} + 0.569\ \text{KCl} + 0.141\ \text{NaCl} + 0.063\ \text{MgCl}_2 + 0.075\ \text{HF} + 0.004\ \text{CaCl}_2 + 2.022\ \text{CO}_2 + 0.057\ \text{H}_2\text{S} + 3.069\ \text{H}_2\text{O}. \qquad \text{(R.7)}$$

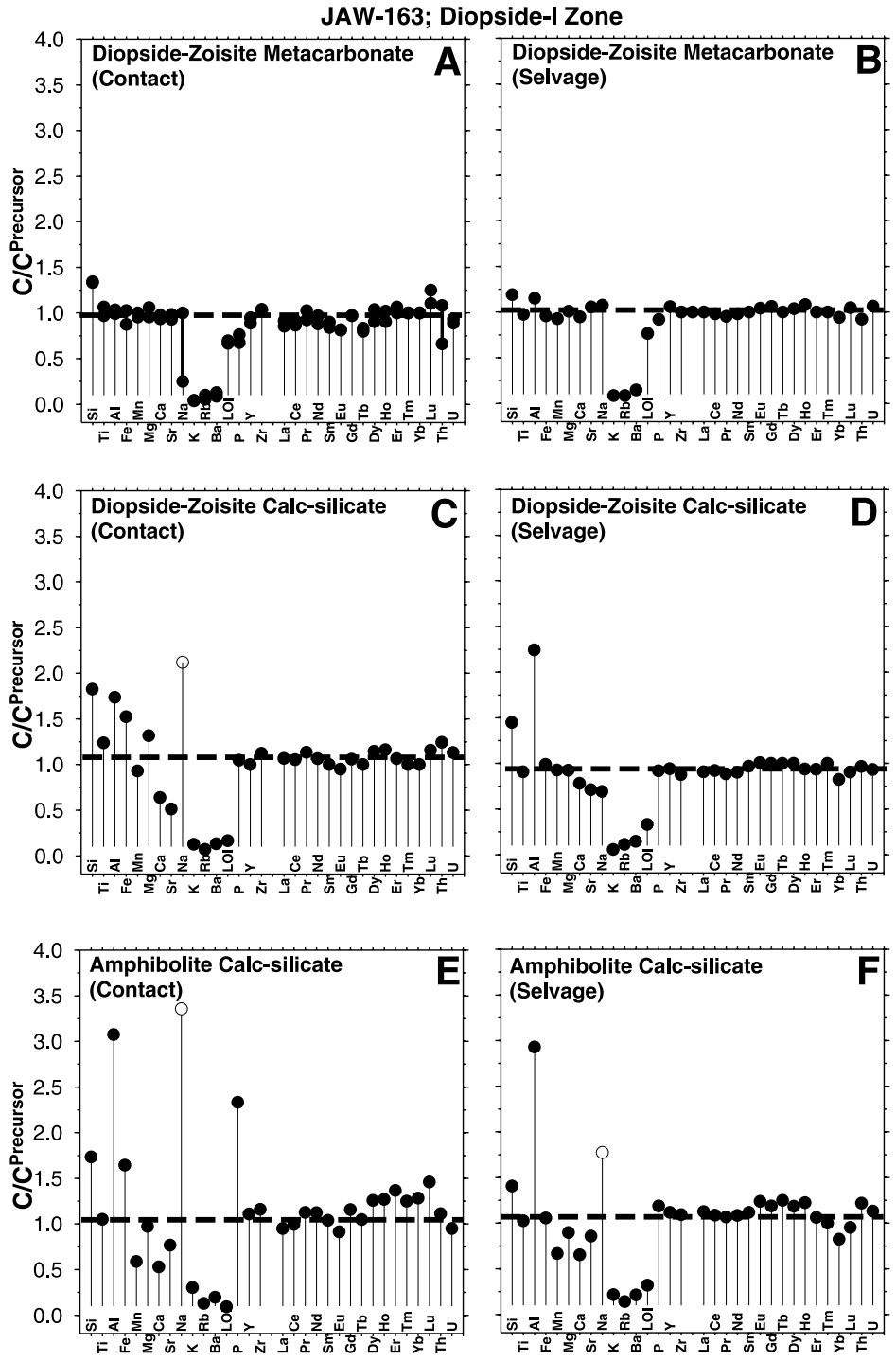

Fig. 12. Concentration ratio diagrams for Diopside-I zone contacts (left panels) and a vein selvage (right panels), JAW-163 locale. Estimate of concentration ratio for immobile elements (r_{inv}) denoted by heavy horizontal dashed lines. (A) Two examples of biotite-free, diopside-zoisite metacarbonates relative to biotite-bearing precursors at lithologic contacts: 1) mean of 163T, U, and V relative to 163Z-2; 2) 163IVAi relative to 163IVAii. (B) Biotite-free, diopside-zoisite metacarbonate in vein selvage (163VIIAiii) relative to biotite-bearing precursor (163VIIAiv). (C) Diopside-zoisite calc-silicate (163IRa) relative to 163Z-2. For this and subsequent figures, the precursor contained little Na, so small gains of Na resulted in large apparent Na increases (open circles). (D) Diopside-zoisite calc-silicate in vein selvage (163VIIAii) relative to 163VIIAiv. (E) Mean amphibolite calc-silicate composition (163Miv, N, O, Pa) for contact relative to 163Z-2. (F) Amphibolite in vein selvage (163VIIAi) relative to 163VIIAiv.

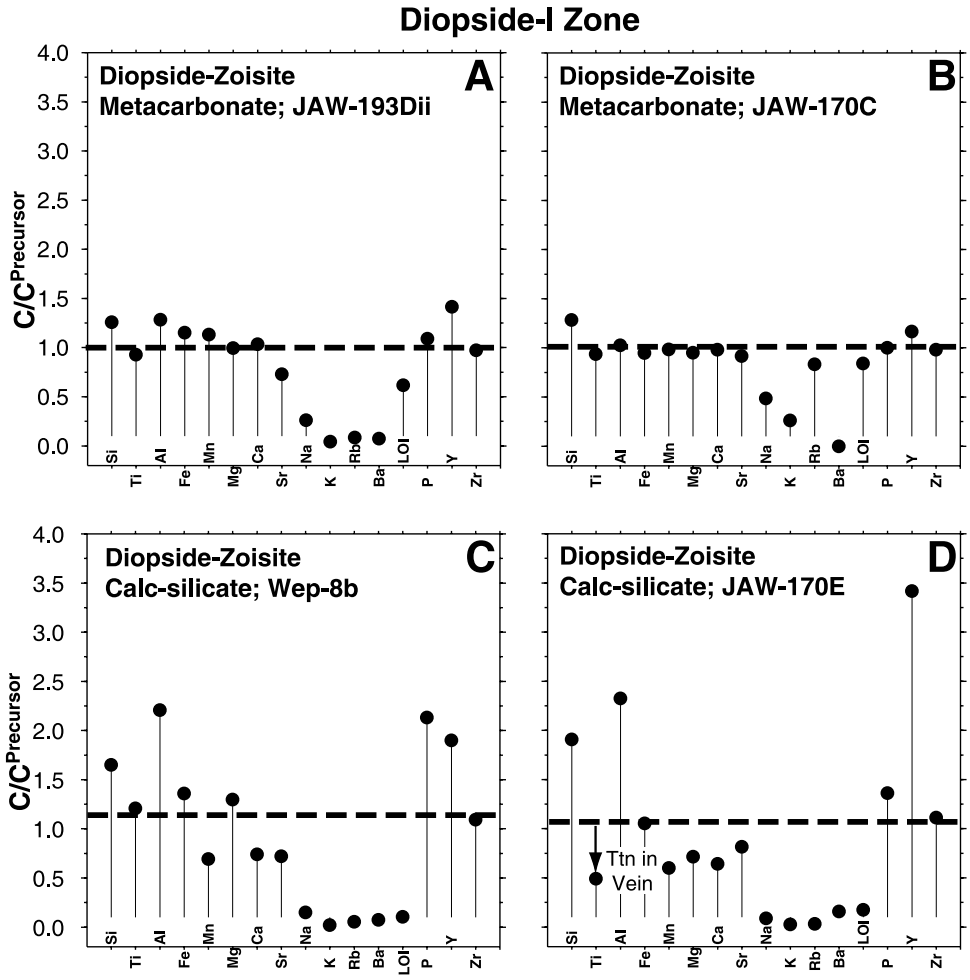

Fig. 13. Concentration ratio diagrams for Diopside-I zone. Estimate of concentration ratio for immobile elements (r_{inv}) denoted by heavy horizontal dashed lines. REE, U, and Th not determined. (A) Diopside-zoisite metacarbonate at lithologic contact (193Dii) relative to hornblende-bearing precursor (193ADi). Note gains of Si, Al, and Y, and losses of Sr, Na, K, Rb, Ba, and volatiles. (B) Diopside-zoisite metacarbonate (170C) relative to biotite- and amphibole-bearing precursor (170A). (C) Diopside-zoisite calc-silicate in vein selvage (Wep-8b) relative to biotite- and amphibole-bearing precursor (Wep-8a). Samples 8a and 8b correspond to mineralogical zones "A" and "F", respectively, of Tracy and others (1983). (D) Diopside-zoisite calc-silicate in vein selvage (170E) relative to biotite- and amphibole-bearing precursor (170A). Ti loss due to local transport to adjacent vein to form titanite (Ttn).

Calcite, the feldspars, biotite, and amphibole were destroyed to make the diopside + zoisite rich product. Losses of K, Na, CO_2, and H_2O were significant, and some Si and Al were gained. R.7 is somewhat atypical because the reactant is the only rock in this study to contain abundant K-feldspar that appears texturally to be prograde (table 3). Note, however, that growth of the diopside-bearing assemblage destroyed the K-feldspar and released K.

The classic Wep-8 sample locality studied by Hewitt (1973), Tracy and others, (1983), and Palin (ms, 1992) is a Di-I zone sequence. Two samples were available: Wep-8a, the little altered biotite-amphibole metacarbonate rock, and Wep-8b, a highly altered diopside-zoisite calc-silicate (mc) rock from the margin of a quartz vein zone.

Tracy and others (1983) and Palin (ms, 1992) concluded that Si, Ca, alkalis, Fe, Mg, and volatiles were all lost adjacent to the vein, resulting in extremely large mass and volume losses of as great as -70 percent. These authors assumed that Al was nearly immobile, except for loss of minor Al in a 1:1 molar ratio to the lost alkalis. A Zr-Ti reference frame indicates loss of Ca, Na, K, and volatiles, consistent with Tracy and others (1983), as well as loss of Mn, Ba, Rb, and Sr (fig. 13C). However, Si, Al and, probably, Fe and Mg were added to the calc-silicate (mc), in contrast to Tracy and others. P and Y were also gained. The pattern of mass transfer resembles that for other diopside-zoisite calc-silicate (mc) rocks (fig. 12C and D). The overall biotite-amphibole metacarbonate → diopside-zoisite calc-silicate (mc) mineralogical transformation was:

$$4.937\ \mathrm{Cal} + 1.132\ \mathrm{Qtz} + 0.462\ \mathrm{Bt} + 0.439\ \mathrm{Pl} + 0.141\ \mathrm{Py} + 3.828\ \mathrm{HCl} +$$
$$2.105\ \mathrm{Si(OH)_4} + 1.254\ \mathrm{Al(OH)_3} + 0.156\ \mathrm{MgCl_2} + 0.099\ \mathrm{FeCl_2} + 0.018\ \mathrm{H_3PO_4} =$$
$$1.158\ \mathrm{Di} + 0.861\ \mathrm{Zo} + 0.101\ \mathrm{Amp} + 0.028\ \mathrm{Ttn} + 0.005\ \mathrm{Ap} +$$
$$1.843\ \mathrm{CaCl_2} + 0.398\ \mathrm{KCl} + 0.232\ \mathrm{NaCl} + 0.011\ \mathrm{MnCl_2} +$$
$$0.088\ \mathrm{HF} + 4.937\ \mathrm{CO_2} + 0.282\ \mathrm{H_2S} + 7.597\ \mathrm{H_2O}. \qquad \text{(R.8)}$$

Si, Al, Mg, and Fe were added to form quartz, zoisite, diopside and lesser amphibole, destroying nearly all calcite and removing the associated CO_2. Much of the Ca was also lost, but some was retained to form product Ca-rich silicates. Destruction of biotite, plagioclase, and sulfides liberated K, Na, and S. P was added to form apatite. The r_{inv} ratio of ~1.15 based on Ti and Zr suggests mass losses of -13 percent for the calc-silicate selvage (Wep-8b) relative to the amphibole and biotite-bearing metacarbonate precursor (Wep-8a).

A final Di-I zone example of diopside-zoisite calc-silicate (mc) formation adjacent to a quartz vein is very similar to other examples, except that Ti was lost locally from the wallrock to make titanite in the adjacent vein (fig. 13D).

Alteration of Metapelitic Rocks, Di-I Zone

Metacarbonate rocks are the focus herein, but alteration of adjacent metapelitic schists provides additional information about mass transfer. Figure 14 compares representative metaclastic schist with: 1) amphibolite calc-silicate (s) rock near the contact (X ~ -0.75 cm) for the Di-I zone profile and 2) biotite-zoisite-garnet rock in the selvage of a ~35 centimeter wide vein that cuts up through the metacarbonate rocks and across the metaclastic rocks near the profile. Si, Al, Na, K, Rb, Ba, and volatiles were lost, and Ca and Y were gained. Mg appears to have been gained and P lost at the contact, with the opposite being true for the selvage. REE were added to both examples, and U was added to the selvage.

Al, Si, and P were gained and Ca was lost on the metacarbonate side of the contact, whereas Al, Si, and P were lost and Ca was gained on the metaclastic side, strongly suggesting that at least some coupled mass transfer across the contact occurred (figs. 11 and 14). The calc-silicate (s) rock directly at the contact lost about -40 percent of its mass relative to the less altered schists away from the contact (fig. 14). This mass loss, while significant, occurs over a narrow (~3 cm) interval and is insufficient to account for all the Al, Si, and P gains in the adjacent calc-silicate (mc) rocks. For example, a simple mass balance calculation demonstrates that the Al added to the calc-silicate (mc) is over 10 times greater than that lost from the calc-silicate (s). The excess Al was likely input by fluids flowing along the quartz veins that cut the calc-silicate (mc) (fig. 2). The gains in Ca and losses of Al in the selvage also suggest fluid exchange with metacarbonate rocks; the Si loss was probably due to local silica transport from the

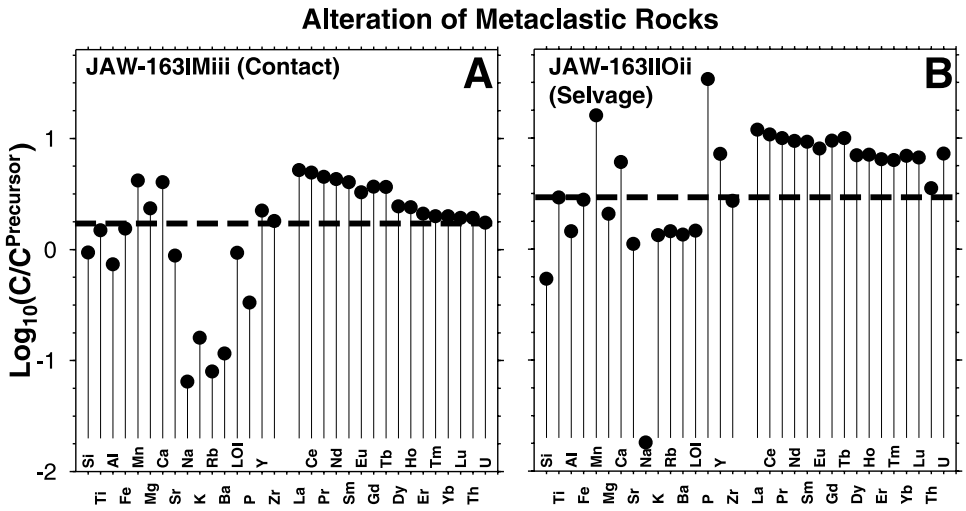

Fig. 14. Concentration ratio diagrams for altered metaclastic schist at lithologic contact with metacarbonate rock or in vein selvage. Logarithmic *y*-axes. Estimate of concentration ratio for immobile elements (r_{inv}) denoted by heavy horizontal dashed lines. Large overall mass losses due mostly to losses of Si and Al. (A) Altered schist at contact (163IMiii) relative to schist ~15 cm from contact (163IL). Overall mass loss about -40 % (eq 3). (B) Altered schist in vein selvage (163IIOii) relative to 163IL. Overall mass loss about -65 % (eq 3).

rock to the vein and contributed to the overall mass loss of about -65 percent (fig. 14). Na, K, Rb, Ba, and Sr were released as zoisite grew and micas and plagioclase broke down within the contact and selvage. Phosphate minerals, zoisite, and/or garnet almost certainly host much of the added REE.

Diopside-II Zone

The example Di-II zone profile extends from the diopside and zoisite-rich metacarbonate rock in the interior of the layer, through diopside-zoisite and amphibolite calc-silicates (mc), to a lithologic contact with metaclastic rock (fig. 2). A ~1.5 centimeter wide quartz vein occupies the contact (vein 1), and a ~0.5 to 3.5 centimeter wide quartz + zoisite vein is present at ~14 to 15 centimeters along the profile (vein 2; fig. 15). The calc-silicates (mc) also contain smaller discontinuous veins and sporadic millimeter scale veinlets (fig. 15). Little of the metaclastic rock is exposed. Si/Zr increases along the profile from ~35 to ~15 centimeters, reaching peak values in the vicinity of vein 2 (fig. 15). Si/Zr then drops in the adjacent amphibolite calc-silicate (mc), but still exceeds values for the interior of the metacarbonate layer. The calc-silicates (mc) gained Al; peak Al/Zr is reached near vein 2 (fig. 15). Profiles for P/Zr, Y/Zr, U/Zr, La/Zr, Sm/Nd, and Sr/Zr are similar (fig. 16). Sm/Eu increases through the calc-silicates (mc) toward vein 1 (fig. 16F). LOI/Zr drops at the diopside-zoisite metacarbonate → diopside-zoisite calc-silicate (ms) transition at ~23 centimeters along the profile (fig. 16H).

Formation of the diopside-zoisite calc-silicate (mc) rocks from the diopside-zoisite metacarbonate precursor involved gains of Si, Al, P, Mg, and Fe, and loss of calcium, Mn, most alkali and alkaline earth metals (except Sr), and volatiles (fig. 17A). The amphibolite calc-silicate (mc) is similar, except that little Mg appears to have been added (not shown). Notably, mid-REE and, to a lesser degree, light REE (LREE) were added near vein 2 (fig. 17B). Eu was not added to the same degree as the surrounding REE, resulting in a Eu "anomaly" and the Sm/Eu increase toward the contact (figs. 16F and 17B). Fluid-rock interaction at lower metamorphic grades is inferred to have

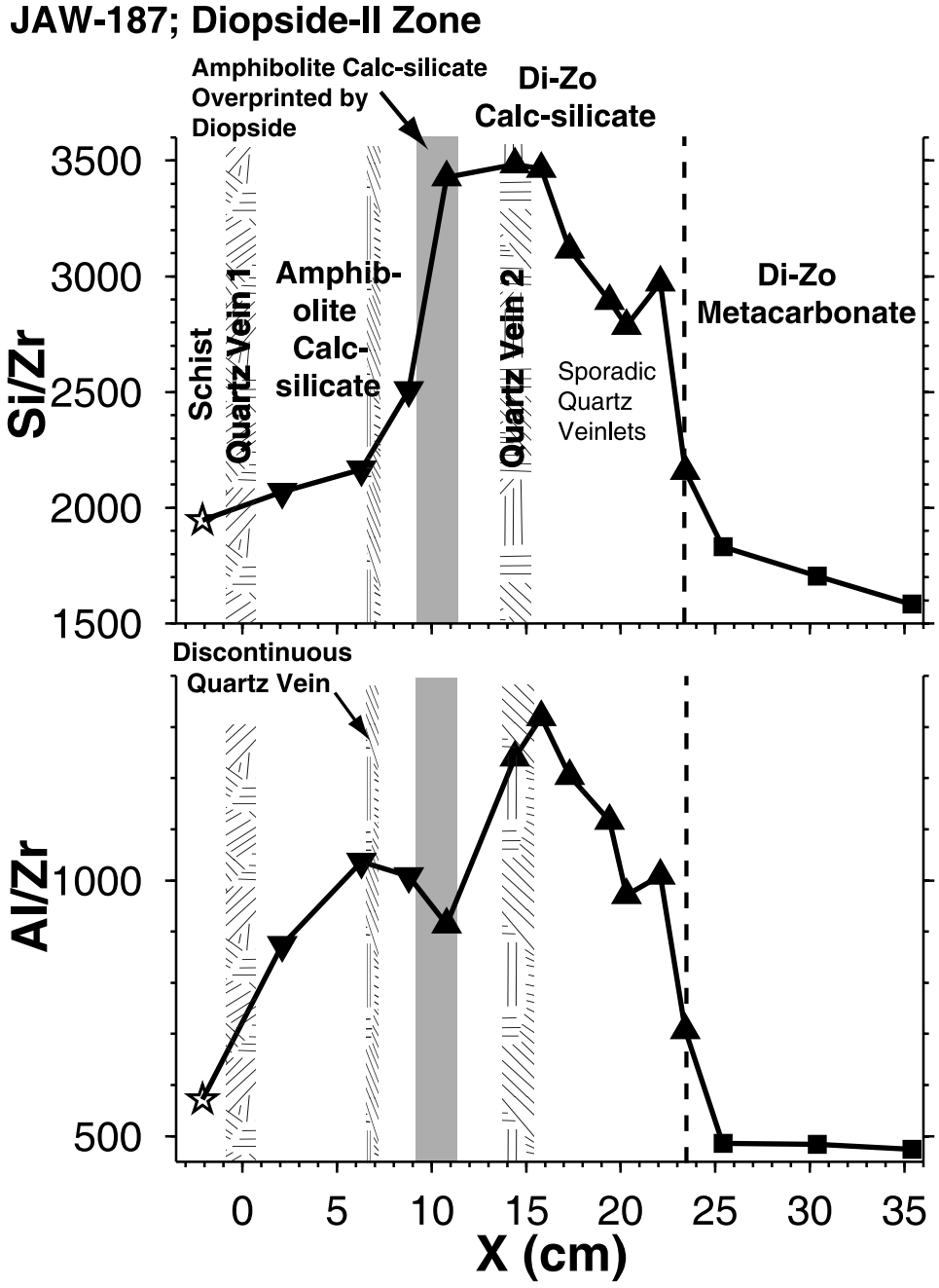

Fig. 15. Si/Zr and Al/Zr profiles for JAW-187 traverse, Diopside-II zone. Area where amphiboles partially replaced by diopside denoted by dark gray band at ~10 cm. Note strong enrichments of Si and Al in calc-silicates (left of vertical dashed line) relative to calcite-rich diopside-zoisite metacarbonate rock (right of vertical dashed line). Rock type symbols given in table 2.

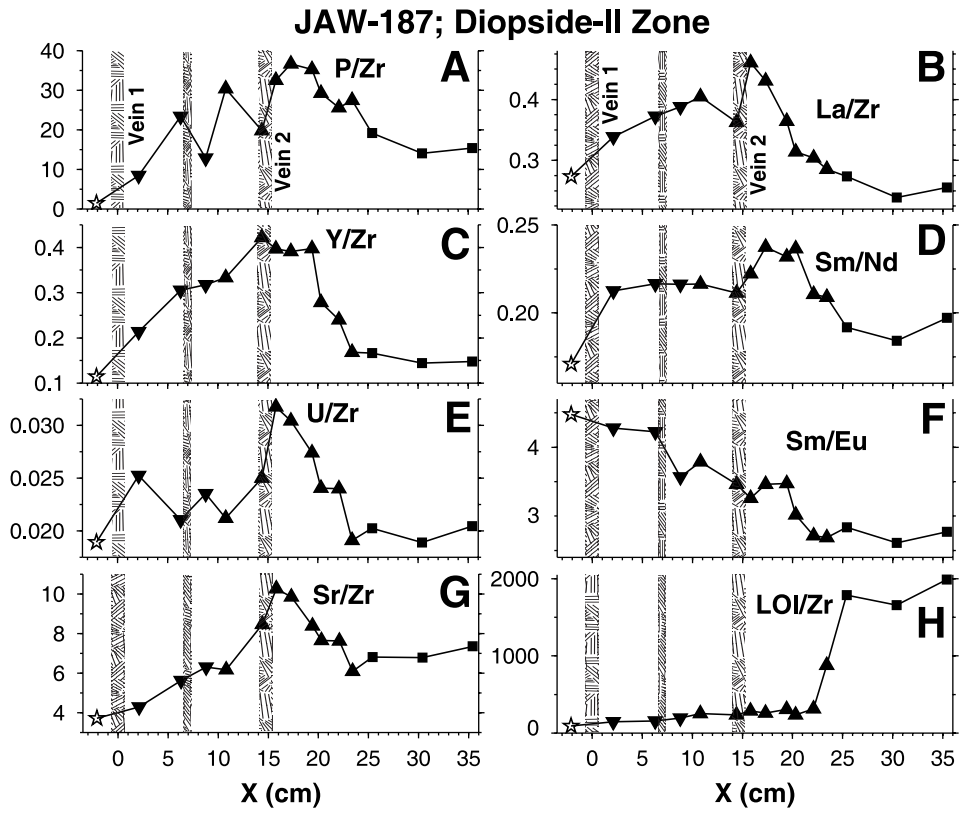

Fig. 16. Geochemical profiles for JAW-187 traverse, Diopside-II zone. See figures 2 and 15 for lithologic descriptions, table 2 for symbol definitions, and text for detailed discussion.

removed Sr from the layer because it contains about half the Sr that little altered Ank-Ab zone metacarbonate rocks do. Infiltrating fluids that produced the diopside-zoisite calc-silicate (mc) must have added Sr back to the rock in the vicinity of vein 2 (fig. 16G).

The reaction that produced diopside-zoisite calc-silicate (mc) from diopside-zoisite metacarbonate rock destroyed calcite and produced considerable quartz, zoisite, and diopside:

$$2.836\ \mathrm{Cal} + 0.010\ \mathrm{Ttn} + 3.162\ \mathrm{Si(OH)_4} + 1.981\ \mathrm{HCl} + 1.472\ \mathrm{Al(OH)_3} + 0.252\ \mathrm{MgCl_2} + 0.180\ \mathrm{FeCl_2} + 0.016\ \mathrm{H_3PO_4} + 0.007\ \mathrm{HF} =$$

$$0.840\ \mathrm{Qtz} + 0.525\ \mathrm{Zo} + 0.345\ \mathrm{Di} + 0.005\ \mathrm{Amp} + 0.004\ \mathrm{Ap} + 1.417\ \mathrm{CaCl_2} + 0.004\ \mathrm{MnCl_2} + 0.003\ \mathrm{NaCl} + 2.836\ \mathrm{CO_2} + 9.286\ \mathrm{H_2O} \quad \text{(R.9)}$$

Si and Al addition resulted in r_{inv} ~0.8 (fig. 17A), and a corresponding overall mass gain of ~25 percent for veined calc-silicate relative to calcite-rich metacarbonate rock in the layer interior.

Another example of the formation of diopside-zoisite calc-silicate (mc) from diopside-zoisite metacarbonate rock resembles that for the profile, although Mg and Fe were less mobile and P addition was extreme (fig. 17C).

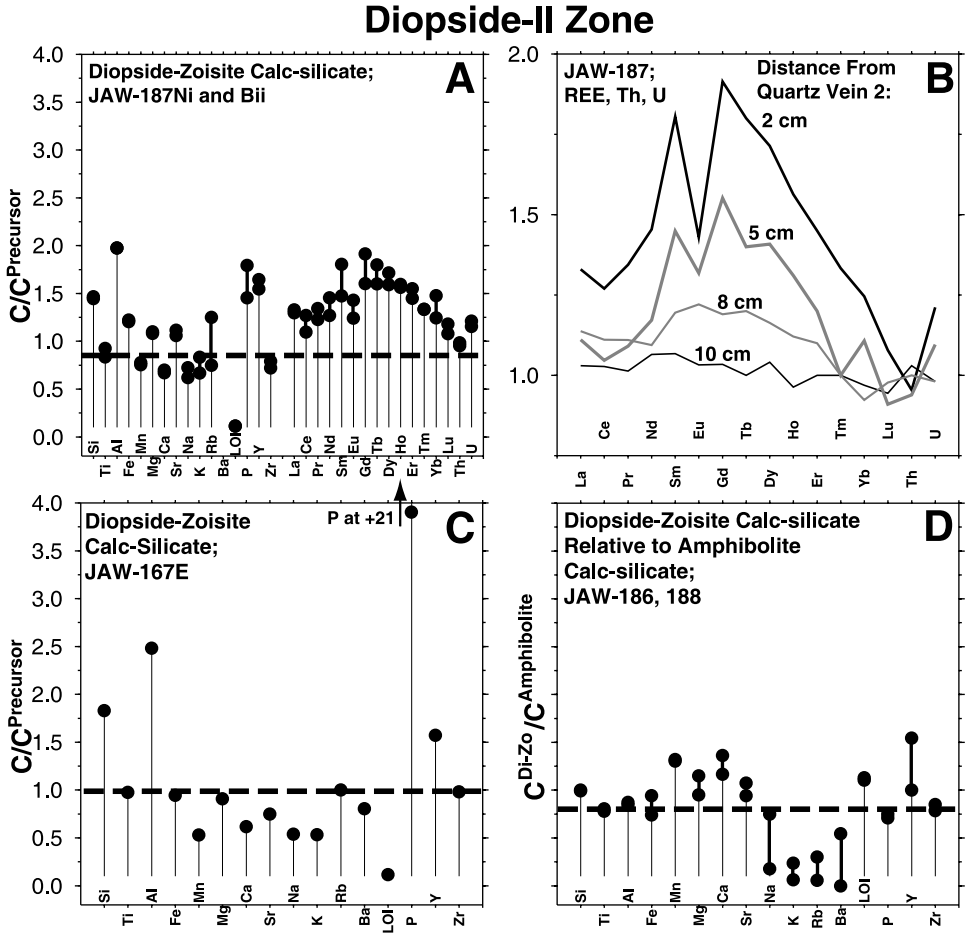

Fig. 17. Concentration ratio diagrams for Diopside-II zone. Estimate of concentration ratio for immobile elements (r_{imv}) denoted by heavy horizontal dashed lines. (A) Two comparisons for the JAW-187 profile (figs. 15 and 16). Two representative diopside-zoisite calc-silicate analyses (187Ni, 187Bii) each relative to diopside-zoisite metacarbonate rock (mean of 187Mi, 187Mii, and 187Miii). Note mass gain of REE with a maximum centered on Gd. (B) Representative REE systematics approaching quartz vein 2 along JAW-187 profile. Note increasing REE gain as vein is approached. Within ~5 cm of vein, Eu gain was not as marked as that for surrounding REE, and U gain occurred. Samples 187Bii (2 cm), 187Ni (5 cm), 187Biii (8 cm), and 187Mi (10 cm) each relative to mean of 187Mi, 187Mii, and 187Miii. (C) Diopside-zoisite calc-silicate (167E) relative to diopside-zoisite metacarbonate (167A). REE not determined. (D) Diopside-zoisite calc-silicates compared to amphibolite calc-silicates (186Bi/186Bii and 188Ai/188Aii). This particular diagram simply compares chemical compositions, and does not imply that one rock type was derived directly from the other. REE not determined.

Strong alteration converted some Di-II zone layers entirely to amphibolite calc-silicate (mc) margins and diopside-zoisite calc-silicate (mc) interiors such that no calcite-rich metacarbonate rock remains. Relative to amphibolite calc-silicate (mc), the diopside-zoisite calc-silicate (mc) tends to be richer in Si, Mn, Mg, Ca, Sr, Y, and volatiles, and poorer in Na, K, Rb, and Ba (fig. 17D).

MOBILITY OF NON-VOLATILE ELEMENTS

This section examines the observed alkali metasomatism, Al addition and associated calc-silicate formation, and the mobility of REE, P, Y, U, and Th in the context of fluid-rock interaction between the metacarbonate layers and surrounding rock types.

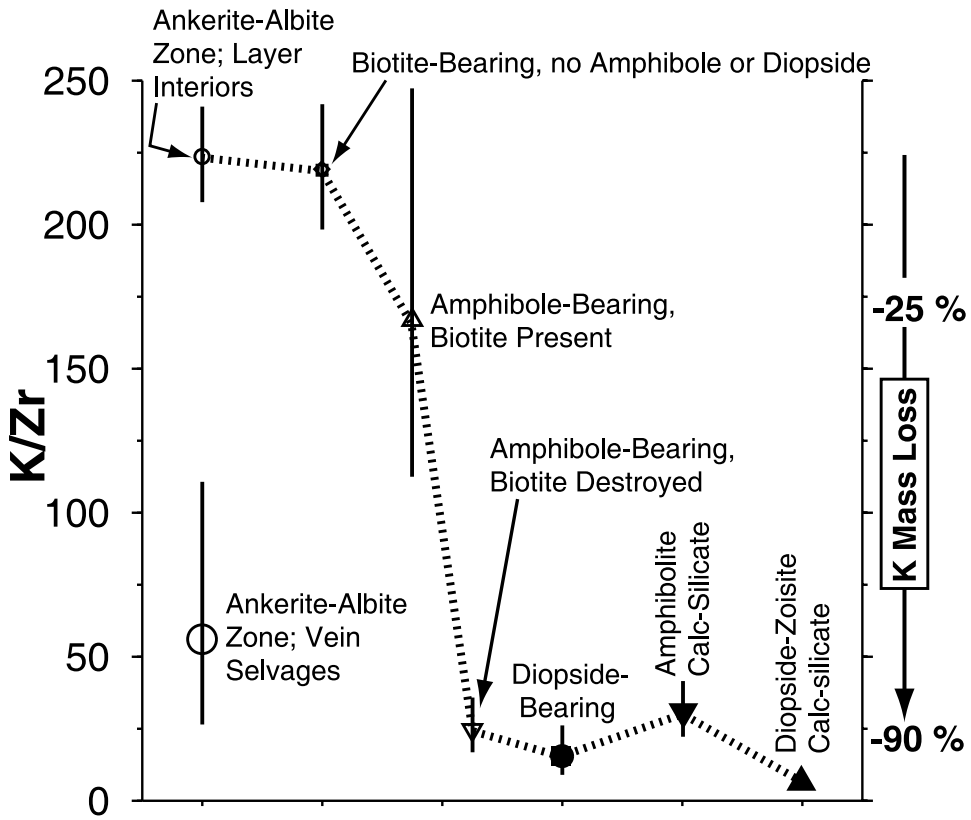

Fig. 18. K loss during metamorphism. K shown relative to immobile Zr. Geometric mean mass ratios $\pm 2\sigma$ (see Ague, 1994a; Ague and van Haren, 1996). Includes data from all rocks with metacarbonate protoliths in appendix E. Major K loss shown for: 1) strongly altered vein selvages in Ankerite-Albite zone in which albite and in some cases chlorite formed at the expense of muscovite and 2) higher grade rocks in which biotite broke down to make amphibole and/or diopside. Selected K mass loss percentages on right edge of diagram relative to mean Ankerite-Albite zone rock.

Alkali Metasomatism in the Ankerite-Albite, Ankerite-Oligoclase, and Biotite Zones

Metacarbonate rocks generally gained Na and lost K at contacts with metaclastic schists and in alteration selvages surrounding syn-metamorphic veins (figs. 4, 5, 6, 7, 8A, and 18). This metasomatism could be the result of: (1) fluid flow in a direction of increasing temperature (Dipple and Ferry, 1992; Ague, 1997a) or (2) input of relatively Na-rich and K-poor fluids derived from surrounding rock types (compare Breeding and Ague, 2002). Mechanism (1) requires that metaclastic schists also gained Na and lost K along lithologic contacts with the metacarbonate layers, but this metasomatism is not observed. In fact, some schists at contacts have noticeably elevated K/Na; for example, metapelite at the JAW-168 profile locality has molar K/Na of ~21, well in excess of the low-grade average of ~1.5 (table 1 in Ague, 1994a). Consequently, only mechanism (2) is viable. The obvious source for metasomatic fluid is the large volume of metaclastic rocks, but such fluid must have more Na and less K than fluid equilibrated with the metacarbonate layers. To test the metaclastic fluid source hypothesis, fluid speciation calculations were done using the model phases quartz, calcite, albitic plagioclase (Ab_{98}), dolomite, muscovite, and clinochlore at representative Ank-Ab zone conditions of 425°C and 7 kbar (app. A) (Ague, 2002).

Many metaclastic rocks at this grade lack carbonate minerals, and are composed mostly of quartz, muscovite, chlorite, and albitic plagioclase. In such rocks, the activities of calcite and dolomite must be less than unity. The Na content of the fluid equilibrated with the solids increases and the K content decreases as the activities of calcite and dolomite are reduced (fig. 19A). Some metaclastic rocks contain ankerite, but lack calcite. Holding the activity (a) of dolomite in the model at $a_{Dol} = 1$ (equivalent to dolomite saturation), the Na content of the fluid increases and the K content decreases as the activity of calcite is reduced (fig. 19A).

These results can also be understood in terms of the pH of fluids coexisting with albite, muscovite, and quartz governed by reactions such as: $2H^+ + K^+ + 3Ab = 3Na^+ + Ms + 6Qtz$. Decreasing the activities of the carbonate minerals decreases pH, and increases the bulk Na^+/K^+ of the fluid (fig. 19B). Fluids in metapelitic rocks that are undersaturated with respect to carbonate minerals will tend to have somewhat lower pH and, thus, elevated Na/K relative to metacarbonate rocks.

Nearly all metacarbonate rocks at this grade lack chlorite; the common mineral assemblage is calcite, ankerite, quartz, muscovite, and albite. Decreasing the clinochlore activity in the calculations models this chlorite undersaturation. The concentration of Na increases and K decreases as the chlinochlore activity is reduced, but the overall amount of fluid composition change is much smaller than that observed for corresponding decreases in the activities of carbonate minerals in the model schists (fig. 19A).

Fluids equilibrated with typical metaclastic rocks in the low-grade parts of the sequence would have had larger Na concentrations and smaller K concentrations than fluids equilibrated with metacarbonate layers (fig. 19). Thus, infiltration of fluids from the schists into the metacarbonate rocks would have driven Na gain and K loss, fully consistent with observations. The metasomatism resulted in the destruction of muscovite and the production of plagioclase (reaction R.1). Fe mass addition around Ank-Ab zone veins (fig. 6) is also consistent with a metaclastic fluid source, since the metaclastic rocks have much larger Fe/Mg than the metacarbonate rocks (compare Ague, 1994a). Infiltration could have occurred by advective flow, diffusion, mechanical dispersion, or some combination (see below). The Ank-Ab zone vein example (figs. 5 and 6A) gained Si and volatiles, strongly suggesting that fluids were flowing in a direction of decreasing temperature through this fracture (Ferry and Dipple, 1991; Ague, 2000). As such, the vein and alteration selvage provide a record of the outflow of fluid released from regional devolatilization. At somewhat higher grades in the Ank-Ol and Bt zones, the situation is a bit more complicated because the activity of anorthite in the plagioclase increases due to reactions that form paragonite or biotite. However, such reactions would increase the Ca/Na of the fluid and, thus, Na would still tend to infiltrate into the metacarbonate layers from the surroundings.

Alkali Metasomatism in the Amphibole and Diopside Zones

A near ubiquitous chemical feature of metacarbonate rocks in these zones is the major loss of K, Rb, and Ba during the growth of amphibole and/or diopside (fig. 18). Na was usually lost from rocks that contained appreciable plagioclase, in contrast to contacts and selvages at lower grades (figs. 10C and 13).

The loss of K, Rb, and Ba coincides with reactions that destroyed biotite and that should have made K-feldspar. Commonly cited model reactions include the production of amphibole: $6\ Cal + 5\ Bt + 24\ Qtz = 3\ Amp + 5\ Kfs + 2\ H_2O + 6\ CO_2$; and diopside: $Bt + 3\ Cal + 6\ Qtz = 3\ Di + Kfs + 3\ CO_2 + H_2O$. However, in the Wepawaug Schist, reactions that consumed biotite and made amphibole or diopside made little or no K-feldspar at the site of reaction (see reactions R.3 through R.8). It should be noted that not all amphibole-bearing rocks are K-depleted. For example, Wep-8a contains abundant biotite and coexisting amphibole, no prograde K-feldspar, and no evidence for K loss (fig. 20) (Ague, 2002). Thus, amphibole formation did not involve biotite

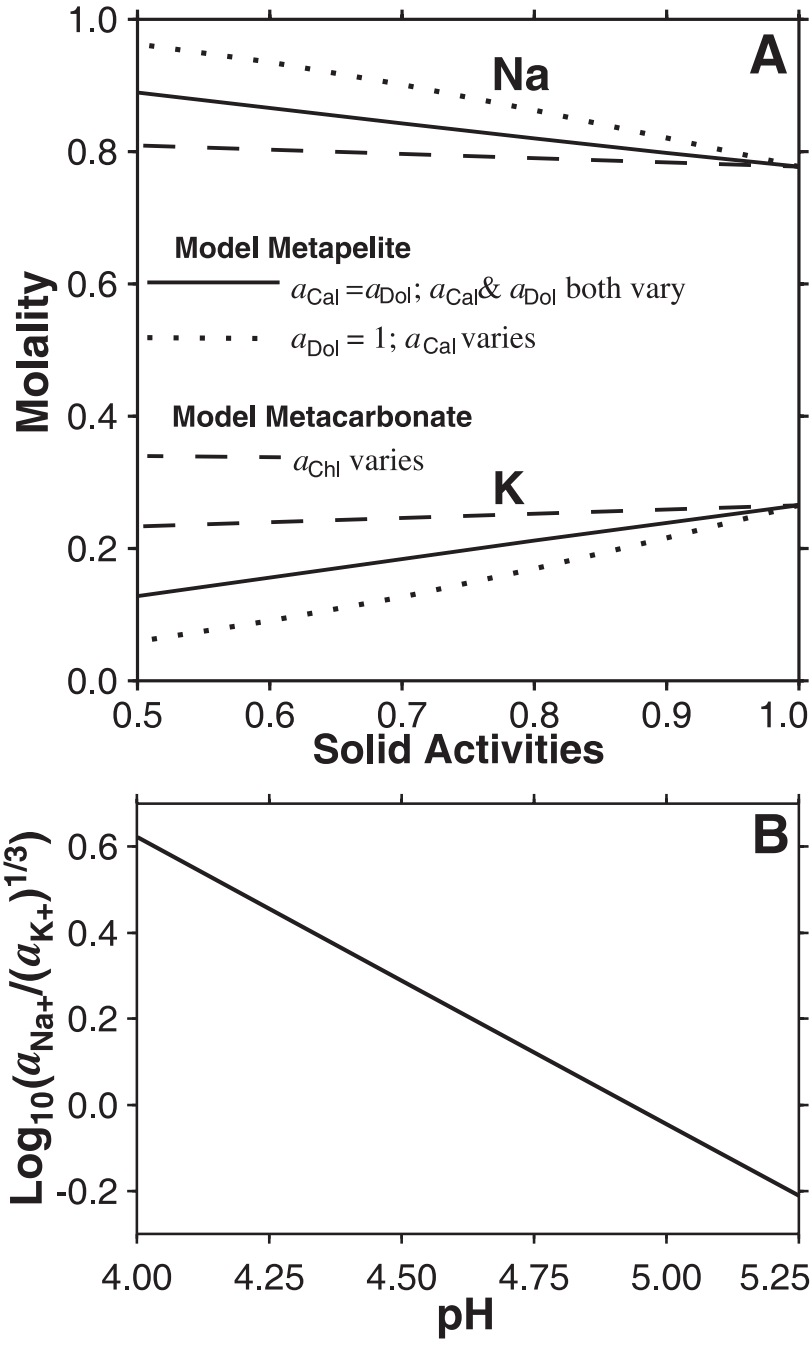

Fig. 19. Fluid compositions calculated for 425°C and 7 kbar (app. A). (A) Relationships between fluid composition and activities of coexisting solids for model metapelitic and metacarbonate rocks. a_{Cal}, a_{Chl}, and a_{Dol} denote activities of calcite, chlinochlore, and dolomite, respectively. Total molality of Na increases and K decreases as activities of carbonate minerals decrease. Metapelitic rocks that contain ankerite but no calcite or that lack carbonate minerals altogether will equilibrate with fluids having larger bulk Na/K than fluids equilibrated with metacarbonate rocks. Variations in a_{Chl} have a considerably smaller impact. (B) Fluids coexisting with albite, muscovite, and quartz. Fluid pH will tend to be higher and Na^+/K^+ lower for metacarbonate rocks rich in calcium-bearing carbonate minerals than for metapelitic rocks.

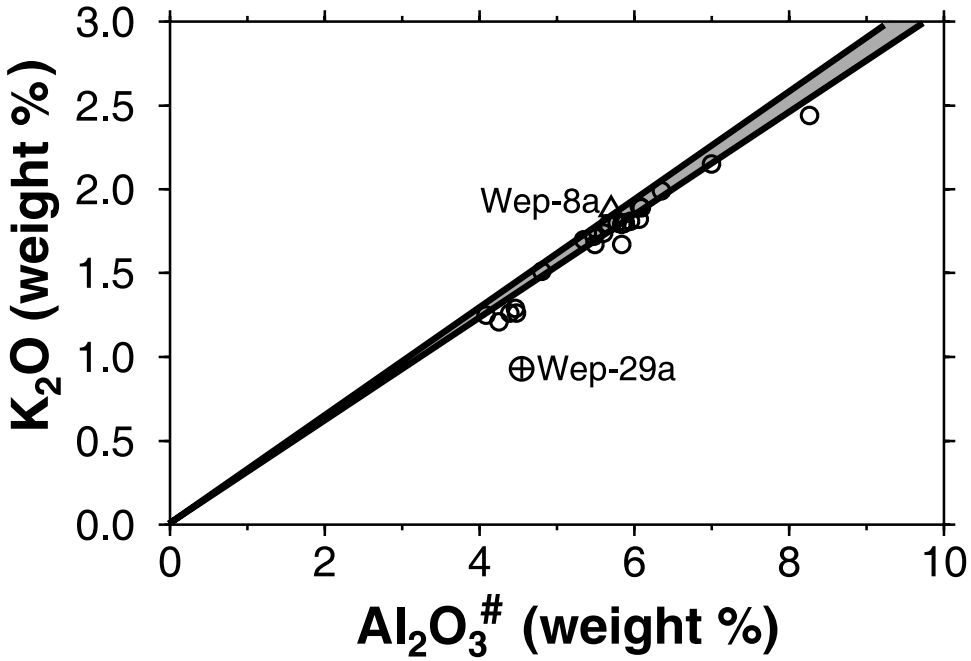

Fig. 20. K_2O-Al_2O_3 relations. $Al_2O_3^{\#}$ estimates bulk-rock Al_2O_3 contained in muscovite, and was obtained by subtracting the fraction of Al_2O_3 in albite from total bulk rock Al_2O_3. Range of muscovite K_2O/Al_2O_3 ratios determined by Ague (2002) denoted by gray shaded trend. Ankerite-Albite zone rocks (open circles) cluster near the trend, indicating that K_2O is hosted by muscovite and that muscovite and albite are the only two significant Al-bearing minerals (does not include highly altered vein selvages). Ankerite-Oligoclase sample Wep-29a falls off the trend because its protolith probably contained paragonite in addition to muscovite and albite. Wep-8a (Diopside-I zone) has $K_2O/Al_2O_3^{\#}$ ratio compatible with muscovite-bearing Ankerite-Albite zone precursor, and thus has not lost K during metamorphism. $Al_2O_3^{\#}$ estimated from bulk rock analysis assuming a Na_2O/K_2O mass ratio of 0.061 for muscovite and a Al_2O_3/Na_2O mass ratio of 1.65 for albite (Ague, 2002). Results are insensitive to reasonable variations in these ratios because muscovite and albite compositions vary little in Ankerite-Albite zone.

and was almost certainly due to a different reaction, most probably the breakdown of ankerite (model reaction: 5 Ank + 8 Qtz + H_2O = Amp + 3 Cal + 7 CO_2).

The K loss requires that the chemical potentials of K species during biotite breakdown in metacarbonate rock were greater than those in surrounding metaclastic and igneous rocks. Fluids equilibrated with quartz + K-feldspar-bearing rocks would have had the largest chemical potentials of K species, greater than the coexisting quartz + muscovite ± K-feldspar found in some felsic igneous and metaigneous rocks, and the quartz + muscovite ± kyanite of metaclastic rocks (fig. 21A). Consequently, when reactions attempted to form K-feldspar, it would have been possible for K to move down chemical potential gradients out of the metacarbonate layers. The rates of biotite destruction and K release at sites of reaction must have been greater than the rates of K-feldspar nucleation and growth, because little or no K-feldspar actually formed (see discussion below and Tracy and others, 1983). The K-feldspar in tiny, millimeter scale veinlets at some localities (JAW-181) may have precipitated as the result of factors such as enhanced surface free energy along crack walls; in addition, the veinlets appear to be late-stage, cross-cutting features (often associated with chlorite) that probably post-date the metamorphic peak. It is worthwhile to note that the precise speciation of the fluid phase is not critical to interpretation of the mineral stability fields on figures like figure 21A. For example, an activity diagram with axes $\log(a_{K^+}/a_{H^+})$ *versus* $\log(a_{Al^{3+}}/(a_{H^+})^3)$ would have stability fields that look identical to

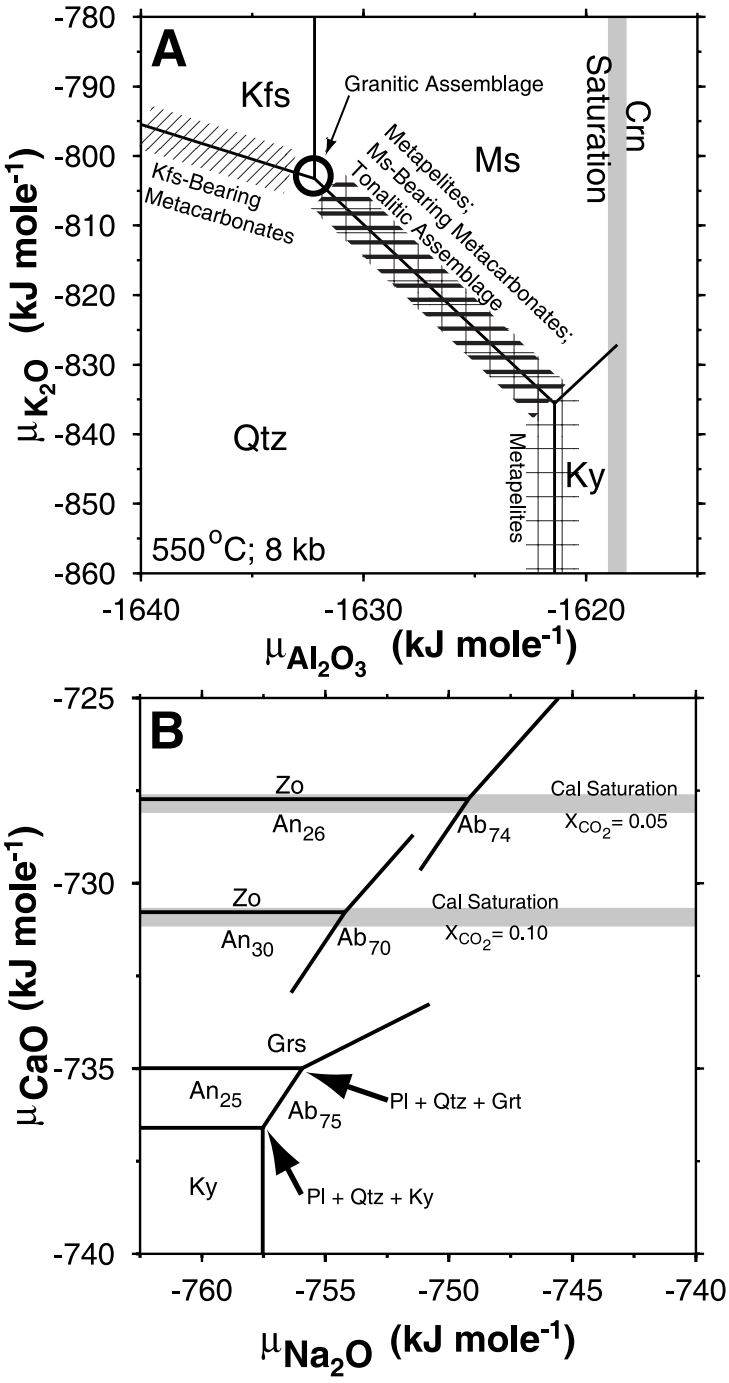

Fig. 21. Chemical potential diagrams, 550°C and 8 kbar. (A) Chemical potential (μ) of K_2O versus chemical potential of Al_2O_3 for minerals coexisting with H_2O. Note large μ_{K_2O} and small $\mu_{Al_2O_3}$ for metacarbonate rocks containing K-feldspar (Kfs) relative to metapelitic or felsic metaigneous rocks. (B) Chemical potential of CaO versus chemical potential of Na_2O for minerals coexisting with quartz and H_2O-CO_2 fluid. Mineral assemblages for model metaclastic schist containing quartz, plagioclase, garnet (grossular component shown), and kyanite occupy lower left part of diagram. Model metacarbonate mineral assemblage of quartz, calcite, plagioclase, and zoisite characterized by larger μ_{CaO}, as well as by μ_{Na_2O} that increases as plagioclase becomes more sodic. Representative grossular (Grs) activity of 0.01 based on Ague (1994b); X_{CO_2} is mole fraction CO_2 in fluid.

those for the chemical potential diagram in figure 21A (although the *x*- and *y*-axis units would obviously be different).

Na loss from plagioclase-bearing metacarbonate rocks was tied to the production of clinozoisite/zoisite from the anorthite component of plagioclase. The bulk plagioclase would have become more albite-rich as the anorthite component was consumed. The chemical potential of Na_2O thus increased and ultimately became much greater than that for assemblages in surrounding schists and igneous rocks (fig. 21B), facilitating removal of Na from the metacarbonate rocks. No albite-enriched plagioclase is evident near the sites of reaction or as compositional zones in the reacted feldspar. Therefore, the Na in the "albite component" generated when the clinozoisite/zoisite formed must have been transported out of the rock down chemical potential gradients at a rate faster than new sodic plagioclase could crystallize. It should be noted that Na loss is not evident in W5/W6A (reaction R.5). The plagioclase is $\sim An_{90}$ (Hewitt, 1973; Ague, 2002), so the chemical potentials of Na species were relatively low.

Al Mobility and the Formation of Calc-silicate Rocks

Major element metasomatism that formed calc-silicates in the Amphibole and Diopside zones included: 1) calcite destruction and loss of Ca and CO_2, 2) Si gain necessary for the growth of amphibole and/or diopside, 3) Al gain mainly to produce clinozoisite/zoisite and, in some cases, garnet, 4) alkali loss (described above) corresponding to the destruction of biotite and feldspar, and 5) Fe gain (figs. 18, 21, and 22). Mg gains occurred in some cases. Some of these metasomatic changes are expected in light of previous studies. For example, calcite-bearing rocks had elevated chemical potentials of Ca species relative to surrounding calcite-free rocks, consistent with the observed Ca losses (fig. 22C) (Vidale, 1969). Fe was gained progressively with increasing metamorphic grade and fluid-rock interaction, almost certainly reflecting infiltration of fluids from metaclastic and igneous/metaigneous rocks having greater Fe/Mg than the metacarbonates (fig. 22D). The Al gains discovered herein are consistent with lower $\mu_{Al_2O_3}$ for metacarbonate rocks relative to surrounding rock types (fig. 21A), but are much larger than documented elsewhere and provide a new avenue for quantification of fluid fluxes.

Time-integrated fluid fluxes (q_{TI}) for Al transport by fluid flow were estimated based on cross-cutting veins surrounded by Al-rich calc-silicate selvages. The q_{TI} needed to propagate a geochemical front from schist or igneous rock into metacarbonate rock can be estimated using an expression for advective mass transport under local fluid-rock equilibrium (Ague, 1998):

$$q_{TI} \approx L\frac{\bar{V}_f M_e}{\Delta X_e} + L\phi \approx L\frac{M_e}{\Delta C_e} + L\phi, \tag{6}$$

in which L is the distance of front propagation, ΔX_e and ΔC_e are the differences in the mole fraction and concentration, respectively, of element e between the input and equilibrium fluids, $\bar{V}_f$ is the molar volume of the fluid, and M_e is the moles of e added (positive) or removed (negative) per volume rock. The $L\phi$ term is negligible, and the change in fluid composition across the front was assumed to dominate the effects of changing P and T along the flow path. The calculations also assume advection-dominated transport directly at the fracture margins and neglect diffusion of Al away from the margins into wallrocks, thus yielding minimum flux estimates. Measurements at over 100 field sites indicate that vein length varies from <1 meter to at least 20 meters. A representative intermediate value of $L = 10$ m was thus used to estimate q_{TI}.

The small concentrations of Al in metamorphic fluids coupled with the large observed Al mass additions indicate that advective fluid flow was needed to transport Al over $L \sim 10$ m length scales. Al is ideal for quantitative application of equation (6) because calculations can be based directly on experimental results, avoiding errors

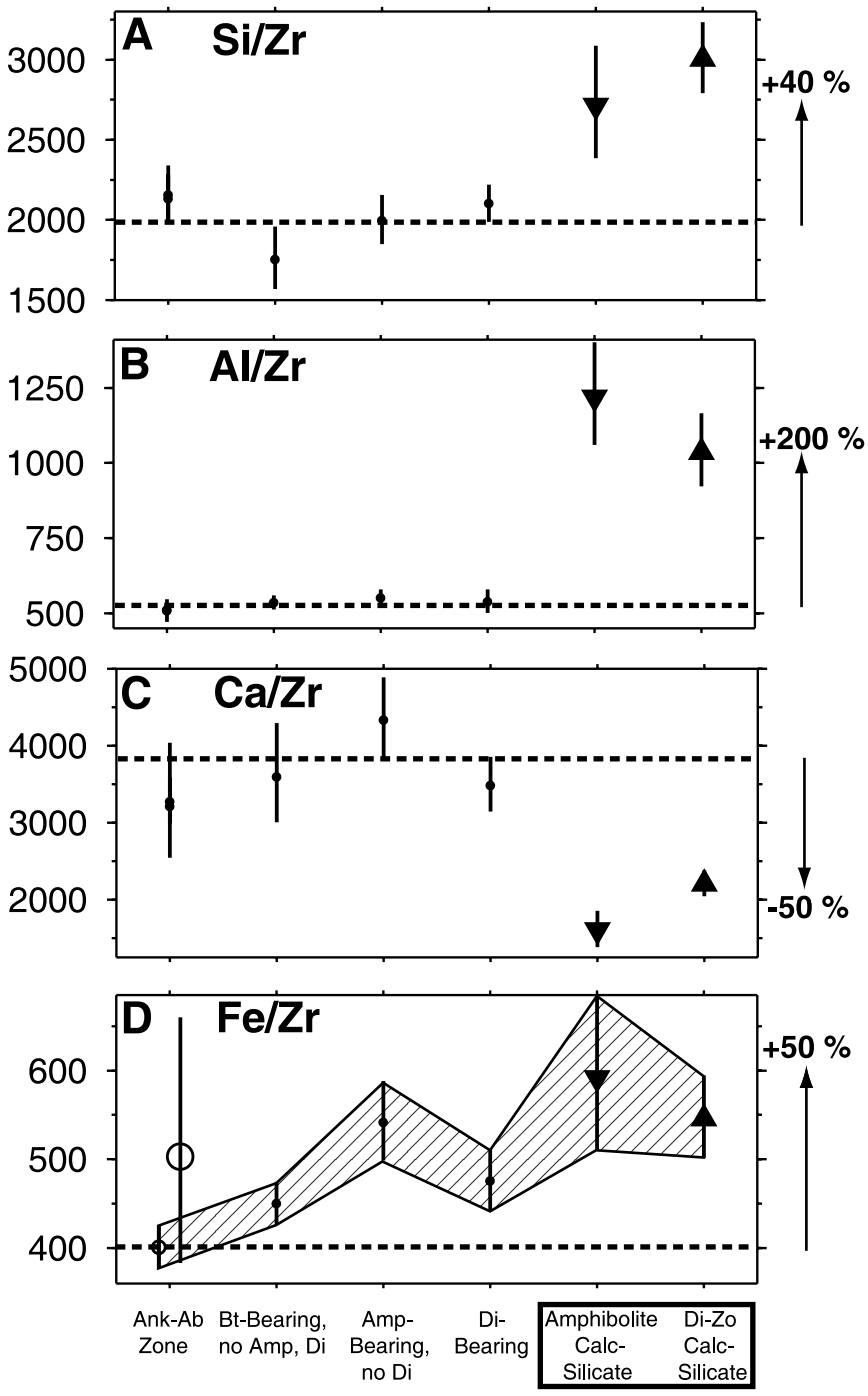

Fig. 22. Si gain, Al gain, Ca loss, and Fe gain (Zr reference frame) for calc-silicate rocks derived from metacarbonate precursors. Geometric mean ratios $\pm 2\sigma$. Percentage mass changes for parts A-C (right edges of graphs) are relative to representative ratios (dashed lines) for four leftmost metacarbonate rock categories on the *x*-axis. Ankerite-Albite zone values for interiors of metacarbonate layers and for vein selvages plotted separately, but are statistically indistinguishable for parts A-C. (A) Si. (B) Al. (C) Ca. (D) Fe. Ank-Ab zone vein selvages (large open circle) and layer interiors (small open circle) are significantly different and are thus distinguished. Fe mass change percentage based on average Ank-Ab zone layer interior. Note Fe added to Ank-Ab vein selvages (fig. 6), and general progressive Fe gain with increasing metamorphic grade and fluid-rock interaction.

associated with theoretical fluid speciation calculations. Recent experiments indicate total Al concentrations of $\sim 10^{-3}$ molal in H_2O coexisting with kyanite and quartz at 500° to 600°C and 8 to 10 kb (Manning, 1999, 2001). Thus, if all Al was deposited into the rock along the advancing front, and if the concentration of Al in fluids equilibrated with the metacarbonate rock was zero, the *maximum* ΔC_{Al} was ~1 mole m^{-3}. This is a maximum value because fluid in the metacarbonate rocks must have contained some Al. For a ΔC_{Al} of 1 mole m^{-3} and a typical mass addition value of 10 g Al per 100 g rock (M_{Al} ~5500 moles Al m^{-3}), the *minimum* calculated flux is $\sim 6 \times 10^4$ m^3 (fluid) m^{-2} (rock) for 10 meter long veins. Similar fluxes must have been required to form Al-rich calc-silicate rocks by layer-parallel flow along fractured lithologic contacts for those cases where little or no Al depletion is evident in adjacent metaclastic rocks (fig. 9A and B). It is important to emphasize that these fluxes are *minimums* because of the neglect of diffusion, the use of a maximum value for ΔC_{Al}, and because kinetic departures from local equilibrium have been ignored. Fluxes of $\sim 10^5$ m^3 m^{-3} are compatible with the independently estimated value of 2.8×10^5 m^3 m^{-3} for veins cutting amphibolite facies metaclastic rocks of the Wepawaug Schist (Ague, 1994b).

Mobility of REE, P, Y, Th, and U

This study indicates that significant REE mobility may occur during regional metamorphism, contrary to most conventional interpretations. Examples from the Ankerite-Albite, Biotite, and Amphibole zones show metasomatic enrichment in the heavy REE (HREE) along contacts and in vein selvages (figs. 4, 5, 6A, 7, 8A, 9E, and 10C). These are accompanied by enrichments in Y and, in most cases, P. In one case, enrichment was sufficient to stabilize xenotime (JAW-197; figs. 5 and 6A). The Diopside-II zone example is different and indicates gain of light to mid-REE combined with a deepening Eu "anomaly" as a quartz vein is approached; Y and P were also added (figs. 16, 17A, and 17B).

Several comments regarding REE behavior can be made based on the available data, although much work remains. First, fluids rich in CO_2, H_2S, and/or halogens have been postulated as transport agents for REE (for example, Grauch, 1989; Gieré and Williams, 1992; Pan and Fleet, 1996), but these were not required for the Wepawaug metacarbonate rocks. Mole fractions of CO_2 were generally low (mostly ~0.01 to ~0.15; Ague, 2002), and are uncorrelated with the nature and extent of the metasomatism. Furthermore, the compositions of micas and amphiboles preclude very halogen-rich fluids (Ague, 1994b, 2002). Second, the association of REE mobility with P and Y addition suggests that the added REE were transported by P and Y complexes and then sequestered largely into phosphate minerals including apatite, monazite, and xenotime (compare Gieré and Williams, 1992). Clinozoisite/zoisite may also host some of the added REE. It is tempting to speculate that the fluids that mobilized and removed P from the surrounding metapelitic rocks during progressive metamorphism were the source of the P deposited in the metacarbonate layers (Ague, 1994a), although "magmatic" fluids may also have played a role. Third, plagioclase is implicated in the mass transfer for the Diopside-II zone profile because it preferentially takes up Eu and excludes the surrounding REE like Sm (compare Hess, 1989), and because it is present in veins near the profile. One scenario is that fluids precipitated plagioclase along flow paths through fractures, becoming progressively depleted in Eu and enriched in the surrounding REE. This characteristic REE pattern was then imprinted on the calc-silicates during fluid infiltration. Fluids derived from or equilibrated with magmatic rocks are inferred to have been important for producing at least some of the Diopside zone mineral assemblages (Palin, ms, 1992; van Haren and others, 1996); the characteristic pattern of REE metasomatism may be a tracer for these fluids.

Th appears to have been essentially immobile, but U was added to several examples including the Diopside-II zone profile (fig. 17B). The general immobility of

Th relative to U in fluids has been inferred for other metamorphic settings, particularly subduction zones (Hawkesworth and others, 1997; Johnson and Plank, 1999).

PROCESSES OF INFILTRATION

Geochemical profiles were modeled using reaction-transport theory to determine processes of fluid infiltration and rates of reaction. A large number of profiles could be studied given the amount of data collected herein; this section focuses on six well-defined examples that provide rigorous controls on infiltration. The JAW-163 profile is not examined because the sample spacing is too coarse for resolving process.

One-dimensional (1-D) tracer transport by advection, diffusion, and mechanical dispersion coupled to linear kinetic fluid-rock exchange in a fully saturated porous medium with constant porosity, pore fluid velocity, and hydrodynamic dispersion coefficient is given by:

$$\frac{\partial C_i}{\partial t} = -v_x \frac{\partial C_i}{\partial x} + D_{HD,i} \frac{\partial^2 C_i}{\partial x^2} + \kappa \frac{1-\phi}{\phi} \left(C_i^{Solid} - \frac{C_i}{K_v} \right), \tag{7}$$

in which C_i is the concentration of species i in the fluid (moles m^{-3}), t is time, v_x is the pore fluid velocity, $D_{HD,i}$ is the hydrodynamic dispersion coefficient incorporating the effects of diffusion through the pore fluid, tortuosity, and mechanical dispersion, ϕ is porosity, C_i^{Solid} is the concentration of i in the solid, κ is a reaction rate constant, and K_v is the equilibrium fluid/solid distribution coefficient by volume. Diffusion and mechanical dispersion are collectively termed "hydrodynamic dispersion" (Bear, 1988). For equation (7), variations in the composition of the solid change the composition of the fluid in equilibrium with the solid as governed by K_v. This type of treatment is widely used for isotopic tracers including Sr and O (Bickle, 1992; Baxter and DePaolo, 2002), but is also appropriate for trace elements like Sr in metacarbonate rocks. The change in concentration for the solid is:

$$\frac{\partial C_i^{Solid}}{\partial t} = -\kappa \left(C_i^{Solid} - \frac{C_i}{K_v} \right). \tag{8}$$

A different, equally widely used treatment is required when the composition of the equilibrium fluid does not necessarily change as the composition of the solid changes:

$$\frac{\partial C_i}{\partial t} = -v_x \frac{\partial C_i}{\partial x} + D_{HD,i} \frac{\partial^2 C_i}{\partial x^2} + \kappa (C_i^{eq} - C_i), \tag{9}$$

in which C_i^{eq} is the concentration of i in equilibrium with the initial solids in the flow domain. The concentration of i in the solid, C_i^{Solid}, is given by:

$$\frac{\partial C_i^{Solid}}{\partial t} = -\kappa \frac{\phi}{1-\phi} (C_i^{eq} - C_i). \tag{10}$$

For example, consider the dissolution of quartz from a rock at constant pressure and temperature; the silica content of the rock decreases with time but the equilibrium aqueous silica concentration in the fluid is invariant. Equations (7) through (10) were solved numerically following Ague (1998, 2000) using "pinned" (fixed value) boundary conditions and initial step-functions in composition at metacarbonate-schist or metacarbonate-vein boundaries. Boundary values were adjusted to optimize the fit of each model profile to the data using an iterative process to minimize chi-square (Press and others, 1992, Chapter 15). Porosity was assumed small (<0.01) and constant for each profile; the interpretations are robust unless porosity underwent large spatial and/or temporal variations (see below). Volume changes for the regions fit by the equations were relatively small and neglected in the modeling.

Ank-Ab Zone Lithologic Contacts; JAW-168 Profile

Fluids equilibrated with carbonate-free metapelitic rock will have relatively low Sr concentrations and thus tend to strip Sr from metacarbonate layers during infiltration. The shape of the Sr profile from the lithologic contact at 0 centimeters to the interior of the layer at ~60 centimeters has the classic shape of an advective reaction front (fig. 23A; see Bickle, 1992). Pure advection would produce a step function-like front; the observed front broadening could be due to sluggish reaction kinetics ("kinetic dispersion") and/or hydrodynamic dispersion. The former possibility could not produce the steep drop in Sr content near the contact at ~70 centimeters, so it is concluded that hydrodynamic dispersion was important. The profile is well fit using equations (7) and (8) assuming local fluid-rock equilibrium (large κ; Bickle, 1992). Note that the precise values of the Sr/Zr ratios are not critical, only the shape of the profile that is fit. The broad front extending from the contact at 0 centimeters into the layer was the result of cross-layer advection from surrounding metapelite into the metacarbonate layer coupled with hydrodynamic dispersion. The drop in Sr at ~70 centimeters was due to hydrodynamic dispersion of Sr from the metacarbonate layer into the metapelite which locally dominated the advection.

The outcrop lies on the westward-dipping, eastern limb of the regional Wepawaug Syncline (Fritts, 1963, 1965a, 1965b; Dieterich, ms, 1968). The contact at 0 centimeters is stratigraphically the lower contact of the layer, so the cross-layer component of advective flow was broadly "upward". A likely possibility is that most of the fluid flow was layer parallel, but that buoyancy drove a component upward into the bottom of the layer. The time-integrated fluid flux for this upward component is approximated by L/K_ν, but K_ν for Sr is poorly known (Bickle, 1992). For example, the preferred values of Evans and others (2002) range from ~0.17 to ~0.0017. The corresponding time-integrated fluid fluxes range from ~2 to ~200 $m^3\ m^{-2}$ for the front propagation distance L = 0.4 m. Oxygen isotopic compositions of carbonate minerals within greenschist facies metacarbonate layers were nearly completely equilibrated with surrounding metapelitic rocks (Palin, ms, 1992), in contrast to the partial equilibration of Sr. Alteration of oxygen isotopic systematics will, in general, occur over longer length scales than Sr because the K_ν for O (~0.6) is larger than that for Sr (Evans and others, 2002).

Equations (7) and (8) would be inapplicable if K_ν varied due to, for example, large gradients in fluid salinity. Biotite compositions indicate that f_{HCl}/f_{H_2O} was, on average, ~1.6 times greater in silica-depleted metapelites adjacent to veins than in rocks far-removed from veins (Ague, 1994b). Analyses of micas and amphiboles in the metacarbonate rocks reveal no systematic variations in halogen content (Ague, 2002). While some level of salinity variation cannot be ruled out, large spatial or temporal variations in salinity (or other factors, including porosity) would almost certainly produce geochemical profiles with more complex shapes than observed, making it extremely unlikely that equations (7) and (8) could be used to fit the data.

Ank-Ab Zone Vein Selvage; JAW-197 Profile

Muscovite destruction and K release was nearly complete in and around the vein; only small relic crystals remain enclosed in quartz or carbonate minerals. Equations (9) and (10) are appropriate for modeling the K release, and indicate that hydrodynamic dispersion can account completely for the mass transfer (fig. 23B). The simplest explanation is that fluid flowed through the vein, and that mass exchange to and from the vein occurred by diffusion along the X direction. Profile shapes for other elements indicate similar behavior (fig. 5). Some component of advection along X is not ruled out by the modeling for this and the following profiles, but is not required by the data. Note that volume increased in the region occupied by the vein and the zone of near

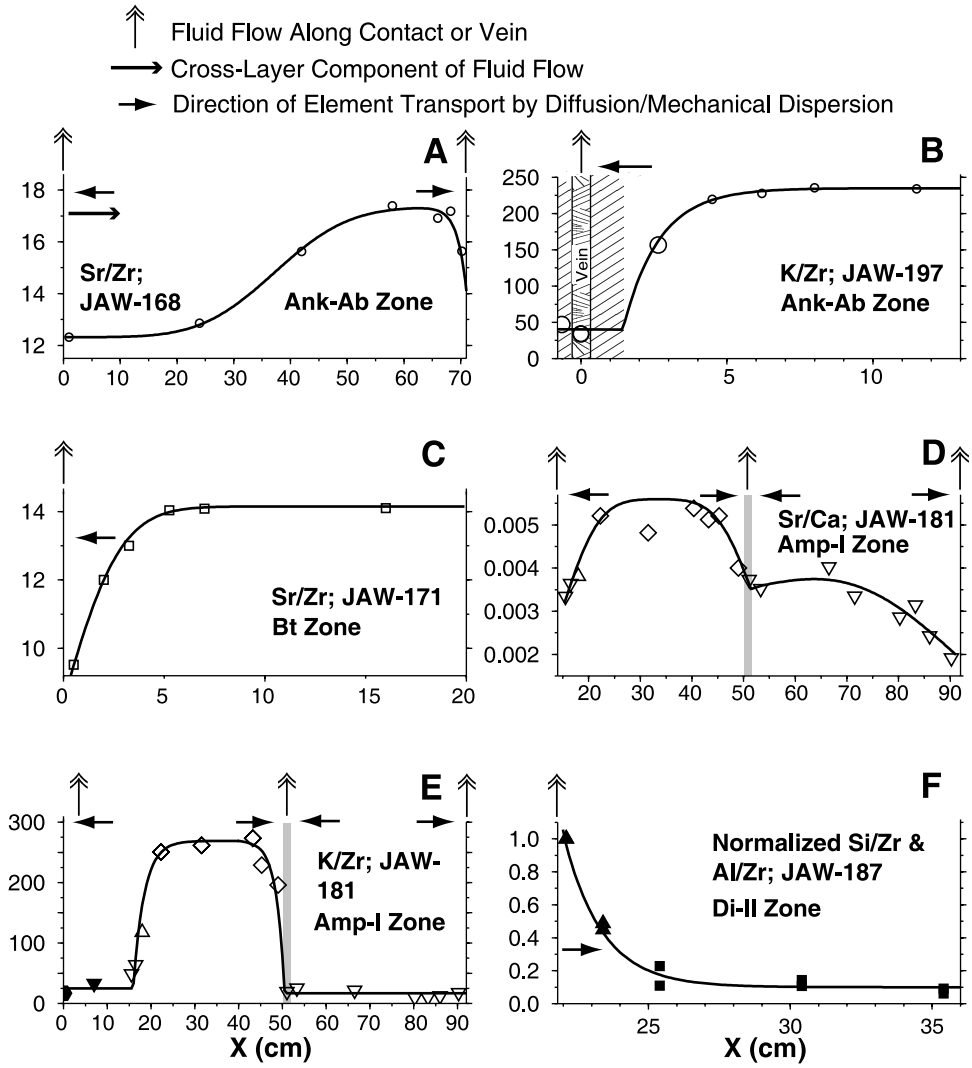

Fig. 23. Results of reaction-transport modeling. Model curves denoted by heavy black lines. (A) Sr/Zr profile across Ankerite-Albite zone layer. Lithologic contacts with metapelitic schists at 0 and 71 cm. (B) K/Zr profile, Ankerite-Albite zone vein and selvage. Zone of near complete muscovite destruction in selvage denoted by diagonal rule. (C) Sr/Zr profile across Biotite zone layer. Lithologic contact with metapelitic schist at 0 cm. (D) Sr/Ca profile across Amphibole-I zone metacarbonate. Inferred internal contact between two lithologically distinct metacarbonate horizons denoted by vertical gray line. Contacts with calc-silicate rocks on layer margins at ~15 cm and ~92 cm. Anomalous data point at ~30 cm was possibly affected by weathering/retrogression and was not included in fit. (E) K/Zr profile for same layer as in part (D), above. Two samples not shown and not included in fit; one contains a tiny K-feldspar-bearing veinlet of probable retrograde origin (at ~72 cm), and the other is near the selvage of a quartz vein and is inferred to have lost K to vein-forming fluids (~40 cm; fig. 2). (F) Normalized Si/Zr and Al/Zr profiles for part of Diopside-II zone profile. Si/Zr and Al/Zr normalized by scaling their maximum values to unity.

complete muscovite destruction in the selvage (see below), but volume changes outside this region were much smaller, allowing use of equations (9) and (10).

Bt Zone Contact; JAW-171 Profile

The Sr profile can be fit using local equilibrium transport by hydrodynamic dispersion (fig. 23C; eqs 7 and 8). Fluid flow probably occurred largely in the

surrounding schists parallel to layering, and cross-layer mass transfer occurred by hydrodynamic dispersion. The zone of Sr depletion corresponds to the zone of maximum biotite production, demonstrating that the fluid infiltration was coupled to reactions that produced biotite (fig. 7).

Amp-I Zone Contacts; JAW-181 Profile

This bed comprises a sequence of thinner layers containing varying fractions of carbonate and silicate minerals, so Sr/Zr is somewhat heterogeneous. In an effort to reduce the impact of these variations, the Sr/Ca ratio was used under the assumption that the Sr content of the carbonate fraction was initially uniform and that Ca within the metacarbonate bed (not including calc-silicates) was immobile. The profile is asymmetrical, so it was modeled in two parts, the first extending from 15 to 51 centimeters, and the second from 51 centimeters to 90 centimeters (fig. 23D). For the modeling, the two parts share a common boundary condition at 51 centimeters. The hypothesis that the first part of the profile initially had a much larger Sr content than the second can be rejected because for this case Sr/Ca should decrease smoothly from the first part to the second around 50 centimeters. Assuming that the entire bed initially had uniform Sr/Ca, both parts of the profile can be fit well using equations (7) and (8) for transport by hydrodynamic dispersion assuming local chemical equilibrium. The second part of the profile (from ~50 to ~90 cm) was more extensively modified than the first, requiring a larger effective hydrodynamic dispersion coefficient and/or a longer timescale of infiltration. A likely explanation for the asymmetric profile across the bed is that the area around ~50 centimeters represents an internal contact of somewhat elevated permeability between two slightly different metacarbonate horizons. In the field, the interval ~50 to 90 centimeters is weathered farther back into the outcrop than ~15 to 50 centimeters, attesting to a physical difference between the two horizons. External fluids flowed parallel to the layering at the edges of the profile and along the internal contact at ~50 centimeters; Sr was stripped out by cross-layer diffusion/mechanical dispersion toward these areas.

The K/Zr profile was fit in two parts (15 - 30 cm and 30 - 51 cm) using equations (9) and (10) assuming transport by hydrodynamic dispersion (fig. 23E). The profile from ~15 to ~50 centimeters is relatively symmetrical and indicates strong K removal due to biotite destruction between 15 and 20 centimeters and between 40 and 50 centimeters. The profile from ~50 to ~ 90 centimeters has been nearly stripped of K; what little remains is sequestered mostly in amphibole and a few small relic biotite grains. The K systematics are consistent with those inferred for Sr, although reaction from ~50 to ~90 centimeters in the K profile has gone essentially to completion.

Diopside-II Zone; JAW-187 Profile

The profile between quartz vein 2 and ~20 centimeters contains small, layer-parallel quartz veinlets (fig. 15) and is poorly fit by 1-D transport theory. However, geochemical profiles for samples beyond 20 centimeters generally show more smoothly varying behavior. Strong metasomatic signals were produced by the Al added to make zoisite and the Si added to make diopside and, to a lesser degree zoisite. The Si/Zr and Al/Zr profiles are well fit by equations (9) and (10) using pure hydrodynamic dispersion transport (fig. 23F). Fluid probably flowed parallel to layering along the veins and veinlets at $X < \sim 20$ centimeters such that metasomatic diffusion haloes developed around them to varying degrees. Beyond ~20 centimeters, the strong advection ceased and transport of Si and Al away from the veined area was dominated by diffusion. The region between ~20 and ~25 centimeters can thus be viewed as a type of "alteration selvage" that developed adjacent to a complex of veins and veinlets.

Comments on Reaction Kinetics

The distance over which the infiltrating fluid was out of equilibrium with the rock (Δx) can be used to place constraints on reaction rates for the major element metasomatism examples (K, Al, Si; fig. 23). For simple dissolution or precipitation reactions and hydrodynamic dispersion transport, Δx for 95 percent approach to equilibrium is approximated by (Lasaga and Rye, 1993):

$$\Delta x \approx \sqrt{\frac{9D_{HD,i}}{\kappa}}. \tag{11}$$

For example, for the K/Zr profile in figure 23B, the region between ~0 and 1.5 centimeters had equilibrated with the external fluid flowing along the fracture, whereas fluid was equilibrated with the rock beyond ~6 centimeters. Thus, Δx is ~4.5 centimeters. The maximum observed Δx is ~10 centimeters (fig. 23E). Assuming transport only by diffusion using a diffusion coefficient of 10^{-8} m^2 s^{-1} and a conservatively small tortuosity of 0.1 ($D_{HD,i}$ = 10^{-9} m^2 s^{-1}; Ague, 1998, 2000, 2002), yields estimates for κ that range over a factor of 5 from 28 yr^{-1} to 140 yr^{-1}. These values are ~50 to ~240 times greater than the representative metamorphic rate of 0.585 yr^{-1} used by Lasaga and Rye (1993), and indicate a fairly close approach to local fluid-rock equilibrium. Note that these are minimum rates because the effects of mechanical dispersion, which could increase $D_{HD,i}$ by factors of 10 or more, have not been considered. The large rates derived for the major elements are consistent with the large, local equilibrium rates needed to fit the Sr profiles.

Kinetic behavior varied widely in the reaction zones. Reactions that involved phases that already existed in the rock proceeded relatively rapidly. Examples include the dissolution of muscovite (fig. 23B), dissolution of biotite (fig. 23E), precipitation of diopside and zoisite (fig. 23F), and local exchange of the trace element Sr between carbonate minerals and fluid (fig. 23A, C, and D). Metamorphic reaction rates are proportional to the rate constant, the mineral surface area available for reaction, and the departure from equilibrium in the system (Lasaga and Rye, 1993). One strong possibility is that infiltration of external fluids that were to some degree out of local equilibrium with the metacarbonate rocks resulted in significant departures from equilibrium, driving the fast kinetics. On the other hand, precipitation reactions that should have formed K-feldspar rarely did so. The destruction of biotite, loss of K and, by inference, the growth of amphibole proceeded at rates that were rapid relative to mass transfer, whereas the precipitation of the product K-feldspar was slow relative to mass transfer for the model profile (fig. 23E). K-feldspar may rarely have reached saturation due to widespread infiltration of fluids from surrounding rock types undersaturated with respect to it (fig. 21A). Another possibility is that activation energy barriers to nucleation were prohibitive and, thus, product K-feldspar nuclei failed to form (see Rubie, 1998). The general lack of K-feldspar across the Amphibole and Diopside zones indicates that K-feldspar precipitation was hindered at the regional scale.

Mass Transfer Processes

The increases in metasomatic mass transfer toward contacts and veins demonstrate the importance of hydrodynamic dispersion along gradients in fluid composition at high angles to layering and in alteration selvages, consistent with the results of reaction-transport modeling (figs. 23 and 24). Furthermore, the regular sequences of mineral assemblages observed at lithologic contacts and in vein selvages (fig. 2) are classic indicators of hydrodynamic-dispersion mass transfer (Vidale, 1969; Hewitt, 1973; Vidale and Hewitt, 1973; Joesten, 1974; Thompson, 1975; Brady 1977; Ashworth and Sheplev, 1997; Abart and others, 2001). This dispersion is inferred to have had a large component of diffusion through fluid-filled pore space, although mechanical

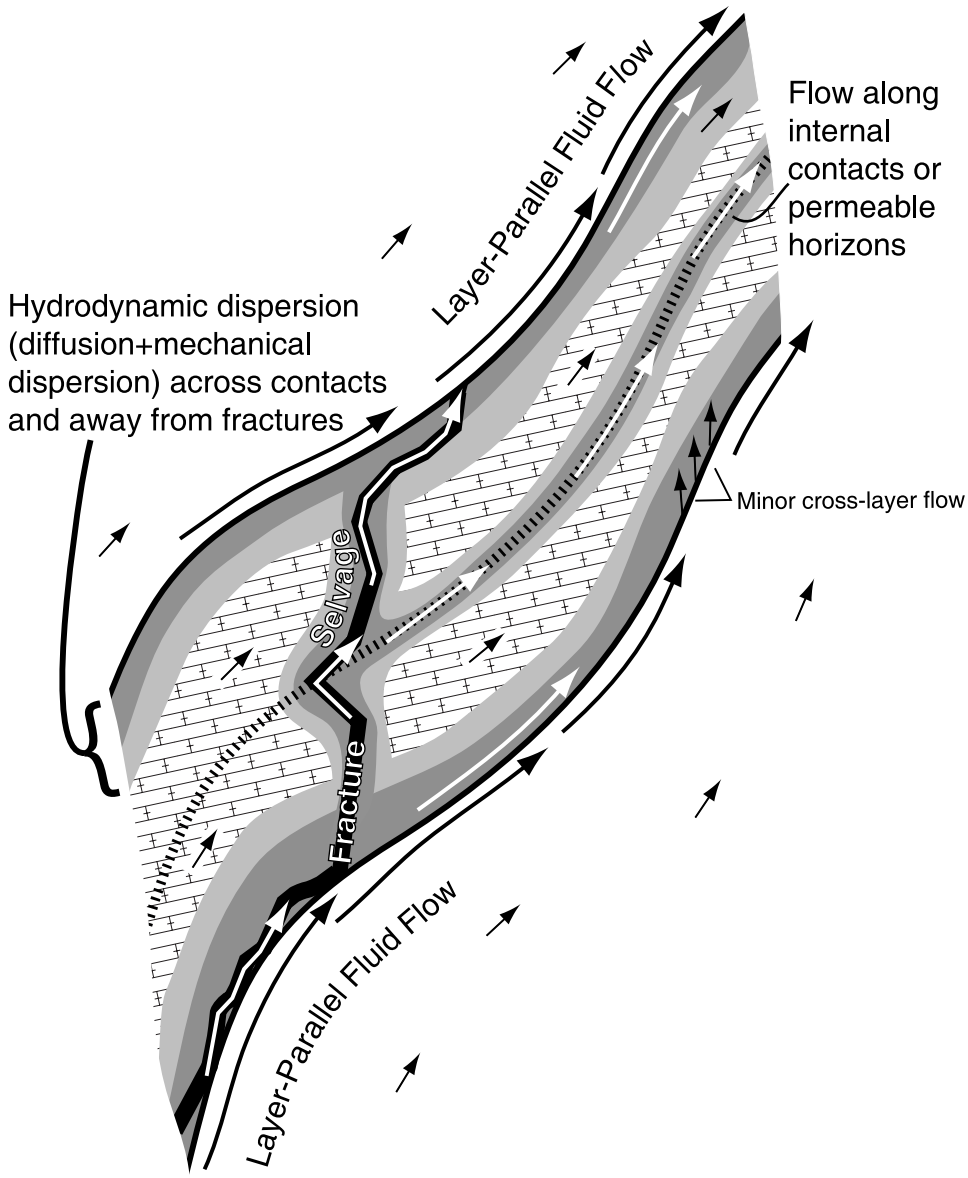

Fig. 24. Schematic cross-section of metacarbonate layer illustrating infiltration processes. Flow mostly layer-parallel or through fractures. Flow concentrated along lithologic contacts and through fractures and permeable horizons. Arrow size qualitatively proportional to fluid flux. Hydrodynamic dispersion (diffusion and mechanical dispersion) occurred at high angles to flow. Largest amounts of fluid-rock reaction and metasomatism denoted by dark gray shading; lesser amounts by lighter gray shading. Metasomatic effects envisioned to have propagated into the metacarbonate layer: 1) inward from its margins and 2) away from fractures or permeable horizons; hydrodynamic dispersion was important in either case.

dispersion may have also been considerable (Ague and Rye, 1999; Ague, 2000, 2002). The reaction-transport modeling indicates limited cross-layer advection, so most of the regional fluid flow must have occurred parallel to layering or through fractures, consistent with a number of earlier studies of Acadian metamorphism in New England (fig. 24) (Hewitt, 1973; Tracy and others, 1983; Palin, ms, 1992; Ague, 1994b; Ferry,

1994; Ague, 2000) and other metamorphic belts (see Rye and others, 1976; Bickle and Baker, 1990).

Two lines of evidence indicate that a considerable component of the layer-parallel flow was concentrated along metaclastic-metacarbonate rock contacts, and internal contacts separating metacarbonate horizons with differing properties (such as grain size and mineralogy) within individual metacarbonate layers (fig. 24). (I) Local source-sink relationships: At some localities, exchange of elements like Al and Ca across lithologic contacts clearly indicates a degree of local communication between metacarbonate and metaclastic rocks (figs. 11 and 14). However, some elements that were lost from the metacarbonates, particularly K, have no obvious enrichment "haloes" in surrounding metaclastic rocks. Moreover, local depletions of Al and Si from metaclastic rocks at contacts were insufficient to produce the observed volumes of calc-silicates for the examples studied herein (figs. 9 and 11). Elements that lack local source-sink relationships must have been transported into/out of the local rock mass by advection-dominated mass transfer along contacts. This advection was coupled to hydrodynamic dispersion that transported the elements to and from the contacts at high angles to the flow direction. (II) Fractures: Lithologic contacts and calc-silicate rocks at lithologic contacts were commonly loci for considerable quartz veining. Metacarbonate and metaclastic rocks have different physical properties, so contacts between them are likely to be areas of mechanical weakness, in some cases related to elevated fluid pressures during reaction (Walther, 1996). Fracturing at lithologic contacts increased porosity and permeability (see Ague, 1995), so highly veined contacts were probably sites of elevated fluid flux relative to more "pervasive" flow through unfractured rock matrix (Breeding and others, 2003). In addition, reactions driven by fluids infiltrating along contacts may have increased rock porosity and permeability at the grain scale and focused layer-parallel flow into the contact areas (compare Balashov and Yardley, 1998).

Most veins that cross-cut metacarbonate layers are surrounded by reaction selvages whose mineral assemblage zonation mirrors that found at lithologic contacts. Advective fluid flow transported the chemical "signature" of the surrounding rock types into the metacarbonate layers along the cracks and in the immediately adjacent wallrock (fig. 24). Hydrodynamic dispersion at high angles to the crack walls operated to transport mass to and from fractures and form the altered selvages.

Next to some veins, quartz, calcite, feldspar, titanite, and/or rutile were removed from the wallrock and deposited in the adjacent vein (figs. 8B and 13D). This local (cm scale) transport or "segregation" is inferred to have occurred by processes dominated by diffusion (for example, "pressure solution"; Ague, 1997b, 2003), and did not necessarily require large fluid fluxes.

Implications for metamorphic volatile release

Volatile mass losses for biotite-, amphibole ± biotite-, and diopside-bearing assemblages in metacarbonate rocks average –11 percent, –23 percent, and –49 percent, respectively (fig. 25; app. D). The –35 to –70 percent range for the diopside-bearing rocks (fig. 25) mainly reflects variations in the total amount of volatiles a given bulk composition could release, rather than large variations in reaction progress.

The regional contour map clearly indicates a maximum in volatile loss centered on the Diopside zones (fig. 26). The southeastern margin of the Diopside zones is the one best constrained by high sampling density, is clearly marked by a strong, 0.5 to 1 kilometer wide increase in volatile loss to the northwest, and runs parallel to the regional northeast-southwest strike of layering. Thermobarometry (Ague, 2002) indicates that the exposed Diopside zones formed at depths increasing from 30 kilometers in the southeast to 35 kilometers in the northwest. This result and the map pattern of volatile loss suggest that the Diopside zones occupy a roughly cylindrical region, elongated northeast-southwest, that was at least 5 kilometers thick during metamor-

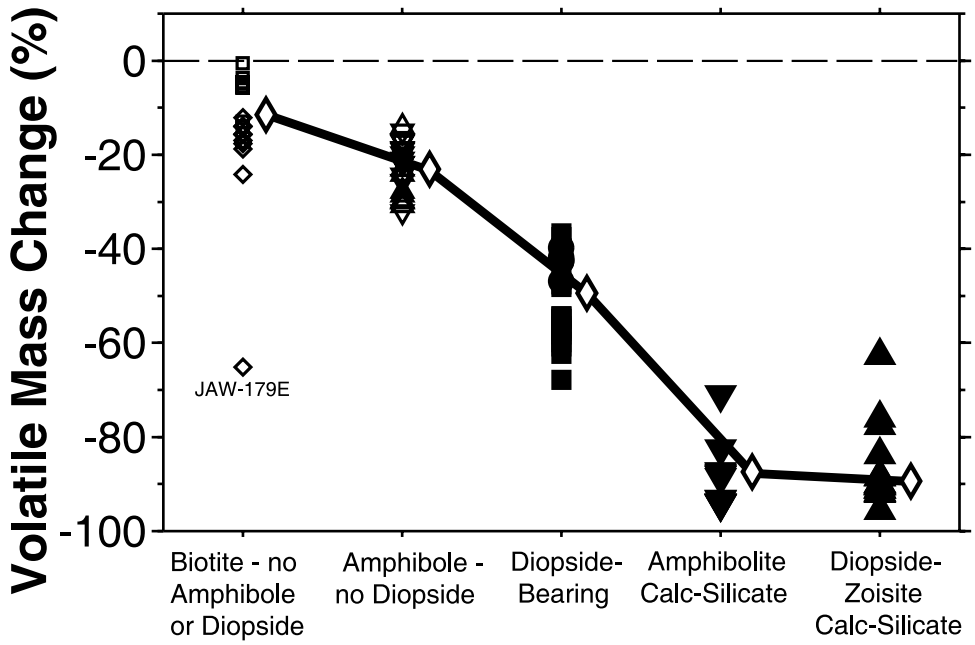

Fig. 25. Volatile mass changes (dominantly CO_2 loss) (see apps. B, C, and D). Mean values $\pm 2\sigma$ denoted by open diamonds. Note progressive volatile depletion for biotite-bearing, amphibole-bearing, and diopside-bearing metacarbonate rocks. Extreme volatile depletions near -90 % observed for calc-silicate rocks derived from metacarbonate precursors. JAW-179E is a selvage that lost CO_2 via local transport of calcite to adjacent vein.

phism. Foliation and lithologic layering are subvertical or dip steeply to the southeast across the Diopside zones (Fritts, 1965a; Dieterich, ms, 1968). Consequently, fluid flow up through the Diopside zones that was mostly layer-parallel would have had a limited northwest-southeast cross-layer component. The steep gradient in volatile loss across the southeastern margin of the zones thus probably reflects a considerable southeastward decrease in the layer-parallel flux of diopside-forming fluids, rather than cross-layer flow to the southeast.

Volatile mass changes for calc-silicates derived from metacarbonate rocks are extreme—mostly between −80 and −95 percent (fig. 25)—and have considerable implications for mass transfer because calc-silicate rocks often make up a significant fraction of the layers at medium and high metamorphic grades. For example, the maximum thickness of the Di-II zone JAW-187 layer is 0.8 meters; 0.3 meters of this is amphibolite and diopside-zoisite calc-silicate rock on the margins of the layer. The metacarbonate interior lost ~50 percent of its volatile mass, whereas the calc-silicates lost ~90 percent (app. D). A simple mass balance calculation shows that the ~38 volume percent of calc-silicate rock released roughly the same amount of volatiles as the ~62 percent of metacarbonate rock. Furthermore, as noted above, some metacarbonate layers in the amphibolite facies were converted entirely to calc-silicate rock. Consequently, studies of mass transfer and devolatilization that neglect calc-silicates will underestimate the CO_2 produced from metamorphic belts.

Coupled transport of H_2O into, and CO_2 out of, metacarbonate layers across contacts or in vein selvages by hydrodynamic dispersion is a powerful means to drive devolatilization reactions during prograde heating (Hewitt, 1973; Ague and Rye, 1999; Ague, 2000, 2002). The coupled transport was sufficient to drive the simultaneous devolatilization of metacarbonate rocks and surrounding schists in a regional flow field

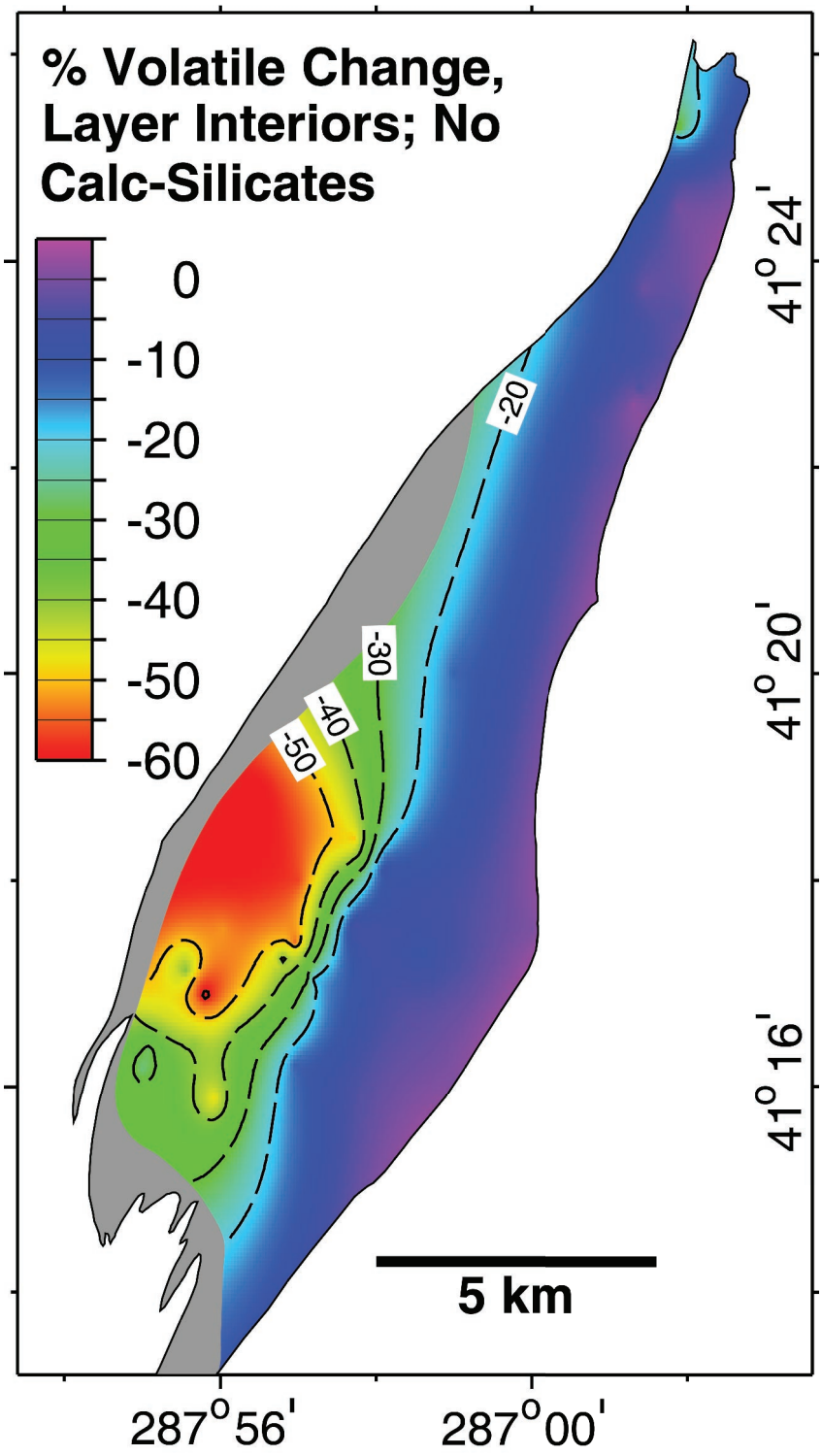

Fig. 26. Regional contour map of percentage volatile mass changes for interiors of metacarbonate layers (excludes calc-silicates). Gray shading denotes area where contours are very uncertain due to limited data coverage. Large volatile mass losses in excess of about -35 % centered on Diopside zones.

in which fluids were ascending and cooling along layering (Ague and Rye, 1999; Ague 2000). The onset of prograde reaction marked by biotite or, more rarely, oligoclase growth in the metacarbonate rocks coincides spatially with the onset of prograde dehydration reactions that consumed muscovite and chlorite and produced garnet, biotite, and H_2O in metaclastic rocks (fig. 1). This relationship reinforces the hypothesis that CO_2 loss from metacarbonate rocks and dehydration of metaclastic rocks were linked and penecontemporaneous. Model calculations indicate that the amount of H_2O produced by the metaclastic rocks was adequate to drive such CO_2 loss (Ague and Rye, 1999). Fluid composition gradients between metacarbonate layers and more water-rich fluids in cracks or adjacent metaclastic schists could have been very small yet still driven the devolatilization (Ague, 2000, 2002). Pervasive infiltration of relatively low X_{CO_2} (mole fraction CO_2) fluids by fluid flow along layers may also have driven devolatilization, but the importance of this process remains to be quantified (see figs. 1, 2C, 10, and 11 in Ague and Rye, 1999). Much of the reactive fluid that infiltrated the metacarbonate rocks was derived from dehydrating metaclastic rocks but, in the Diopside zones, oxygen isotope data indicate that fluids released from or equilibrated with igneous/metaigneous rocks were also probably important (Palin, ms, 1992; van Haren and others, 1996; Ague, 2002).

CHANGES IN ROCK VOLUME

Metasomatic reactions produced significant changes in rock volume ($\varepsilon_{\rho m}$; table D1). Relative to Ank-Ab zone protoliths, the interiors of metacarbonate beds became denser and lost volume progressively with increasing metamorphic grade, reaching -20 to -30 percent volume loss in the Di-II zone (fig. 27). Volume was lost due to increases in average mineral density (fig. 27A) and loss of volatiles (fig. 25). Volume-reducing reactions may have transiently increased rock porosity and permeability, facilitating increased infiltration and mass transfer (compare Balashov and Yardley, 1998; Bolton and others, 1999).

Calc-silicates are the densest rocks and underwent the most extreme devolatilization (fig. 27). However, $\varepsilon_{\rho m}$ spans a wide range because of variable metasomatic mass additions of Si, Al, and other constituents. Calc-silicates containing abundant quartz veins or veinlets exhibit the smallest volume losses (0 to -10 %) due mostly to mass additions of silica (quartz) and Al (in zoisite or clinozoisite) that offset losses of Ca and volatiles to varying degrees.

Volume gains are less common for the metacarbonates, but were possible if veins added large amounts of mass to the rock. For example, an Ank-Ab vein+selvage (JAW-197Ai; fig. 6) underwent +19 percent volume gain due to precipitation of carbonate minerals, quartz, and albite in and around the vein (fig. 27, table D1). Rock density was little affected by the alteration for this example, so density changes did not contribute significantly to the volume change. When assessing mass and volume changes, it is important to emphasize that $\varepsilon_{\rho m}$ values depend on the precursor to which the altered rock is compared. For example, relative to Ank-Ab zone protoliths, the veined JAW-187Oiv Di-Zo calc-silicate lost about –3 percent of its volume (table D1; Di-II zone). Relative to unveined Di-Zo metacarbonate from the interior of the JAW-187 layer, however, the sample gained ~+15 percent volume. This percentage is positive because the interior did not undergo vein mass addition, and because it has greater density and fewer volatiles than little metamorphosed Ank-Ab zone rocks.

Relative to the Ank-Ab zone precursor, the classic Wep-8b calc-silicate vein selvage has an $\varepsilon_{\rho m}$ of -27 percent (table D1). Relative to the adjacent hornblende-biotite metacarbonate rock (Wep-8a), the volume loss is around -20 percent. These volume losses, while significant, are considerably less than the -70 percent inferred by Tracy and others (1983).

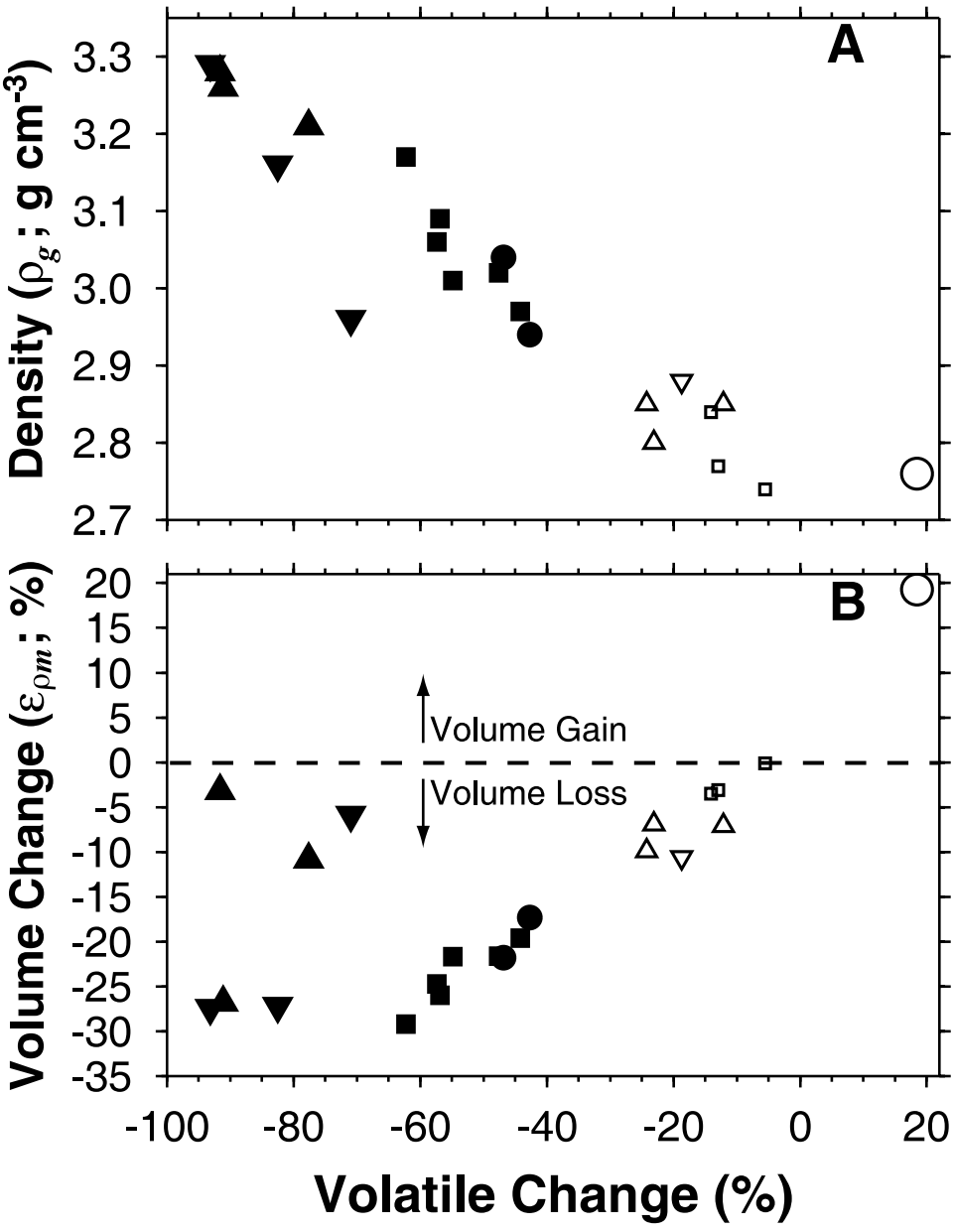

Fig. 27. Density and volume changes as functions of volatile mass change for representative samples. (A) Grain density (ρ_g; rock density on a porosity-free basis) versus volatile mass change (see fig. 25). Density generally increases with increasing devolatilization. (B) Volume change relative to Ank-Ab zone protoliths calculated using density and mass changes ($\varepsilon_{\rho m}$; table D1). Rocks that lost ~70 % or more of their volatiles are calc-silicates.

CONCLUSIONS

This study demonstrates that interaction of fluids derived from different rock types in lithologically heterogeneous settings is important for driving metasomatic and devolatilization reactions during metamorphism, and that diffusion and mechanical

dispersion must be considered when evaluating mineral reactions, fluid fluxes, and flow paths (compare Hewitt, 1973; Ague and Rye, 1999; Ague, 2000, 2002; Evans and others, 2002).

In the Ank-Ab and Bt zones, mass transfer of non-volatile elements was more limited than at higher grades, but was considerable in alteration selvages around veins and at some lithologic contacts. Mass transfer caused gains of Na, Y, heavy REE (HREE) and, in many cases, P and Fe. K, Rb, and Ba were generally lost, and Sr was lost except where calcite precipitated in and around calcite-rich veins. The Na gain and K loss resulted from reactions that destroyed muscovite and produced albite, and are consistent with metasomatism triggered by infiltration of fluids equilibrated with metaclastic rocks (fig. 19). Detailed study of a representative calcite-rich Ank-Ab zone vein (figs. 2, 5, and 6A) suggests that it was a conduit for cooling fluids ascending through the metasedimentary sequence.

At higher grades in the Amphibole and Diopside zones, calc-silicates formed at lithologic contacts and in vein selvages due in large part to major gains of Si, Al, and Fe, losses of volatiles and alkali and alkaline earth metals, and destruction of calcite (figs. 18, 22, and 24). K, Rb, and Ba were lost quantitatively when biotite broke down to make amphibole or diopside in calc-silicates and the calcite-rich interiors of the metacarbonate beds (fig. 18). The K-feldspar that should have formed as a result of these breakdown reactions is rarely present, reflecting transport of K (and Ba and Rb) down chemical potential gradients toward lithologic contacts or fractures that was rapid relative to K-feldspar precipitation. Similarly, the growth of clinozoisite/zoisite from plagioclase liberated Na. As was the case at lower grades, Y and P were generally gained, and HREE addition is evident in some outcrops. Enrichment of light REE, mid REE, Sr, and U was observed for a Di-II zone example in the highest grade part of the Formation.

Average prograde mass loss of volatiles from the interiors of the metacarbonate layers increases from -11 percent in the Biotite zone to -49 percent in the Diopside zones, relative to little reacted Ankerite-Albite zone protoliths (figs. 25 and 26). Furthermore, the open-system reactions that formed calc-silicate rocks in the Amphibole and Diopside zones led to massive volatile depletions averaging near -90 percent. Consequently, studies of CO_2 release from mountain belts should carefully consider calc-silicate rocks to avoid underestimating devolatilization budgets. Metamorphism was generally accompanied by S loss; S was largely or completely removed from most calc-silicates and from the interiors of Di-II zone metacarbonate layers (compare Ferry, 1981; Ague and van Haren, 1996).

The interiors of metacarbonate beds progressively lost volume due to increases in average mineral density and losses of volatiles; volume losses reached -20 to -30 percent in the highest grade rocks (Di-II zone) relative to Ank-Ab zone protoliths (fig. 27). Volume losses for calc-silicates were highly variable, ranging from near zero to -30 percent, depending on the amount of externally-derived mass added in the form of veins and veinlets. Volume gains were less common, but were possible if very large local vein mass additions occurred, even in the Ank-Ab zone.

The bulk of the non-volatile element metasomatism occurred due to infiltration of external fluids; most of these were derived from dehydrating metaclastic rocks. The documented Na gains and K losses at lower grades, K and Na losses at higher grades, and progressive Fe gains should be useful for tracing infiltration of external fluids in other field areas. The region of heavily decarbonated Diopside zone rocks coincides spatially with scattered outcrops of felsic, syn-metamorphic igneous rocks. Within this region, oxygen is isotopically light in metacarbonate interiors, calc-silicates, and some quartz veins (Tracy and others, 1983; Palin, ms, 1992; van Haren and others, 1996), suggesting that fluids derived from or equilibrated with igneous rocks augmented the regional dehydration flux (Palin, ms, 1992; van Haren and others, 1996).

Fluid flow was mostly sub-parallel to foliations and lithologic layering, and through cracks found along contacts or cross-cutting the metacarbonate layers (fig. 24). Diffusion with some contribution from mechanical dispersion at high angles to fluid flow facilitated exchange of mass across lithologic contacts and in selvages around veins. Progressive biotite, amphibole, and diopside index mineral growth and associated mass transfer are envisioned to have propagated into the metacarbonate layers inward from lithologic contacts, away from veins, or along permeable horizons (fig. 24; see Hewitt, 1973; Ague and Rye, 1999). The permeability along layers and foliations was presumably greater than across them, so pervasive, cross-layer flow was not favored (compare Ferry, 1994; Ingebritsen and Manning, 1999). Lithologic contacts were zones of mechanical weakness that commonly fractured and were loci for large fluid fluxes and vein formation (fig. 24). Al mass balance for the Amphibole and Diopside zones indicates that time-integrated fluid fluxes as great as $\sim 10^5$ m^3 m^{-2} were channelized along: 1) large fractures with calc-silicate-bearing selvages and 2) heavily altered, calc-silicate-bearing lithologic contacts (eq 6). Pervasive flow along grain boundaries through the interiors of the metacarbonate beds is more difficult to quantify. Nonetheless, given the absence of metasomatic signatures indicative of pervasive flow along regional T and P gradients for non-volatile elements like Na and K, it is probable that any such fluxes must have been less than $\sim 10^4$ m^3 m^{-2} (Dipple and Ferry, 1992; Ague, 1997a).

Detailed geochemical profiles done across low-grade Ankerite-Albite zone rocks indicate that fluid flow was broadly "upward" and in a direction of decreasing temperature (JAW-168 and -197 profiles). These results, together with those for quartz veins in metapelitic rocks at higher grades (Ague, 1994b; van Haren and others, 1996), are consistent with regional upward-directed fluid expulsion from the metamorphic pile during prograde heating.

An important finding to emphasize is that a number of key elements that are often assumed to be immobile or nearly so, including Al and REE, underwent significant mass transfer. Al mass additions in some cases exceeding +250 percent were necessary to make amphibolite and diopside-zoisite calc-silicates. Fluids equilibrated with metaclastic rocks or igneous rocks have greater chemical potentials of Al species than metacarbonate layers and were the source of the Al. Zr and Th, on the other hand, were essentially immobile. Ti was also largely inert, but two examples indicate that it could be transported locally over centimeter length scales from wallrocks to adjacent veins (figs. 8B and 13D). REE were added to the metacarbonate rocks at a variety of metamorphic grades. REE addition was commonly accompanied by P and Y addition, suggesting that P and Y complexes transport REE and that phosphate minerals like apatite, monazite, and xenotime are major hosts for the REE. Other phases including clinozoisite/zoisite could also contain added REE, but detailed REE budgets remain to be determined. The P lost from metapelitic rocks with increasing metamorphic grade (Ague, 1994a) may have been the source for at least some of the P added to the metacarbonate layers. The discovery of significant REE mobility indicates that isotopic systems including La/Ce, Sm/Nd, and Lu/Hf may be valuable tracers of the sources and flow paths of metamorphic fluids.

ACKNOWLEDGMENTS

I thank E. W. Bolton, C. M. Breeding, C. J. Carson, J. M. Palin, D. M. Rye, J. L. M. van Haren, and B. A. Wing for discussions, J. M. Ferry, G. Markl, and B. W. D. Yardley for critical reviews, and D. R. MacPhee for laboratory assistance. Financial support from National Science Foundation grants EAR-9706638, EAR-9727134, and EAR-9810089, and Department of Energy grant DE-FG02-01ER15216 is gratefully acknowledged.

Appendix A

Methods

Chemical analyses of minerals were done on the JEOL-JXA-8600 electron microprobe at Yale University. These analyses are given in Ague (2002) unless otherwise noted. Rock density on a porosity-free basis (ρ_g) was measured using a Micromeretics gas pycnometer (Ague, 1994a). Bulk chemical analyses of rocks were done by X-ray Assay Laboratories, Don Mills, Ontario. The quality of this laboratory's chemical analyses has been evaluated previously (see Ague, 1994a). Major and minor elements were determined by XRF on fused disks, Rb, Sr, Zr, Nb, Ba (and Y in some samples) were determined by XRF on pressed powder pellets, and REE, U, Th, and the remainder of the Y determinations were done by ICP-MS. High precision Zr analyses are critical to the present study. For example, Zr determinations across the homogenous JAW-168 and JAW-171 layers vary by only ± 7 ppm and ± 3 ppm, respectively (±2σ sample standard deviation), far superior to the ca. ± 20-30 ppm obtained with older methods using fused disks.

Calculation of the speciation of Si-Al-Mg-Ca-Na-K-H-C-O-Cl fluids for the model Ank-Ab zone was done using standard methods (see Sverjensky, 1987; Ague, 1997a) and thermodynamic data from: 1) Berman (1991) for solids, as modified by Sverjensky and others, (1991); 2) Pokrovskii and Helgeson (1995) for Al species in the fluid and Shock and others (1997) for all other ions and aqueous complexes; and 3) Kerrick and Jacobs (1981) for fugacities and activities of CO_2 and H_2O. Total Cl molality was set to 1 molal consistent with mica compositions (Ague, 1994b). These calculations involve many difficult to quantify uncertainties, including use of aqueous species data beyond the recommended maximum P of 5 kb, and the behavior of aqueous species in CO_2-bearing fluids (it should be noted, however, that X_{CO_2} values for the model fluids, as well as those recorded by actual Ank-Ab zone rocks, are small, $<\sim 0.02$; see Ague, 2002). Thus, the calculations should be considered as approximations useful for elucidating general fluid infiltration processes. Ank-Ab zone calculations used the activity model of Furhman and Lindsley (1988) for plagioclase and a typical muscovite activity (0.65; Ague, 2002); all other solids were taken as pure. Considerable uncertainty surrounds anorthite activity in albitic plagioclase at Ank-Ab zone *P-T* conditions. However, the compositions of feldspar in the metaclastic rocks and the adjacent metacarbonate layers are nearly identical in the Ank-Ab zone, so anorthite activity is constant across the layers and large shifts in feldspar composition can be ruled out as a cause of the variations in fluid composition.

Appendix B

Modes, Balancing Reactions, and Volatile Mass Changes

Modes and balancing reactions.—Alteration reactions are invaluable for assessing open system processes, and must be balanced using reaction progress analysis based on quantitative mineral abundances (for example, Brimhall, 1979; Ferry, 1983b). The modal amounts of pyrite, pyrrhotite, and calcic amphibole were estimated in a few samples directly from thin sections using line integration (compare Brimhall, 1979). Molar calcite, ankerite, quartz, muscovite, albite, plagioclase, biotite, diopside, clinozoisite, zoisite, garnet, rutile, titanite, apatite, and, in most cases, pyrite, and amphibole were determined using mass balance expressions for Si, Ti, Al, Fe (all as Fe^{2+}), Mg, Ca, Na, K, and P, each with the form:

$$\sum_p w_{e,p} x_p = w_{e,r}, \tag{B.1}$$

in which $w_{e,p}$ is the weight percent of element e in mineral p, $w_{e,r}$ is the weight percent of e in the rock (app. E), and x_p is the mass fraction of mineral p in the rock (kg p per kg rock). Together, these form the linear matrix equation:

$$\mathbf{Wx} = \mathbf{w}, \tag{B.2}$$

in which the coefficient matrix **W** contains the elemental weight percents for minerals, the vector **w** contains the corresponding elemental weight percents for the rock, and **x** is the vector of mass fractions for the minerals. Dividing mineral mass fractions by molecular weights, then multiplying by 10^3, yields the mineral abundance vector **n** in terms of moles mineral per kilogram rock (table 3). The calculations used pure quartz, rutile, and F-apatite, and measured compositions for other phases (table 3). Apatite is the dominant phosphate in the Wepawaug; monatite and xenotime are also found in some rocks but were not considered. Small amounts of graphite and chalcopyrite were ignored.

Equation (B.2) was solved using least-squares methods based on the singular value matrix decomposition (Lawson and Hanson, 1974; Press and others, 1992). Solutions were constrained to be as consistent as possible with observed mineralogy using, for example, inequality constraints which insure that all mineral abundances are

positive, and equality constraints for those minerals whose modes were estimated from thin sections (compare Lawson and Hanson, 1974). Multiple correlation coefficients were >0.9998 for all solutions.

To obtain the balancing coefficients for solids, the moles per kilogram of the reactant minerals were subtracted from those of the products, accounting for any overall rock mass changes that accompanied reaction (see Ague, 1994b):

$$\mathbf{\Delta} = r\mathbf{n}' - \mathbf{n}^\circ, \tag{B.3}$$

in which $\mathbf{\Delta}$ is the vector of balancing coefficients and $\mathbf{n}'$ and $\mathbf{n}^\circ$ are the vectors of mineral abundances for the product and reactant rocks, respectively. The $\mathbf{\Delta}$ coefficients are thus relative to 1 kilogram of reactant rock. The mineral changes were converted to fluid-rock reactions by balancing with fluid species using mass and charge balance constraints. Because the precise fluid speciation was not determined, the "generic" species $Si(OH)_4$, $Ti(OH)_4$, $Al(OH)_3$, $FeCl_2$, $MgCl_2$, $MnCl_2$, $CaCl_2$, NaCl, KCl, HCl, H_2S, H_3PO_4, HF, H_2O, and CO_2 were used. Most reactions are slightly imbalanced because of roundoff errors, neglect of changes in redox state, and because some solid and fluid species with negligible stoichiometric coefficients were omitted for clarity.

If one stage of a geochemical alteration process is compared to the next one in the sequence, and the moles of reactants and products are linear functions of reaction progress, then equation (B.3) estimates the true stoichiometric coefficients for solids for the alteration reaction. On the other hand, if the beginning and end stages of reaction progress are compared directly, ignoring the details of the intermediate stages of reaction, then the overall mineralogical changes are represented accurately by equation (B.3), but the balancing coefficients ($\mathbf{\Delta}$) need not correspond to any of the individual reactions that actually occurred during the various stages of alteration. This latter case is referred to as an "overall mineralogical transformation" herein.

JAW-181DDiv-v has undergone some retrograde chloritization. To better estimate initial mineralogy, equation (B.2) was solved by: 1) assuming that chloritization was isochemical except for H_2O gain, 2) excluding chlorite as one of the phases in the rock, and 3) multiplying the right side of equation (B.2) by the value of the factor r (eq 2) that yields a mass fraction sum of 1 (see next section for additional discussion of r).

Estimates of volatile loss.—For the calcite-rich interiors of metacarbonate layers, it is possible to reconstruct the initial Ank-Ab zone mineralogy to estimate metamorphic volatile loss. Mineral assemblages and most mineral compositions vary little in the Ank-Ab zone. Ankerite compositions are dependent on bulk rock Mg/Fe, but can be predicted accurately (app. C). In most low-grade metacarbonate rocks far-removed from metasomatic zones such as vein selvages, nearly all of the bulk-rock Al_2O_3 is found in muscovite; albite contains the remainder (fig. 20). Consequently, other aluminous phases like paragonite were, with one exception, not considered (see below). Under the assumption that Al mobility was limited in the interiors of the metacarbonate layers, estimates of protolith muscovite contents can be made based on measured Al_2O_3 concentrations, irrespective of any metamorphic K mobility. Albite abundances in the protolith reconstructions are probably the least accurate because of Na mobility, but, with the exception of some lithologic contacts and vein selvages, albite was generally not abundant enough in Ank-Ab zone layers to affect strongly a given rock's overall volatile budget.

For each rock, a linear system similar to equation (B.2) was solved for the mass fractions of calcite, ankerite, quartz, muscovite, albite, rutile, and pyrite using the elements Si, Ti, Al, Fe (all Fe^{2+}), Mg, Ca, and Na. The calculations used representative mineral compositions for calcite, muscovite, and albite from thin section JAW-197A-2 (Ague, 2002), estimated ankerite compositions (app. C), and pure quartz, rutile, and pyrite. As devolatilization proceeds, the mass of volatiles in a rock decrease, which, in the absence of other mass changes, increases the weight percents of other elements (a form of "residual enrichment"; Ague, 1994a). Thus, equation (B.2) yields mineral mass fraction sums that exceed one because the concentrations of the elements are greater than they were in the protolith state. The vector of rock elemental weight percents, $\mathbf{w}$, needs to be multiplied by the ratio of each element in the protolith relative to the final composition. This ratio, r, is given by equation (2), and is also equivalent to:

$$r = \frac{1}{\sum_p x_p}. \tag{B.4}$$

Thus, the Ank-Ab zone mineral mass fractions ($\mathbf{x}^*$) can be obtained from:

$$\mathbf{W}\mathbf{x}^* = r\mathbf{w}, \tag{B.5}$$

using r from equation (B.4). Estimates of Ank-Ab bulk chemistry can also be obtained by multiplying measured concentrations by r. A powerful check on the procedure is to solve equation (B.5) for Ank-Ab zone rocks, and compare the computed and measured volatile contents. Loss on ignition (LOI) was taken as a measure of total volatile content for the rock analyses. Because ankerite contains most of the Fe in the Ank-Ab zone, Fe in the bulk rock analyses was taken as Fe^{2+} and, thus, LOI values were increased to account for the amount of oxygen added when the rock samples were fused and all Fe was converted to Fe^{3+}. For the computed reconstructions, total

volatile content was estimated from the CO_2 or H_2O contents of each mineral. The effects of graphite and pyrite were considered small and ignored. The mean difference between the estimated $CO_2 + H_2O$ contents and the Fe^{2+}-corrected LOI values is only -0.38 ± 1.12 weight percent (±2σ sample standard deviation), strongly suggesting that reconstructed volatile contents are accurate enough to quantify prograde devolatilization. The input of Si and Al into some diopside-bearing metacarbonate rocks introduces errors into the protolith reconstructions, but these effects have small impact on estimates of volatile loss.

Sample Wep-29a contains abundant oligoclase, implying that paragonite was present in the Ank-Ab zone protolith. Solving equation (B.5) for the mass fractions of calcite, ankerite, quartz, muscovite, albite, paragonite, rutile, and pyrite using the elements Si, Ti, Al, Fe (all Fe^{2+}), Mg, Ca, K, and Na and the average paragonite composition for similar Ank-Ab zone rocks from table 2 in Ferry (1992) yields 5.2 weight percent paragonite for the inferred protolith. Paragonite has not been observed in the Wepawaug Schist, but the solution for Wep-29a indicates that it was probably present, albeit rare.

The above procedures are inappropriate for highly altered vein selvages and lithologic contacts due to mobility of Si, Al, Ca, and other elements. For these rocks, the initial Ank-Ab zone Zr, CO_2, and H_2O contents were estimated using mean values for less altered rocks from the same layer or outcrop. For this problem, averaging using methods based on the geometric mean (Ague and van Haren, 1996) and the standard arithmetic mean give nearly identical results, so arithmetic means were used for simplicity. Volatile loss for a given rock was estimated assuming a Zr reference frame using equation (4) together with the measured Zr (C_i') and Fe^{2+}-corrected LOI (C_j'); and the estimated mean Zr (C_i^o) and CO_2+H_2O (C_j^o) for the Ank-Ab zone protolith.

Less altered rocks suitable for estimating Ank-Ab zone Zr, CO_2, and H_2O contents were unavailable for several calc-silicate samples. For these calc-silicates, a representative initial bulk volatile content of 29 weight percent was assumed, and the percentage volatile loss estimated using: 100*(measured Fe^{2+}-corrected LOI)/(29) – 1. To assess uncertainties, this equation was tested against the procedure described in the previous paragraph for samples whose initial Ank-Ab zone Zr, CO_2, and H_2O contents could be estimated. Uncertainties on volatile loss estimates are significant – approximately ±5 percent. However, this uncertainty level has little impact because the overall volatile losses for calc-silicates are extremely large and easily distinguishable from those for less altered rocks.

Appendix C

Ankerite Compositions

The ankerite compositions needed for the volatile loss calculations (app. B) were estimated using the representative whole-rock and ankerite analyses presented in table C1. Ankerite compositions in low-grade Ank-Ab and Ank-Ol zone rocks are a strong function of whole-rock chemistry. The following linear relationships between weight percent oxide in ankerite and $Mg/(Mg+Fe^{Total})$ (moles) for whole rocks were obtained: 1) MgO_{Ank} = 24.3713 ($Mg/(Mg+Fe^{Total})$ – 1.3817 (r^2 = 0.994); 2) FeO_{Ank} = -29.1657 ($Mg/(Mg+Fe^{Total})$ + 28.9645 (r^2 = 0.996); CaO_{Ank} = 2.0719 ($Mg/(Mg+Fe^{Total})$ + 28.2022 (r^2 = 0.758); $CO_{2,Ank}$ = 7.3504 ($Mg/(Mg+Fe^{Total})$ + 40.5404 (r^2 = 0.996). Here, r^2 is the square of the linear correlation coefficient. The somewhat lower r^2 for CaO has little impact on the results because the overall amount of CaO variation in the ankerites is small (<0.5 wt percent; table C1). Ankerite MnO contents are relatively small and do not appear to vary systematically, so the average MnO content of 0.69 weight percent (table C1) was used. The above equations and average MnO content allow low-grade ankerite compositions to be estimated given bulk-rock $Mg/(Mg+Fe^{Total})$.

Table C1

Ankerite compositions and bulk-rock $Mg/(Mg + Fe^T)$

Sample	$Mg/(Mg+Fe^T)$ Rock (Moles)	FeO Ank	MgO Ank	MnO Ank	CaO Ank	CO_2 Ank
JAW-190Bii	0.791	6.09	17.72	0.37	29.92	46.35
JAW-197Avi	0.687	8.87	15.51	0.55	29.70	45.63
JAW-197Ai	0.662	9.76	14.62	0.95	29.61	45.43
Wep-29a	0.652	9.87	14.54	1.21	29.45	45.28
JvH-W-38	0.813	5.09	18.56	0.37	29.80	46.51

General Notes: Ankerite (Ank) oxides in weight percent. Ank composition for JAW-197Ai is bulk average for zoned grains. Ank CO_2 content estimated from microprobe analyses assuming 1 mole CO_2 per mole of cations (Fe + Mg + Mn + Ca) in matrix correction iterations. Fe^T is total Fe (moles) in bulk rock.

Appendix D

Estimates of Volatile Loss (table D1)

Table D1

Calculated calcite, ankerite and muscovite abundances for the Ank-Ab zone, volatile budgets, densities, and volume changes

Sample	Rock Type Code	Cal (mol kg^{-1})	Ank (mol kg^{-1})	Ms (mol kg^{-1})	Initial Zr (ppm)	Initial CO_2 (wt. %)	Initial H_2O (wt. %)	% Volatile Mass Change	ρ_g (g cm^{-3})	ε_{pm} (%)
119B	8	2.945	1.473	0.516	54.7	25.98	0.92	-62.3	3.17	-29.2
119Di	9							-83.8[a]		
163IMiv	10				58.5	29.34	0.74	-94.0[b]		
163IN	10				58.5	29.34	0.74	-93.3[b]		
163IO	10				58.5	29.34	0.74	-94.2[b]		
163IPa	10				58.5	29.34	0.74	-94.1[b]		
163IRa	9				58.5	29.34	0.74	-90.3[b]		
163IT	8	3.235	1.532	0.423	61.7	27.75	0.76	-59.8		
163IU	8	3.047	1.578	0.443	59.4	27.32	0.79	-60.8		
163IV	8	3.526	1.520	0.365	62.6	28.92	0.65	-54.3		
163IW	7	3.972	1.496	0.413	52.6	30.67	0.74	-41.8		
163IX	7	3.977	1.504	0.417	52.4	30.77	0.75	-42.2		
163IZ-2	7	3.905	1.519	0.417	62.2	30.59	0.75	-42.6		
163IVAi	8	3.146	1.611	0.428	55.1	28.05	0.76	-58.2		
163IVAii	6	3.277	1.815	0.424	55.9	30.44	0.76	-39.8		
163VIIAi	10				58.5	29.34	0.74	-82.5[b]	3.16	-27.2
163VIIAii	9				58.5	29.34	0.74	-77.6[b]	3.21	-10.8
163VIIAiii	8	3.100	1.560	0.481	53.7	27.41	0.86	-57.4	3.06	-24.7
163VIIAiv	7	3.464	1.614	0.430	55.4	29.49	0.77	-46.8	3.04	-21.8
167A	8	4.261	1.377	0.363	46.2	30.91	0.65	-39.9		
167C	8	4.655	1.306	0.333	45.9	32.01	0.60	-37.5		
167D	8	4.090	1.413	0.372	49.7	30.48	0.66	-41.5		
167E	9				47.3	31.13	0.64	-91.8[c]		
168J	1	4.450	1.005	0.452		28.46	0.81			
168A	1	4.190	0.952	0.445		26.85	0.79			
168C	1	4.136	1.098	0.489		27.90	0.87			
168K	1	4.002	1.086	0.431		27.20	0.77			
168D	1	4.087	1.148	0.449		28.12	0.80			
168Ei	1	3.999	1.081	0.437		27.15	0.78			
168Eii	1	4.121	1.073	0.421		27.61	0.75			
169Ai	5	3.561	1.210	0.496	56.6	26.36	0.89	-29.8		
169Aii	9				56.6	26.36	0.89	-62.6[d]		
169B	8	3.812	1.118	0.464	52.8	26.65	0.83	-41.0		
170A	5	3.580	1.475	0.450	64.9	28.76	0.80	-30.8		
170C	8	3.374	1.322	0.584	56.7	26.52	1.04	-58.1		
170E	9				60.8	27.64	0.92	-88.5[e]		
171A	3	4.929	1.160	0.356	63.9	31.94	0.64	-5.7		
171B	3	5.176	1.031	0.388	62.4	31.89	0.69	-5.5		
171Ci	3	5.064	1.106	0.439	61.1	32.06	0.78	-5.7		
171Cii	3	5.931	0.531	0.483	61.3	30.81	0.86	-4.5		
171Ciii	3	6.194	0.381	0.502	62.1	30.63	0.90	-4.7		
171D	3	5.457	0.972	0.434	60.2	32.61	0.78	-3.7		
172A	4	4.066	1.136	0.520	62.1	27.93	0.93	-18.8		
173A	5	3.735	1.175	0.530	64.4	26.84	0.95	-30.1		
179B	4	3.210	1.062	0.662	87.8	23.53	1.18	-24.2		
179E	4				87.8	23.53	1.18	-65.1[f]		
181SII	10				47.9	30.31	0.69	-87.7[g]		
181SI	10				47.9	30.31	0.69	-87.4[g]		
181Bi	6	6.170	0.631	0.295	43.4	32.75	0.53	-17.1		
181Bii	6	6.398	0.560	0.302	45.1	33.12	0.54	-17.3		
181Biii	5	6.784	0.483	0.324	47.5	34.13	0.58	-14.0		
181C	4	5.620	0.578	0.382	46.8	29.85	0.68	-15.7		
181FF	4	5.639	0.601	0.366	51.1	30.14	0.65	-13.9		
181E	4	5.553	0.580	0.402	48.3	29.57	0.72	-16.9		
181Fiv	4	5.233	0.639	0.391	48.5	28.69	0.70	-15.6		
181D	4	5.349	0.618	0.422	50.4	29.01	0.75	-17.7		

TABLE D1

(continued)

Sample	Rock Type Code	Cal (mol kg^{-1})	Ank (mol kg^{-1})	Ms (mol kg^{-1})	Initial Zr (ppm)	Initial CO_2 (wt. %)	Initial H_2O (wt. %)	% Volatile Mass Change	ρ_g (g cm^{-3})	ε_{pm} (%)
181Fiii	4	5.954	0.507	0.361	50.3	30.69	0.64	-14.0		
181Fii	6	4.809	0.731	0.451	50.2	27.63	0.81	-24.3		
181Fi	6	4.864	0.725	0.448	51.3	27.83	0.80	-25.6		
181GG	6	5.477	0.582	0.385	46.3	29.26	0.69	-21.9		
181G	6	5.057	0.662	0.429	48.7	28.12	0.77	-21.8		
181Hiv	6	6.547	0.454	0.326	45.3	32.83	0.58	-14.9		
181Hiii	6	5.648	0.535	0.419	43.2	29.59	0.75	-20.9		
181Hii	6	5.952	0.544	0.368	42.6	31.01	0.66	-19.0		
181Hi	6	5.991	0.533	0.484	55.3	31.09	0.87	-19.8		
181Rii	10				47.9	30.31	0.69	-88.2[g]		
181DDia	6	5.799	0.604	0.370	54.4	30.87	0.66	-18.7	2.88	-10.6
181DDiia	5	5.661	0.603	0.368	49.3	30.25	0.66	-12.1	2.85	-7.1
181DDiv-v	10				51.9	30.56	0.66	-71.0[h]	2.96	-5.9
184A	1	4.621	0.925	0.406		28.51	0.72			
185A	8	4.740	1.013	0.488	43.8	29.81	0.87	-40.0		
185C	8	5.043	1.180	0.271	50.5	32.61	0.48	-36.8		
185D	9				47.2	31.21	0.68	-90.4[i]		
186Bi	9							-90.0[a]		
186Bii	10							-88.6[a]		
187Ai	10				72.8	27.56	0.92	-94.1[j]		
187Aii-iii	10				72.8	27.56	0.92	-94.0[j]		
187Aiv	10				72.8	27.56	0.92	-93.2[j]	3.29	-27.4
187Av	9				72.8	27.56	0.92	-91.0[j]		
187Oiv	9				72.8	27.56	0.92	-91.6[j]	3.28	-3.2
187Ni	9				72.8	27.56	0.92	-90.3[j]		
187Bii	9				72.8	27.56	0.92	-91.1[j]		
187Oii	9				72.8	27.56	0.92	-90.0[j]		
187Biii	9				72.8	27.56	0.92	-92.0[j]		
187Biv	9				72.8	27.56	0.92	-89.9[j]		
187Nii	9				72.8	27.56	0.92	-76.0[j]		
187Mi	8	3.644	1.295	0.494	69.2	27.47	0.88	-55.0		
187Mii	8	3.480	1.336	0.534	74.7	27.12	0.95	-54.5		
187Miii	8	4.007	1.185	0.523	74.6	28.10	0.93	-47.6	3.02	-21.6
188Ai	9							-88.4[a]		
188Aii	10							-88.0[a]		
189A	1	3.447	1.486	0.43		28.27	0.83			
190Bi	2				48.8	29.92	0.59	-34.8[k]		
190Bii	1	3.899	1.464	0.311		30.07	0.56			
190D	1	3.947	1.440	0.335		30.06	0.60			
190F	1	3.899	1.455	0.337		29.98	0.60		2.81	
190H	1	3.901	1.404	0.324		29.55	0.58			
191A	1	3.308	0.797	0.630		21.61	1.13			
192A	3	5.300	0.728	0.391	68.5	29.76	0.70	-0.6[l]		
193ADi	6	4.770	1.330	0.351	45.1	32.74	0.63	-32.1		
193Dii	8	4.604	1.206	0.370	42.9	30.92	0.66	-41.4		
195Aii	8	3.137	1.171	0.427	89.4	24.15	0.76	-56.4		
195Aiii	8	2.666	1.319	0.678	88.8	23.39	1.21	-67.9		
196Ai	9				43.0	28.74	0.82	-95.6[m]		
196Aii	8	4.093	1.214	0.458	43.0	28.74	0.82	-48.1		
197AS	2				66.5	26.91	0.82	+6.7[n]		
197Ai	2				66.5	26.91	0.82	+18.5[n]	2.76	+19.3
197Aii	2				66.5	26.91	0.82	+8.4[n]		
197Aiii	1-2				66.5	26.91	0.82	+1.8[n]		
197Aiv	1	4.143	0.974	0.456		26.84	0.82			
197Av	1	4.166	0.969	0.465		26.90	0.83		2.77	
197B-2	1	4.108	0.999	0.468		26.91	0.84			
197Avi	1	4.020	1.054	0.449		27.00	0.80			
JvH-W-16	8	3.804	1.200	0.470	54.1	27.33	0.84	-54.9	3.01	-21.7
JvH-W-24A	7	3.610	1.688	0.410	61.0	30.77	0.73	-42.7	2.94	-17.3
JvH-W-27	3	5.652	0.403	0.432	52.0	28.44	0.77	-5.5	2.74	-0.1
JvH-W-28	3	3.189	1.451	0.477	64.9	26.85	0.85	-14.1	2.84	-3.5
JvH-W-32	3	4.388	0.786	0.566	63.5	26.27	1.01	-12.9	2.77	-3.1
JvH-W-34	8	4.625	1.119	0.421	44.5	30.23	0.75	-44.2	2.97	-19.6
JvH-W-35	8	3.782	1.257	0.510	51.6	27.74	0.91	-56.9	3.09	-26.0
JvH-W-36	1	4.463	0.904	0.540		27.64	0.96		2.82	

TABLE D1

(continued)

Sample	Rock Type Code	Cal (mol kg^{-1})	Ank (mol kg^{-1})	Ms (mol kg^{-1})	Initial Zr (ppm)	Initial CO_2 (wt. %)	Initial H_2O (wt. %)	% Volatile Mass Change	ρ_g (g cm^{-3})	$\varepsilon_{\rho m}$ (%)
JvH-W-37	1	3.359	1.455	0.340		27.61	0.61		2.80	
JvH-W-38	1	3.626	1.546	0.310		29.57	0.55		2.79	
JvH-W-39	1	4.028	1.217	0.364		28.46	0.65		2.77	
Wep-8a	5	3.954	1.164	0.409	60.7	27.68	0.73	-23.1	2.80	-6.9
Wep-8b	9				60.7	27.68	0.73	-91.1[n]	3.26	-26.8
Wep-29a	1	3.651	1.543	0.215	64.8	29.71	0.63	-9.4		
Wep-35a	5	3.378	1.257	0.551	74.6	25.97	0.99	-27.7		
W-5	5	4.449	1.202	0.379	56.1	30.21	0.68	-24.2	2.85	-9.9
W-6i	6	4.330	1.250	0.389	48.3	30.12	0.69	-28.5		

General Notes: All sample numbers begin with prefix JAW unless noted otherwise. ρ_g is grain density (rock density on a porosity-free basis); $\varepsilon_{\rho m}$ is volume strain computed using changes in rock density and mass. $\varepsilon_{\rho m}$ relative to Ank-Ab zone protoliths except for JAW-197Ai computed relative to JAW-197Av protolith. Average Ank-Ab zone ρ_g of 2.79 ±0.017 g cm^{-3} (2σ) used to compute $\varepsilon_{\rho m}$, except for JAW-197Ai which is based on ρ_g = 2.77 g cm^{-3} for protolith sample JAW-197Av. Density measurements from this study and Ague and Van Haren (1996). All volume change estimates made using Zr reference frame.

[a]Estimated assuming 29 weight % initial volatiles.
[b]Based on mean initial Zr, CO_2, and H_2O for samples 163T, U, V, W, X, Z-2.
[c]Based on mean initial Zr, CO_2, and H_2O for samples 167A, C, D.
[d]Based on initial Zr, CO_2, and H_2O for sample 169Ai.
[e]Based on mean initial Zr, CO_2, and H_2O for samples 170A, C.
[f]Based on initial Zr, CO_2, and H_2O for sample 179B.
[g]Based on mean initial Zr, CO_2, and H_2O for samples 181B, C, D, E, F, G, H, FF, GG.
[h]Based on mean initial Zr, CO_2, and H_2O for samples 181DDia, DDiia.
[i]Based on mean initial Zr, CO_2, and H_2O for samples 185A, C.
[j]Based on mean initial Zr, CO_2, and H_2O for samples 187Mi, Mii, Miii.
[k]Based on mean initial Zr, CO_2, and H_2O for samples 190Bii, D, F, H.
[l]Sample JAW-192A is in Biotite Zone but biotite heavily retrograded to Ankerite + Muscovite.
[m]Based on initial Zr, CO_2, and H_2O for sample 196Aii.
[n]Based on mean initial Zr, CO_2, and H_2O for samples 197Aiv, v, vi, B-2.
[o]Based on initial Zr, CO_2, and H_2O for sample Wep-8a.

APPENDIX E

Rock Chemistry Tables

General Notes for Rock Chemistry Tables

(1) Sample numbers begin with prefix JAW unless noted otherwise. Rb, Sr, Ba, Zr, Nb, Y, rare earth element, U, and Th concentrations tabulated in ppm, all others in weight percent. All Fe as Fe_2O_3. *LOI:* loss on ignition; *Total:* weight percent total including Rb, Sr, Ba, Zr, Nb, and Y summed as oxides. *b.d.*: below detection.

(2) Analyses for JvH samples and JAW-119B from Ague and van Haren (1996), except for Zr concentrations reanalyzed using pressed pellet for internal consistency with the other data presented herein.

(3) Y concentrations for JAW-163, -168, -171, -181, -187, and -197 series samples determined using ICP-MS; all other Y concentrations determined using XRF (pressed pellet).

(4) X is distance along geochemical profile measured in centimeters.

(5) JAW-163VIIA and JAW-181DD are profiles that extend across alteration selvages adjacent to quartz veins. Distances (X) are approximate due to irregular thickness of alteration zones, and are measured relative to X = 0 cm at the center of the veins. JAW-190 profile extends away from a contact with metapelite at X = 0 cm; sample -190Bi is a selvage surrounding an ~8 cm wide, cross-cutting quartz vein.

(6) Samples from vein selvages, in addition to those from measured profiles discussed in text and note (5), are: JAW-119D, -169Aii, -170E, -179E, -185D, -190Bi, -196Ai, and Wep-8b.

(7) Rock Type Codes. *1:* Ank-Ab zone and, for Wep-29a, Ank-Ol zone; *2:* Ank-Ab zone vein selvage; *3:* Bt zone metacarbonate rock including Ank and Ms; *4:* Biotite-bearing metacarbonate rock, no Ank; *5:* Amp + Bt-bearing metacarbonate rock; *6:* Amp-bearing metacarbonate rock, no Bt; *7:* Di + Bt-bearing metacarbonate rock; *8:* Di-bearing metacarbonate rock, little or no Amp or Bt; *9:* Di-Zo calc-silicate (metacarbonate protolith); *10:* Amphibolite calc-silicate (metacarbonate protolith); *11:* Amphibolite calc-silicate (metaclastic protolith); *12:* Amphibolite at contact between metacarbonate and metaclastic rocks; *13:* Czo/Zo-rich metapelite at contact with calc-silicate or in vein selvage; *14:* Metaclastic schist. See tables 1, 2, and 3 for additional detail.

TABLE E1

Major oxides, minor oxides, Rb, Sr, Ba, Zr, Nb, and Y

Sample	Zone	Rock Type Code	X (cm)	SiO_2	TiO_2	Al_2O_3	Fe_2O_3	MgO	MnO	CaO	K_2O	Na_2O	P_2O_5	LOI	Total	Rb	Sr	Ba	Zr	Nb	Y
119B	Di-II	8	-	36.5	0.32	8.40	6.23	6.14	0.42	29.80	0.01	0.20	0.26	12.00	100.3	0.54	427	0.14	68	19	20
119Di	Di-II	9	-	45.9	0.50	13.70	6.19	6.82	0.38	21.20	0.09	0.10	0.44	3.85	99.2	3	380	31	84	15	39
119Dii	Di-II	13	-	41.3	1.02	23.10	7.10	5.26	0.23	14.60	3.15	0.03	0.11	2.10	98.2	214	605	1020	179	20	34
163IG	Di-I	14	-47.75	72.0	0.70	13.30	4.06	1.80	0.05	1.19	3.05	1.82	0.11	2.00	100.3	143	203	846	225	14	19
163IL	Di-I	14	-14.75	69.2	0.77	14.00	3.84	1.93	0.05	2.50	1.93	3.87	0.06	1.50	99.9	113	492	1130	249	14	11
163IMi	Di-I	14	-6.25	79.5	0.42	9.31	2.99	1.32	0.03	1.74	1.27	2.57	0.06	0.90	100.3	84	364	1010	165	9	13
163IMii	Di-I	11	-2.75	86.2	0.55	4.50	2.52	1.72	0.07	1.63	1.25	0.31	0.03	0.85	99.8	92	109	939	208	15	18
163IMiii	Di-I	11	-0.75	65.1	1.16	10.30	5.94	4.53	0.21	10.10	0.31	0.25	0.02	1.40	99.5	9	434	131	450	25	43
163IMiv	Di-I	10	0.75	48.8	0.40	16.00	8.08	7.54	0.29	15.50	0.35	0.37	0.47	1.70	99.6	10	666	127	82	8	12
163IN	Di-I	10	5.25	45.2	0.47	16.50	8.28	8.15	0.31	17.00	0.33	0.39	0.57	1.90	99.2	8	632	67	79	12	19
163IO	Di-I	10	17.25	43.3	0.29	21.90	5.75	5.19	0.22	19.60	0.21	0.23	0.43	1.95	99.2	4	1080	76	85	7	23
163IPa	Di-I	10	22.25	43.0	0.20	22.10	5.75	4.85	0.22	19.50	0.25	0.22	0.49	2.10	98.8	7	1040	101	88	4	20
163IRa	Di-I	9	32.25	47.5	0.40	10.80	6.45	8.71	0.41	21.60	0.12	0.19	0.22	3.40	99.9	4	569	63	81	8	16
163IT	Di-I	8	38.25	34.9	0.34	6.61	4.39	6.91	0.44	31.20	0.04	0.09	0.15	13.50	98.7	2	1030	34	75	6	15
163IU	Di-I	8	52.25	36.0	0.36	6.98	4.44	7.19	0.43	30.60	0.04	0.09	0.15	13.10	99.5	3	1050	50	73	6	10
163IV	Di-I	8	66.25	33.2	0.33	5.72	4.18	6.91	0.44	32.90	0.04	0.09	0.19	16.00	100.1	3	1020	40	76	6	10
163IW	Di-I	7	72.25	26.1	0.32	6.16	4.01	6.61	0.44	34.00	1.06	0.09	0.19	20.80	100.0	48	1160	525	61	5	12
163IX	Di-I	7	82.25	25.9	0.33	6.23	4.01	6.68	0.44	34.20	1.14	0.08	0.19	20.80	100.2	53	1170	476	61	6	12
163IZ-2	Di-I	7	107.25	26.0	0.32	6.22	4.23	6.61	0.44	33.70	0.94	0.09	0.21	20.40	99.4	56	1110	469	72	6	13
163IIOii	Di-I	13	-	37.3	2.26	20.30	10.70	4.02	0.80	15.20	2.57	0.07	2.04	2.20	97.8	164	548	1530	678	67	120
163IVAi	Di-I	8	-	34.0	0.31	6.67	4.61	7.21	0.44	31.20	0.03	0.08	0.21	14.20	99.1	5	856	43	67	7	18
163IVAii	Di-I	6	-	25.3	0.32	6.72	5.27	7.53	0.46	32.00	0.79	0.32	0.31	21.30	100.5	50	869	338	65	7	19
163VIIAi	Di-I	10	3	40.1	0.38	19.20	5.07	6.19	0.28	21.00	0.15	0.23	0.44	5.90	99.0	5	751	45	71	12	16
163VIIAii	Di-I	9	9	41.3	0.33	14.70	4.74	6.38	0.39	25.10	0.04	0.09	0.34	6.10	99.6	4	624	31	57	9	13
163VIIAiii	Di-I	8	13	34.0	0.36	7.54	4.60	6.96	0.39	30.40	0.06	0.14	0.34	14.10	99.0	3	925	31	65	8	14
163VIIAiv	Di-I	7	18	28.5	0.37	6.55	4.79	6.89	0.42	32.10	0.69	0.13	0.37	18.40	99.3	35	876	209	65	8	13
167A	Di-II	8	77.70	25.7	0.29	5.76	4.58	5.88	0.47	35.30	0.15	0.26	0.13	21.70	100.4	5	1090	46	54	4	14
167C	Di-II	8	132.50	23.2	0.29	5.30	4.34	5.59	0.46	36.80	0.18	0.28	0.15	23.10	99.8	6	1200	92	53	5	14
167D	Di-II	8	17.40	26.4	0.32	5.89	4.83	5.93	0.46	34.50	0.12	0.26	0.14	20.80	99.8	5	939	55	58	7	17
167E	Di-II	9	7.30	47.0	0.28	14.30	4.33	5.35	0.25	21.80	0.08	0.14	2.73	2.50	98.9	5	817	37	53	4	22
168J	Ank-Ab	1	1.00	24.5	0.36	6.66	3.51	3.83	0.37	29.20	1.80	0.58	0.24	28.60	99.8	59	776	377	63	7	20
168A	Ank-Ab	1	24.00	29.2	0.32	6.01	3.37	3.62	0.33	27.50	1.80	0.25	0.15	27.00	99.7	60	720	315	56	6	14
168C	Ank-Ab	1	42.00	26.1	0.35	6.55	3.46	4.19	0.32	28.00	1.99	0.24	0.15	28.40	99.9	64	1000	385	64	5	10
168K	Ank-Ab	1	58.00	28.9	0.31	5.76	3.57	4.04	0.34	27.30	1.74	0.20	0.15	27.40	99.9	55	974	339	56	4	11
168D	Ank-Ab	1	66.00	26.4	0.32	6.02	3.72	4.26	0.36	28.10	1.79	0.22	0.23	28.50	100.1	58	981	341	58	6	11
168Ei	Ank-Ab	1	68.25	28.7	0.32	5.88	3.45	4.04	0.33	27.10	1.79	0.24	0.15	27.40	99.6	55	962	359	56	7	10
168Eii	Ank-Ab	1	70.25	27.5	0.33	6.18	3.37	4.08	0.33	27.90	1.67	0.52	0.14	27.90	100.1	53	938	344	60	6	12
169Ai	Di-I	5	-	32.2	0.35	6.92	4.64	4.67	0.50	28.10	2.06	0.06	0.27	20.50	100.4	99	668	515	62	5	19

TABLE E1

(continued)

Sample	Zone	Rock Type Code	X (cm)	SiO_2	TiO_2	Al_2O_3	Fe_2O_3	MgO	MnO	CaO	K_2O	Na_2O	P_2O_5	LOI	Total	Rb	Sr	Ba	Zr	Nb	Y
169Aii	Di-I	9	-	39.3	0.43	8.62	5.26	5.59	0.49	26.30	0.13	0.13	0.32	13.50	100.2	5	656	28	78	7	22
169B	Di-I	8	-	34.2	0.31	6.89	4.35	4.71	0.51	30.50	0.08	0.10	0.17	18.30	100.2	3	601	26	61	4	13
170A	Di-I	5	-	27.0	0.38	7.14	3.80	6.10	0.30	29.70	2.69	0.57	0.11	22.00	100.0	93	903	328	71	4	12
170C	Di-I	8	-	34.0	0.36	9.17	4.38	6.08	0.34	30.70	0.12	0.15	0.12	13.60	99.1	8	658	24	69	6	17
170E	Di-I	9	-	51.5	0.19	16.60	4.01	4.36	0.18	19.10	0.07	0.05	0.15	3.85	100.2	3	738	52	79	4	41
171A	Bt	3	0.50	18.6	0.35	5.42	4.32	4.22	0.64	33.10	1.06	0.52	0.13	30.80	99.3	31	619	245	65	6	23
171B	Bt	3	2.00	19.2	0.31	5.17	3.87	3.90	0.57	33.40	1.58	0.15	0.24	30.70	99.2	39	756	304	63	6	16
171Ci	Bt	3	3.25	17.8	0.33	5.87	4.05	4.19	0.56	33.40	1.76	0.17	0.24	31.00	99.5	42	806	307	62	6	14
171Cii	Bt	3	5.25	18.9	0.36	6.35	3.71	2.35	0.50	34.60	1.92	0.13	0.19	30.20	99.4	40	870	287	62	7	13
171Ciii	Bt	3	7.00	18.7	0.38	6.61	3.54	1.98	0.50	35.20	2.03	0.13	0.18	30.10	99.5	42	887	357	63	4	12
171D	Bt	3	16.00	16.4	0.35	5.81	4.03	3.73	0.54	34.70	1.72	0.17	0.23	32.20	100.0	36	860	277	61	5	11
172A	Bt	4	-	26.7	0.38	7.35	4.11	4.47	0.46	29.60	2.31	0.25	0.16	24.50	100.5	66	1020	391	66	7	14
173A	Amp-II	5	-	27.5	0.44	8.77	6.09	4.20	0.59	29.60	0.84	0.80	0.21	21.10	100.2	36	439	299	72	7	30
174A	Amp-II	13	-	39.6	1.22	23.80	11.80	5.12	0.38	9.59	4.05	0.45	0.11	2.65	99.0	243	371	819	249	19	69
179B	Bt	4	-	32.1	0.54	9.93	5.88	3.67	0.52	25.00	2.28	0.56	0.16	19.70	100.5	96	672	340	95	7	22
179E	Bt	4	-	34.1	0.63	16.30	8.59	5.00	0.43	18.30	3.08	0.28	0.49	13.10	100.4	177	412	482	142	9	25
181W	Amp-I	14	-88.50	62.6	0.94	18.70	6.72	2.30	0.07	0.29	4.45	0.36	0.11	3.80	100.5	131	90	703	185	18	25
181Z	Amp-I	14	-43.50	53.4	1.09	21.40	7.26	2.56	0.12	1.95	3.15	4.69	0.03	3.20	99.0	145	471	811	217	23	23
181UV	Amp-I	14	-23.50	51.9	1.16	22.00	8.81	3.16	0.28	3.41	2.98	4.62	0.00	2.10	100.6	171	501	624	233	18	31
181SIV	Amp-I	11	-8.50	38.4	1.09	24.60	10.30	2.76	0.34	16.70	0.68	0.33	0.06	4.00	99.4	32	682	225	228	19	25
181SIII	Amp-I	11	-2.50	49.5	0.95	21.30	6.68	1.43	0.24	16.40	0.22	0.29	0.04	2.95	100.1	13	615	56	181	21	20
181Y	Amp-I	12	0.00	62.0	0.46	13.30	5.07	2.62	0.16	11.90	0.18	0.12	0.88	2.70	99.5	14	418	39	89	7	19
181SII	Amp-I	10	2.50	52.4	0.29	14.40	10.80	6.73	0.29	10.10	0.56	0.36	0.02	4.10	100.1	37	220	82	65	0	18
181SI	Amp-I	10	7.00	38.4	0.24	26.50	5.59	0.67	0.21	22.70	0.26	0.21	0.71	4.80	100.4	16	953	82	66	3	51
181Bi	Amp-I	6	15.50	19.1	0.23	4.12	4.28	2.57	0.60	38.20	0.27	0.12	0.58	28.80	99.0	8	912	40	46	4	18
181Bii	Amp-I	6	16.49	18.3	0.24	4.19	4.05	2.44	0.57	39.20	0.37	0.09	0.35	29.20	99.1	10	1020	75	48	3	16
181Biii	Amp-I	5	18.00	15.3	0.23	4.38	3.86	2.27	0.60	40.40	0.71	0.06	0.33	31.00	99.3	22	1100	167	50	4	18
181C	Amp-I	4	22.25	24.4	0.27	5.19	3.64	2.49	0.42	34.40	1.48	0.10	0.20	26.60	99.4	38	1280	212	49	5	7
181FF	Amp-I	4	31.50	22.9	0.29	5.35	3.82	2.48	0.45	34.30	1.67	0.35	0.19	27.10	99.1	40	1180	250	53	9	10
181E	Amp-I	4	40.35	25.1	0.28	5.39	3.57	2.55	0.45	34.30	1.25	0.04	0.18	26.20	99.5	37	1320	233	51	5	8
181Fiv	Amp-I	4	43.25	26.4	0.30	5.62	3.91	2.60	0.46	32.80	1.68	0.27	0.17	25.70	100.1	42	1200	246	51	7	10
181D	Amp-I	4	45.25	25.8	0.29	5.63	3.77	2.61	0.45	33.30	1.46	0.03	0.18	25.40	99.1	42	1240	244	53	5	7
181Fiii	Amp-I	4	49.00	22.7	0.25	4.95	3.72	2.28	0.59	36.00	1.25	0.11	0.18	28.00	100.2	34	1030	224	53	3	9
181Fii	Amp-I	6	51.05	29.0	0.33	6.37	4.55	2.91	0.57	32.30	0.13	0.10	0.19	23.10	99.7	5	862	26	55	6	12
181Fi	Amp-I	6	53.30	28.6	0.33	6.31	4.46	2.91	0.56	32.50	0.17	0.10	0.18	22.80	99.0	6	818	33	56	6	11
181GG	Amp-I	6	66.50	26.6	0.29	5.40	3.68	2.58	0.47	34.70	0.13	0.11	0.19	24.90	99.2	5	999	29	50	5	9
181G	Amp-I	6	71.50	28.6	0.31	6.03	3.96	2.81	0.47	33.10	0.44	0.10	0.18	24.20	100.3	14	792	61	53	6	10
181Hiv	Amp-I	6	80.25	19.0	0.24	4.47	3.30	2.27	0.55	39.20	0.06	0.08	0.21	29.80	99.3	4	802	b.d.	48	4	9

TABLE E1

(continued)

Sample	Zone	Rock Type Code	X (cm)	SiO_2	TiO_2	Al_2O_3	Fe_2O_3	MgO	MnO	CaO	K_2O	Na_2O	P_2O_5	LOI	Total	Rb	Sr	Ba	Zr	Nb	Y
181Hiii	Amp-I	6	83.25	25.1	0.27	5.87	3.78	2.47	0.49	35.60	0.06	0.09	0.22	25.70	99.8	3	800	25	47	4	10
181Hii	Amp-I	6	86.00	22.6	0.28	5.13	3.73	2.49	0.55	37.10	0.07	0.09	0.21	27.30	99.6	2	643	b.d.	46	4	10
181Hi	Amp-I	6	90.25	19.5	0.32	6.75	4.23	2.49	0.68	37.50	0.13	0.09	0.25	27.40	99.4	4	514	32	60	5	24
181Rii	Amp-I	10	92.00	47.7	0.31	20.70	5.88	2.57	0.23	17.30	0.24	0.05	0.41	3.85	99.3	14	709	80	58	5	26
181OI	Amp-I	12	101.50	47.9	0.62	18.80	8.30	4.48	0.23	14.80	0.39	0.17	0.63	3.45	99.9	30	500	106	93	11	53
181Qii	Amp-I	13	115.00	63.9	1.10	13.10	6.58	3.95	0.14	4.61	2.77	0.98	0.11	2.20	99.6	157	223	496	246	22	39
181Qi	Amp-I	13	126.50	45.4	1.38	22.40	9.99	4.38	0.23	4.28	4.49	2.42	0.11	4.00	99.3	225	342	1310	253	26	46
181DDia	Amp-I	6	5	22.9	0.29	5.15	4.03	2.63	0.49	36.80	0.16	0.07	0.23	27.40	100.3	8	781	28	59	4	8
181DDiia	Amp-I	5	7	23.8	0.29	4.98	3.86	2.54	0.45	35.00	0.82	0.07	0.20	28.25	100.4	35	897	145	52	4	9
181DDiv-v	Amp-I	10	0	51.3	0.33	13.3	4.90	2.38	0.23	17.90	0.39	0.12	1.09	8.58	100.3	22	433	63	52	6	18
184A	Ank-Ab	1	-	27.0	0.29	5.44	3.26	3.65	0.29	30.00	1.70	0.16	0.15	28.40	100.5	55	1040	409	54	5	9
185A	Di-II	8	-	25.8	0.28	7.33	4.11	4.56	0.42	35.70	0.21	0.12	0.14	21.00	99.8	8	855	70	51	4	12
185B	Di-II	11	-	46.4	2.05	15.70	8.48	6.18	0.37	17.20	0.39	0.24	0.02	2.25	99.4	9	454	70	282	35	49
185C	Di-II	8	-	23.2	0.32	4.10	4.19	5.03	0.47	38.10	0.09	0.12	0.15	23.60	99.5	8	988	69	58	5	9
185D	Di-II	9	-	44.3	0.25	17.10	6.31	5.10	0.31	22.30	0.30	0.10	0.27	3.15	99.6	17	743	81	58	4	25
186Bi	Di-II	9	-	48.2	0.40	15.00	5.72	6.16	0.30	21.10	0.05	0.08	0.39	2.10	99.6	3	292	b.d.	70	7	51
186Bii	Di-II	10	-	48.1	0.50	17.20	7.71	6.48	0.23	15.50	0.80	0.45	0.55	1.90	99.5	52	272	64	89	11	33
187Ao	Di-II	13	-2.10	61.6	1.09	16.00	5.01	1.63	0.24	11.80	0.59	0.63	0.05	1.35	100.1	30	551	133	148	26	17
187Ai	Di-II	10	2.10	45.6	0.63	17.00	8.66	7.98	0.41	16.30	0.39	0.42	0.20	1.50	99.2	6	442	34	103	14	22
187Aii-iii	Di-II	10	6.30	44.0	0.53	18.60	7.42	6.30	0.39	18.80	0.33	0.31	0.51	1.50	98.8	5	535	27	95	14	29
187Aiv	Di-II	10	8.80	45.6	0.58	16.20	6.08	6.17	0.42	21.80	0.09	0.10	0.25	1.65	99.0	5	536	b.d.	85	16	27
187Av	Di-II	9	10.80	48.4	0.49	11.40	6.63	7.79	0.42	21.70	0.04	0.11	0.46	1.66	99.2	3	407	b.d.	66	14	22
187Oiv	Di-II	9	14.40	47.7	0.34	15.00	6.00	6.17	0.36	21.50	0.04	0.09	0.29	1.50	99.1	3	542	44	64	8	27
187Ni	Di-II	9	15.80	46.7	0.35	15.70	5.76	6.12	0.34	21.50	0.05	0.07	0.47	1.80	99.0	5	647	46	63	8	25
187Bii	Di-II	9	17.30	46.0	0.38	15.70	5.84	6.03	0.35	22.40	0.04	0.06	0.58	1.80	99.3	3	680	b.d.	69	11	27
187Oii	Di-II	9	19.40	45.2	0.41	15.40	6.06	6.08	0.36	22.40	0.04	0.08	0.59	2.25	99.0	5	612	24	73	10	29
187Biii	Di-II	9	20.30	47.1	0.42	14.50	6.27	6.75	0.38	22.20	0.05	0.06	0.53	1.85	100.2	2	605	b.d.	79	9	22
187Biv	Di-II	9	22.10	47.7	0.40	14.30	6.04	6.58	0.40	22.10	0.04	0.07	0.44	2.35	100.5	4	572	36	75	12	18
187Nii	Di-II	9	23.40	41.1	0.43	11.90	5.43	6.07	0.42	25.90	0.04	0.08	0.56	7.80	99.8	4	542	25	89	10	15
187Mi	Di-II	8	25.40	32.9	0.43	7.71	4.93	5.67	0.45	32.20	0.04	0.11	0.37	15.00	99.9	3	572	b.d.	84	9	14
187Mii	Di-II	8	30.40	32.8	0.41	8.23	4.90	5.84	0.46	31.20	0.03	0.09	0.29	14.90	99.2	3	611	b.d.	90	7	13
187Miii	Di-II	8	35.40	29.8	0.41	7.89	4.51	5.20	0.44	32.80	0.11	0.09	0.31	17.50	99.1	6	647	20	88	6	13
188Ai	Di-II	9	-	47.7	0.50	15.30	5.34	6.24	0.37	21.60	0.05	0.09	0.27	2.60	100.1	3	564	24	90	16	27
188Aii	Di-II	10	-	48.1	0.64	18.10	5.67	5.43	0.28	18.50	0.21	0.12	0.36	2.30	99.8	10	599	44	106	21	27
189A	Ank-Ab	1	-	27.2	0.34	6.07	3.45	5.73	0.21	26.90	1.82	0.10	0.13	28.30	100.4	56	834	354	66	6	11
190Bi	Ank-Ab	2	368.00	26.7	0.33	6.31	8.20	8.37	0.37	19.60	0.28	2.72	0.72	26.50	100.2	13	507	112	67	6	19
190Bii	Ank-Ab	1	366.00	26.0	0.25	4.36	2.99	5.72	0.25	29.00	0.99	0.25	0.13	30.40	100.5	37	772	300	51	4	9

TABLE E1

(continued)

Sample	Zone	Rock Type Code	X (cm)	SiO_2	TiO_2	Al_2O_3	Fe_2O_3	MgO	MnO	CaO	K_2O	Na_2O	P_2O_5	LOI	Total	Rb	Sr	Ba	Zr	Nb	Y
190D	Ank-Ab	1	295.00	26.1	0.24	4.43	2.91	5.70	0.24	29.20	1.26	0.10	0.13	29.80	100.3	44	918	356	49	5	8
190F	Ank-Ab	1	200.00	26.8	0.25	4.47	2.94	5.86	0.25	29.50	1.29	0.07	0.13	28.50	100.2	44	906	350	47	5	8
190H	Ank-Ab	1	0.00	27.1	0.24	4.38	3.14	5.45	0.27	28.80	1.21	0.15	0.14	29.30	100.3	41	862	348	48	4	10
191A	Ank-Ab	1	-	36.2	0.49	8.73	3.98	2.92	0.26	22.30	2.44	0.43	0.16	21.80	99.9	87	868	399	105	8	14
192A	Bt	3	-	21.4	0.38	6.17	4.04	2.73	0.44	32.30	1.67	0.73	0.14	30.10	100.3	48	1440	329	69	6	10
193ADi	Di-I	6	-	19.7	0.31	5.56	4.91	5.37	0.66	36.90	0.23	0.35	0.14	25.10	99.3	6	475	24	51	3	18
193Dii	Di-I	8	-	25.3	0.29	5.70	4.65	5.11	0.65	36.20	0.06	0.17	0.14	21.10	99.4	5	436	b.d.	50	5	21
195Aii	Di-II	8	-	42.4	0.40	6.52	4.65	4.85	0.38	27.50	0.04	0.10	0.15	12.40	99.5	2	701	b.d.	106	6	24
195Aiii	Di-II	8	-	40.1	0.58	10.70	5.34	5.81	0.36	26.70	0.05	0.10	0.15	9.25	99.3	3	886	37	110	9	20
196Ai	Di-II	9	-	48.8	0.49	15.30	5.34	5.44	0.30	20.80	0.05	0.06	0.32	1.85	98.8	4	661	27	79	7	30
196Aii	Di-II	8	-	29.4	0.31	7.11	4.79	5.21	0.48	33.70	0.12	0.18	0.15	17.70	99.2	5	600	49	51	3	19
197AS	Ank-Ab	2	-0.65	27.3	0.32	6.43	3.98	4.02	0.43	28.00	0.34	2.98	0.16	26.30	100.4	14	822	87	60	3	20
197Ai	Ank-Ab	2	0.00	27.1	0.27	5.36	3.77	3.72	0.48	29.50	0.23	2.33	0.15	27.30	100.3	13	963	56	56	5	25
197Aii	Ank-Ab	2	2.65	28.4	0.32	6.00	3.70	4.13	0.35	27.20	1.15	1.43	0.16	27.20	100.2	43	856	264	61	5	12
197Aiii	Ank-Ab	1-2	4.50	28.6	0.35	6.31	3.77	3.99	0.31	27.10	1.72	0.61	0.14	27.20	100.3	61	873	392	65	6	12
197Aiv	Ank-Ab	1	6.20	28.8	0.33	6.28	3.57	3.66	0.31	27.50	1.81	0.31	0.16	27.30	100.2	63	850	412	66	7	11
197Av	Ank-Ab	1	8.00	28.5	0.34	6.37	3.61	3.64	0.31	27.60	1.90	0.30	0.16	27.50	100.4	62	863	393	67	6	10
197B-2	Ank-Ab	1	11.50	28.3	0.35	6.43	3.61	3.74	0.29	27.40	1.89	0.32	0.13	27.80	100.4	62	876	370	67	6	12
197Avi	Ank-Ab	1	-	28.7	0.34	6.20	3.56	3.95	0.31	27.30	1.67	0.32	0.14	27.50	100.2	61	858	399	66	7	12
JvH-W-16	Di-II	8	-	33.0	0.30	7.39	4.29	5.27	0.43	31.70	1.22	0.25	0.18	14.60	98.7	30	662	226	64	15	11
JvH-W-24A	Di-I	7	-	25.6	0.26	6.18	4.19	7.29	0.36	32.70	1.28	0.16	0.23	20.30	98.7	63	1170	172	70	22	0
JvH-W-27	Bt	3	-	26.8	0.22	5.72	2.44	2.12	0.34	32.60	1.81	0.11	0.15	27.90	100.4	63	1170	201	53	17	11
JvH-W-28	Bt	3	-	29.0	0.31	7.43	4.08	5.53	0.29	26.20	1.56	0.69	0.12	24.50	99.8	46	635	257	68	15	15
JvH-W-32	Bt	3	-	28.7	0.31	7.61	4.08	3.08	0.29	28.70	1.98	0.13	0.16	24.30	99.5	49	941	270	66	18	0
JvH-W-34	Di-II	8	-	26.6	0.22	6.46	3.93	5.04	0.36	35.80	0.11	0.17	0.17	19.80	98.8	6	920	38	52	21	0
JvH-W-35	Di-II	8	-	32.0	0.25	8.22	4.68	5.67	0.42	33.00	0.04	0.24	0.31	14.60	99.5	3	823	6	63	22	12
JvH-W-36	Ank-Ab	1	-	24.4	0.30	7.11	4.61	3.17	0.41	28.70	2.15	0.20	0.25	27.70	99.2	70	1180	161	68	12	0
JvH-W-37	Ank-Ab	1	-	31.3	0.20	4.78	2.93	5.71	0.25	26.30	1.26	0.26	0.12	27.20	100.5	43	925	217	56	17	15
JvH-W-38	Ank-Ab	1	-	27.9	0.17	4.26	2.80	6.15	0.21	28.20	1.25	0.18	0.13	28.90	100.3	43	1080	186	49	12	0
JvH-W-39	Ank-Ab	1	-	28.8	0.21	5.02	2.78	4.89	0.19	28.50	1.51	0.22	0.15	27.40	99.9	44	1300	171	61	17	12
Wep-8a	Di-I	5	-	28.4	0.37	6.84	4.10	4.51	0.49	29.40	1.90	0.80	0.15	23.00	100.2	55	1130	394	65	6	10
Wep-8b	Di-I	9	-	46.9	0.45	15.10	5.57	5.86	0.34	21.80	0.04	0.12	0.32	2.40	99.0	3	815	29	71	7	19
Wep-29a	Ank-Ol	1	-	21.2	0.42	7.40	5.42	5.12	0.84	29.10	0.93	1.79	0.25	27.90	100.5	24	652	203	67	13	23
Wep-35a	Amp-II	5	-	30.5	0.45	8.37	4.53	4.88	0.33	27.10	1.97	0.51	0.14	20.70	99.7	56	1020	333	81	6	13
W-5	Amp-II	5	-	23.9	0.29	5.44	5.66	4.26	0.72	33.00	1.41	0.16	0.32	24.90	100.2	36	1110	192	61	6	16
W-6i	Amp-II	6	-	24.0	0.30	5.83	6.40	4.37	0.75	33.60	0.42	0.22	0.34	24.00	100.3	11	614	59	54	2	26

TABLE E2

Rare earth elements, Th, and U

Sample	Zone	Rock Type Code	X (cm)	La	Ce	Pr	Nd	Sm	Eu	Gd	Tb	Dy	Ho	Er	Tm	Yb	Lu	Th	U
163IG	Di-I	14	-47.75	15.0	34.6	3.4	15.3	3.2	1.11	2.5	0.5	2.8	0.51	1.9	0.4	2.3	0.34	11.1	2.7
163IL	Di-I	14	-14.75	7.8	19.6	2.3	9.8	2.1	0.43	2.2	0.3	2.9	0.55	2.0	0.3	2.0	0.30	12.4	2.4
163IMi	Di-I	13	-6.25	11.1	24.2	2.8	12.5	2.8	0.44	2.6	0.3	2.6	0.47	1.6	0.2	1.8	0.24	7.1	1.8
163IMii	Di-I	11	-2.75	13.4	38.4	3.9	15.9	3.6	0.65	3.5	0.5	3.4	0.69	2.3	0.4	2.8	0.42	11.3	1.8
163IMiii	Di-I	11	-0.75	40.6	96.5	10.4	42.3	8.5	1.41	8.1	1.1	7.1	1.32	4.2	0.6	4.0	0.58	23.9	4.2
163IMiv	Di-I	10	0.75	18.2	36.8	4.2	18.6	3.6	0.85	3.3	0.4	2.8	0.50	1.7	0.2	1.6	0.23	6.1	1.3
163IN	Di-I	10	5.25	15.5	29.5	3.5	15.6	3.1	0.90	2.9	0.4	2.6	0.50	1.7	0.2	1.7	0.25	5.3	1.3
163IO	Di-I	10	17.25	19.1	37.7	4.4	19.6	4.3	1.33	4.5	0.6	4.2	0.78	2.5	0.3	2.2	0.31	5.4	1.5
163IPa	Di-I	10	22.25	21.0	43.7	4.6	20.9	4.8	1.27	4.6	0.7	4.0	0.71	2.3	0.3	2.2	0.32	5.0	1.6
163IRa	Di-I	9	32.25	20.7	39.1	4.2	17.7	3.8	1.13	3.5	0.5	3.1	0.57	1.6	0.2	1.5	0.22	6.1	1.7
163IT	Di-I	8	38.25	19.2	38.6	4.4	19.5	4.0	1.13	4.0	0.5	3.5	0.60	1.9	0.2	1.6	0.22	5.7	1.6
163IU	Di-I	8	52.25	15.6	30.0	3.5	14.8	2.9	0.86	2.9	0.4	2.5	0.43	1.4	0.2	1.4	0.18	5.0	1.4
163IV	Di-I	8	66.25	14.9	28.1	3.4	14.1	2.8	0.92	2.8	0.4	2.4	0.48	1.6	0.2	1.5	0.22	5.2	1.3
163IW	Di-I	7	72.25	18.1	34.9	4.2	18.8	3.8	1.17	3.9	0.5	3.2	0.56	1.9	0.2	1.4	0.20	5.8	1.6
163IX	Di-I	7	82.25	17.1	32.7	3.9	16.9	3.3	1.12	3.3	0.4	2.8	0.50	1.6	0.2	1.4	0.20	5.4	1.5
163IZ-2	Di-I	7	107.25	19.4	37.1	3.7	16.6	3.8	1.19	3.3	0.5	2.7	0.49	1.5	0.2	1.5	0.19	4.9	1.5
163IIOii	Di-I	13	-	93.0	211.0	23.0	92.3	19.4	3.47	20.8	3.0	20.3	3.90	12.9	1.9	13.8	2.00	43.8	17.4
163IVAi	Di-I	8	-	19.3	37.5	3.8	17.1	3.6	1.26	3.6	0.5	2.9	0.58	1.7	0.3	1.6	0.25	5.1	1.6
163IVAii	Di-I	6	-	21.1	41.0	4.1	19.4	4.0	1.55	3.7	0.6	3.2	0.64	1.7	0.3	1.6	0.20	7.7	1.8
163VIIAi	Di-I	10	3	21.1	38.1	4.7	19.1	3.8	1.45	3.8	0.5	3.2	0.60	1.7	0.2	1.4	0.20	7.8	1.7
163VIIAii	Di-I	9	9	17.0	32.3	3.9	15.9	3.3	1.18	3.2	0.4	2.7	0.46	1.5	0.2	1.4	0.19	6.2	1.4
163VIIAiii	Di-I	8	13	18.7	34.4	4.2	17.3	3.4	1.22	3.4	0.4	2.8	0.53	1.6	0.2	1.6	0.22	5.9	1.6
163VIIAiv	Di-I	7	18	18.7	35.0	4.4	17.6	3.4	1.17	3.2	0.4	2.7	0.49	1.6	0.2	1.7	0.21	6.4	1.5
168J	Ank-Ab	1	1.00	20.0	36.0	4.4	18.5	3.6	0.91	3.7	0.5	3.9	0.79	2.5	0.3	2.2	0.28	5.5	1.3
168A	Ank-Ab	1	24.00	17.5	33.1	3.9	16.9	3.4	1.03	3.4	0.4	2.9	0.53	1.6	0.2	1.5	0.21	5.3	1.3
168C	Ank-Ab	1	42.00	17.1	32.8	3.9	16.0	3.2	1.02	3.2	0.4	2.7	0.51	1.6	0.2	1.5	0.20	5.4	1.2
168K	Ank-Ab	1	58.00	17.4	32.8	3.9	16.2	3.3	1.05	3.4	0.4	3.0	0.54	1.7	0.2	1.5	0.19	5.0	1.2
168D	Ank-Ab	1	66.00	17.6	32.8	4.1	17.4	3.5	1.11	3.6	0.5	3.0	0.57	1.7	0.2	1.5	0.22	5.3	1.4
168Ei	Ank-Ab	1	68.25	15.6	29.8	3.5	15.2	3.0	0.91	3.1	0.4	2.6	0.48	1.5	0.2	1.3	0.17	4.9	1.1
168Eii	Ank-Ab	1	70.25	17.4	33.3	3.9	17.2	3.4	0.95	3.2	0.4	3.1	0.56	2.0	0.2	1.5	0.22	5.8	1.2

TABLE E2
(continued)

Sample	Zone	Rock Type Code	X (cm)	La	Ce	Pr	Nd	Sm	Eu	Gd	Tb	Dy	Ho	Er	Tm	Yb	Lu	Th	U
171A	Bt	3	0.50	19.6	40.1	4.6	19.4	4.3	1.23	4.5	0.6	4.4	0.84	3.0	0.4	3.3	0.44	5.4	1.5
171B	Bt	3	2.00	20.5	39.6	4.6	19.7	3.9	1.14	4.0	0.5	3.8	0.71	2.2	0.3	1.9	0.27	5.8	1.3
171Ci	Bt	3	3.25	19.8	39.0	4.5	19.1	4.0	1.20	4.0	0.5	3.6	0.64	2.1	0.3	1.9	0.24	5.7	1.3
171Cii	Bt	3	5.25	19.8	38.8	4.6	18.7	3.8	1.36	3.8	0.5	3.4	0.63	2.0	0.3	1.8	0.24	5.9	1.5
171Ciii	Bt	3	7.00	20.5	40.2	4.7	19.4	3.7	1.41	3.8	0.5	3.4	0.62	2.0	0.3	1.8	0.26	6.2	1.6
171D	Bt	3	16.00	20.2	38.9	4.5	18.8	3.5	1.31	3.5	0.5	3.2	0.57	1.9	0.2	1.6	0.24	5.7	1.5
181W	Amp-I	14	-88.50	16.5	99.0	4.0	15.2	2.8	0.56	3.0	0.6	4.4	0.94	3.1	0.5	3.5	0.50	15.1	3.6
181Z	Amp-I	14	-43.50	43.6	97.0	10.6	41.7	7.2	1.16	5.3	0.7	4.8	0.95	3.2	0.5	3.6	0.49	20.0	3.7
181UV	Amp-I	14	-23.50	19.6	37.0	4.8	19.2	3.9	0.74	3.3	0.5	4.1	0.96	4.2	0.8	7.0	1.08	21.2	3.8
181SIV	Amp-I	11	-8.50	45.9	100.0	11.2	45.4	8.7	1.88	8.5	1.1	6.5	1.08	2.9	0.3	2.9	0.34	16.6	3.3
181SIII	Amp-I	11	-2.50	41.4	89.4	10.2	40.5	8.0	1.71	7.3	0.9	5.6	0.97	2.6	0.3	2.5	0.36	14.9	2.9
181Y	Amp-I	12	0.00	28.7	51.5	6.6	26.2	5.1	2.62	4.8	0.6	3.9	0.72	2.2	0.3	1.8	0.24	7.8	2.5
181SII	Amp-I	10	2.50	12.8	27.3	3.1	13.0	2.4	0.62	2.6	0.3	2.6	0.57	2.5	0.4	3.6	0.48	5.2	1.0
181SI	Amp-I	10	7.00	21.2	38.3	4.8	19.5	4.2	1.48	3.8	0.6	5.5	1.60	7.1	1.2	8.3	1.01	5.3	1.7
181Bi	Amp-I	6	15.50	18.3	34.0	4.2	19.6	4.9	1.35	5.5	0.7	4.3	0.72	2.1	0.3	2.0	0.25	4.7	1.3
181Bii	Amp-I	6	16.49	16.3	30.0	3.7	15.4	3.2	1.31	3.7	0.5	3.7	0.73	2.3	0.3	2.2	0.29	4.6	1.2
181Biii	Amp-I	5	18.00	16.6	30.1	3.7	15.2	2.9	1.19	3.3	0.5	3.9	0.80	2.6	0.4	2.7	0.36	4.6	1.2
181C	Amp-I	4	22.25	15.4	27.7	3.4	14.5	2.8	1.38	2.8	0.3	2.4	0.42	1.3	0.2	1.3	0.16	5.2	1.2
181FF	Amp-I	4	31.50	18.3	35.8	4.2	16.9	3.3	1.37	3.0	0.4	2.7	0.53	1.6	0.2	2.0	0.20	4.7	1.4
181E	Amp-I	4	40.35	16.5	29.8	3.6	15.1	3.0	1.38	2.7	0.3	2.4	0.43	1.4	0.2	1.2	0.15	4.4	1.0
181Fiv	Amp-I	4	43.25	16.3	29.4	3.6	14.8	3.0	1.33	2.9	0.4	2.5	0.47	1.4	0.2	1.2	0.18	5.4	1.2
181D	Amp-I	4	45.25	18.4	33.7	4.1	17.3	3.0	1.49	3.1	0.4	2.7	0.49	1.6	0.2	1.4	0.18	5.1	1.3
181Fiii	Amp-I	4	49.00	19.5	35.9	4.4	18.4	4.0	1.29	4.0	0.5	3.3	0.55	1.6	0.2	1.7	0.22	5.4	1.4
181Fii	Amp-I	6	51.05	20.8	38.0	4.6	19.3	4.3	1.28	4.5	0.6	3.7	0.65	1.9	0.2	1.7	0.23	5.5	1.6
181Fi	Amp-I	6	53.30	18.9	34.8	4.2	17.6	3.6	1.21	3.9	0.5	3.1	0.56	1.6	0.2	1.6	0.19	5.0	1.6
181GG	Amp-I	6	66.50	18.6	33.8	4.2	17.0	3.4	1.56	3.0	0.4	2.5	0.48	1.5	0.2	1.4	0.20	5.0	1.7
181G	Amp-I	6	71.50	17.8	32.3	4.0	16.5	3.4	1.42	3.3	0.4	2.7	0.49	1.5	0.2	1.3	0.19	5.5	2.2
181Hiv	Amp-I	6	80.25	15.3	27.9	3.4	13.7	2.6	1.36	2.5	0.3	2.1	0.37	1.2	0.2	1.4	0.15	4.6	1.4
181Hiii	Amp-I	6	83.25	14.6	26.4	3.2	14.0	2.7	1.41	2.7	0.3	2.3	0.40	1.3	0.2	1.3	0.14	4.7	1.4
181Hii	Amp-I	6	86.00	14.8	26.5	3.3	13.4	2.7	1.23	2.5	0.3	2.4	0.47	1.5	0.2	1.3	0.22	4.7	1.4

TABLE E2

(continued)

Sample	Zone	Rock Type Code	X (cm)	La	Ce	Pr	Nd	Sm	Eu	Gd	Tb	Dy	Ho	Er	Tm	Yb	Lu	Th	U
181Hi	Amp-I	6	90.25	22.6	43.2	5.3	21.9	4.9	1.30	4.9	0.7	5.2	1.04	3.2	0.5	3.1	0.40	7.1	1.7
181Rii	Amp-I	10	92.00	19.0	33.9	4.2	17.0	3.3	1.26	3.8	0.6	4.8	0.96	3.2	0.5	3.4	0.43	4.8	1.6
181OI	Amp-I	12	101.50	30.5	52.6	6.7	27.0	5.1	1.98	5.7	0.9	7.6	1.69	5.6	0.8	5.3	0.64	8.4	2.9
181Qii	Amp-I	13	115.00	51.7	110.0	12.5	50.5	9.5	1.71	8.3	1.1	7.3	1.38	4.1	0.6	3.8	0.51	20.8	3.6
181Qi	Amp-I	13	126.50	60.9	107.0	14.4	55.8	10.4	2.23	9.5	1.2	7.7	1.39	4.4	0.5	3.9	0.55	19.5	3.6
181DDia	Amp-I	6	5	19.0	35.2	4.0	17.5	3.6	1.43	3.2	0.5	2.4	0.46	1.3	0.2	1.3	0.20	6.3	1.6
181DDiia	Amp-I	5	7	16.0	29.2	3.3	14.0	3.0	1.47	2.4	0.4	2.1	0.41	1.3	0.2	1.2	0.18	5.0	1.4
181DDiv-v	Amp-I	10	0	17.2	31.3	3.2	15.5	3.2	1.80	3.0	0.5	2.9	0.64	2.0	0.3	1.6	0.26	5.3	2.0
187Ao	Di-I	13	-2.10	40.5	88.0	9.7	35.1	6.0	1.34	4.9	0.6	4.4	0.84	2.7	0.4	3.0	0.44	15.6	2.8
187Ai	Di-I	10	2.10	34.9	64.6	8.1	32.0	6.8	1.59	6.5	0.8	5.1	0.92	2.9	0.4	3.0	0.37	10.1	2.6
187Aii-iii	Di-I	10	6.30	35.4	58.2	7.8	31.4	6.8	1.61	7.1	1.0	5.7	1.09	3.3	0.5	3.3	0.45	8.9	2.0
187Aiv	Di-I	10	8.80	33.0	52.7	7.1	28.2	6.1	1.71	6.4	0.8	5.5	1.06	3.2	0.4	3.0	0.44	8.4	2.0
187Av	Di-I	9	10.80	26.7	40.7	5.7	23.1	5.0	1.32	5.3	0.7	4.4	0.84	2.4	0.3	2.2	0.29	5.8	1.4
187Oiv	Di-I	9	14.40	23.2	38.7	5.1	21.3	4.5	1.30	5.0	0.6	4.3	0.85	2.5	0.4	2.1	0.28	6.6	1.6
187Ni	Di-I	9	15.80	29.0	45.7	6.3	26.1	5.8	1.78	6.2	0.8	5.2	1.01	3.1	0.4	3.2	0.35	6.5	2.0
187Bii	Di-I	9	17.30	29.7	52.9	6.9	29.9	7.1	2.05	7.4	0.9	5.6	0.99	2.9	0.4	2.7	0.32	6.3	2.1
187Oii	Di-I	9	19.40	26.6	48.7	6.4	28.9	6.7	1.93	6.8	0.9	5.2	0.97	2.8	0.4	2.3	0.27	7.3	2.0
187Biii	Di-I	9	20.30	24.8	43.6	5.6	24.1	5.7	1.89	6.0	0.7	4.6	0.83	2.4	0.3	2.4	0.27	6.2	1.9
187Biv	Di-I	9	22.10	22.8	40.7	5.1	20.9	4.4	1.62	4.4	0.6	3.6	0.69	2.1	0.3	2.0	0.27	6.3	1.8
187Nii	Di-I	9	23.40	25.4	46.3	5.7	22.5	4.7	1.75	4.6	0.6	3.8	0.71	2.2	0.3	2.0	0.29	6.6	1.7
187Mi	Di-I	8	25.40	23.0	42.8	5.2	21.9	4.2	1.48	4.0	0.5	3.4	0.61	2.0	0.3	2.1	0.28	6.8	1.7
187Mii	Di-I	8	30.40	21.5	40.0	4.9	19.0	3.5	1.34	3.5	0.5	3.0	0.60	1.9	0.3	2.2	0.27	6.1	1.7
187Miii	Di-I	8	35.40	22.5	42.2	5.3	20.8	4.1	1.48	4.1	0.5	3.4	0.69	2.1	0.3	2.2	0.34	6.9	1.8
197AS	Ank-Ab	2	-0.65	17.1	33.2	3.4	17.0	3.7	1.35	3.4	0.7	4.6	0.97	2.9	0.4	2.6	0.34	6.3	1.4
197Ai	Ank-Ab	2	0.00	13.8	26.8	2.7	14.0	3.1	1.10	3.2	0.5	4.3	1.15	3.6	0.6	4.6	0.64	4.8	1.2
197Aii	Ank-Ab	2	2.65	17.7	34.6	3.5	17.5	3.6	1.45	3.5	0.6	3.0	0.63	1.6	0.3	1.6	0.22	6.3	1.6
197Aiii	Ank-Ab	1-2	4.50	19.7	37.7	3.8	17.6	4.1	1.41	3.2	0.6	3.3	0.61	1.8	0.3	1.7	0.22	7.1	1.8
197Aiv	Ank-Ab	1	6.20	20.2	39.5	4.0	19.4	3.9	1.40	3.3	0.5	3.1	0.64	2.0	0.3	1.6	0.21	7.0	1.7
197Av	Ank-Ab	1	8.00	19.4	37.6	4.0	18.5	4.1	1.37	3.4	0.6	3.1	0.57	1.9	0.3	1.5	0.27	6.5	1.5
197B-2	Ank-Ab	1	11.50	19.3	36.8	3.7	17.3	3.6	1.20	3.1	0.5	2.7	0.56	1.6	0.2	1.3	0.15	7.0	1.2
197Avi	Ank-Ab	1	-	20.1	37.9	3.9	19.0	4.1	1.48	3.3	0.5	3.0	0.60	1.7	0.3	1.7	0.25	6.0	1.4

References

Abart, R., Schmud, R., and Harlov, D., 2001, Metasomatic coronas around hornblendite xenoliths in granulite facies marble, Ivrea zone, N Italy, I: Constraints on component mobility: Contributions to Mineralogy and Petrology, v. 141, p. 473–493.

Ague, J. J., 1994a, Mass transfer during Barrovian Metamorphism of Pelites, south-central Connecticut, I: Evidence for composition and volume change: American Journal of Science, v. 294, p. 989–1057.

——— 1994b, Mass transfer during Barrovian Metamorphism of Pelites, south-central Connecticut, II: Channelized fluid flow and the growth of staurolite and kyanite: American Journal of Science, v. 294, p. 1061–1134.

——— 1995, Deep crustal growth of quartz, kyanite, and garnet into large aperture, fluid-filled fractures, north-eastern Connecticut, USA: Journal of Metamorphic Geology, v. 13, p. 299–314.

——— 1997a, Crustal mass transfer and index mineral growth in Barrow's garnet zone, Northeast Scotland: Geology, v. 25, p. 73–76.

——— 1997b, Compositional variations in metamorphosed sediments of the Littleton Formation: American Journal of Science, v. 297, p. 440–449.

——— 1998, Simple models of coupled fluid infiltration and redox reactions in the crust: Contributions to Mineralogy and Petrology, v. 132, p. 180–197.

——— 2000, Release of Co_2 from carbonate rocks during regional metamorphism of lithologically heterogeneous crust: Geology, v. 28, p. 1123–1126.

——— 2002, Gradients in fluid composition across metacarbonate layers of the Wepawaug Schist, Connecticut, USA: Contributions to Mineralogy and Petrology, v. 143, p. 38–55.

——— 2003, Fluid Flow in the Deep Crust, *in* Rudnick, R. L., editor, Treatise on geochemistry: The Netherlands, Elsevier, v. 3, chapter 6.

Ague, J. J., and Rye, D. M., 1999, Simple models of CO_2 release from metacarbonates with implications for interpretation of directions and magnitudes of fluid flow in the deep crust: Journal of Petrology, v. 40, p. 1443–1462.

Ague, J. J., and van Haren, J. L. M., 1996, Assessing metasomatic mass and volume changes using the bootstrap, with application to deep-crustal hydrothermal alteration of marble: Economic Geology, v. 91, p. 1169–1182.

Ashworth, J. R., and Sheplev, V. S., 1997, Diffusion modelling of metamorphic layered coronas with stability criterion and consideration of affinity: Geochimica et Cosmochimica Acta, v. 61, p. 3671–3689.

Ayers, J. C., and Watson, E. B., 1991, Solubility of apatite, monazite, zircon, and rutile in supercritical aqueous fluids with implications for subduction zone geochemistry: Philosophical Transactions of the Royal Society of London Series A, v. 335, p. 365–375.

Balashov, V. N., and Yardley, B. W. D., 1998, Modeling metamorphic fluid flow with reaction-compaction-permeability feedbacks: American Journal of Science, v. 298, p. 441–470.

Baxter, E. F., and DePaolo, D. J., 2002, Field measurement of high temperature bulk reaction rates I: Theory and technique: American Journal of Science, v. 302, p. 442–464.

Bear, J., 1988, Dynamics of fluids in porous media: New York, Dover, 764 p.

Berman, R. G., 1991, Thermobarometry using multi-equilibrium calculations: A new technique, with petrological applications: Canadian Mineralogist, v. 29, p. 833–855.

Bickle, M. J., 1992, Transport mechanisms by fluid flow in metamorphic rocks: Oxygen and strontium decoupling in the Trois Seigneurs Massif – a consequence of kinetic dispersion?: American Journal of Science, v. 292, p. 289–316.

Bickle, M. J., and Baker, J., 1990, Advective-diffusive transport of isotopic fronts: An example from Naxos, Greece: Earth and Planetary Science Letters, v. 97, p. 78–93.

Bolton, E. W., Lasaga, A. C., and Rye, D. M., 1999, Long-term flow/chemistry feedback in a porous medium with heterogeneous permeability: Kinetic control of dissolution and precipitation: American Journal of Science, v. 299, p. 1–68.

Brady, J. B., 1977, Metasomatic zones in metamorphic rocks: Geochimica et Cosmochimica Acta, v. 41, p. 113–125.

Breeding, C. M., and Ague, J. J., 2002, Slab-derived fluids and quartz-vein formation in an accretionary prism, Otago Schist, New Zealand: Geology, v. 30, p. 499–502.

Breeding, C. M., Ague, J. J., Brocker, M., and Bolton, E. W., 2003, Blueschist preservation in a retrograded, high-pressure, low-temperature metamorphic terrane, Tinos, Greece: Implications for fluid flow paths in subduction zones: Geochemistry, Geophysics, Geosystems, v. 4, 9002, doi:10.1029/2002GC000380.

Brimhall, G. H., Jr., 1979, Lithologic determination of mass transfer mechanisms of multiple-stage porphyry copper mineralization at Butte, Montana: Vein formation by hypogene leaching and enrichment of potassium silicate protore: Economic Geology, v. 74, p. 556–589.

Carlson, W. D., 2002, Scales of disequilibrium and rates of equilibration during metamorphism: American Mineralogist, v. 87, p. 185–204.

Carson, C. J., Ague, J. J., Grove, M., Coath, C. D., and Harrison, T. M., 2002, Zircon isotopic behavior during upper-amphibolite facies fluid infiltration in the Napier Complex, East Antarctica: Earth and Planetary Science Letters, v. 199, p. 287–310.

Dieterich, J. H., ms, 1968, Sequence and mechanics of folding in the area of New Haven, Naugatuck, and Westport, Connecticut: Ph.D. thesis, Yale University, New Haven, 153 p.

Dipple, G. M., and Ferry, J. M., 1992, Metasomatism and fluid flow in ductile fault zones: Contributions to Mineralogy and Petrology, v. 112, p. 149–164.

Evans, K. A., Bickle, M. J., Skelton, A. D. L., Hall, M., and Chapman, H., 2002, Reductive deposition of graphite at lithological margins in East Central Vermont: a Sr, C, and O isotope study: Journal of Metamorphic Geology, v. 20, p. 781–798.

Ferry, J. M., 1981, Petrology of graphitic, sulfide-rich schists from south-central Maine – An example of desulfidation during prograde regional metamorphism: American Mineralogist, v. 66, p. 908–931.
——— 1982, A comparative geochemical study of pelitic schists and metamorphosed carbonate rocks from south-central Maine, USA: Contributions to Mineralogy and Petrology, v. 80, p. 59–72.
——— 1983a, Mineral reactions and element migration during metamorphism of calcareous sediments from the Vassalboro Formation, south-central Maine: American Mineralogist, v. 68, p. 334–354.
——— 1983b, On the control of temperature, fluid composition, and reaction progress during metamorphism: American Journal of Science, v. 283-A, p. 201–232.
——— 1992, Regional Metamorphism of the Waits River Formation, eastern Vermont, Delineation of a new type of giant metamorphic hydrothermal system: Journal of Petrology, v. 33, p. 45–94.
——— 1994, Overview of the petrologic record of fluid flow during regional metamorphism in northern New England: American Journal of Science, v. 294, p. 905–988.
Ferry, J. M., and Dipple, G. M., 1991, Fluid flow, mineral reactions, and metasomatism: Geology, v. 19, p. 211–214.
Fritts, C. E., 1963, Bedrock geology of the Mount Carmel quadrangle, Connecticut: U.S. Geological Survey Quadrangle Map GQ-199.
——— 1965a, Bedrock geologic map of the Ansonia quadrangle, Fairfield and New Haven Counties, Connecticut: U.S. Geological Survey Quadrangle Map GQ-426.
——— 1965b, Bedrock geologic map of the Milford quadrangle, Fairfield and New Haven Counties, Connecticut: U.S. Geological Survey Quadrangle Map GQ-427.
Fuhrman, M. L., and Lindsley, D. H., 1988, Ternary feldspar modelling and thermometry: American Mineralogist, v. 73, p. 201–215.
Gieré, R., and Williams, C. T., 1992, REE-bearing minerals in a Ti-rich vein from the Adamello contact aureole (Italy): Contributions to Mineralogy and Petrology, v. 112, p. 83–100.
Grant, J. A., 1986, The isocon diagram – a simple solution to Gresens' equation for metasomatic alteration: Economic Geology, v. 81, p. 1976–1982.
Grauch, R. I., 1989, Rare earth elements in metamorphic rocks, *in* Lipin, B. R., and McKay, G. A., editors, Geochemistry and mineralogy of rare earth elements: Mineralogical Society of America, Reviews in Mineralogy, v. 21, p. 147–167.
Hawkesworth, C., Turner, S., Peate, D., McDermott, F., and van Calsteren, P., 1997, Elemental U and Th variations in island arc rocks: Implications for U-series isotopes: Chemical Geology, v. 139, p. 207–221.
Hess, P. C., 1989, Origins of igneous rocks: Cambridge, Harvard University Press, 336 p.
Hewitt, D. A., 1973, The metamorphism of micaceous limestones from south-central Connecticut: American Journal of Science, v. 273-A, p. 444–469.
Ingebritsen, S. E., and Manning, C. E., 1999, Geological implications of a permeability-depth curve for the continental crust: Geology, v. 27, p. 1107–1110.
Joesten, R., 1974, Local equilibrium and metasomatic growth of zoned calc-silicate nodules from a contact aureole, Christmas Mountains, Big Bend Region, Texas: American Journal of Science, v. 274, p. 876–901.
Johnson, M. C., and Plank, T., 1999, Dehydration and melting experiments constrain the fate of subducted sediments: Geochemistry, Geophysics, Geosystems, v. 1, 1999GC000014.
Kerrick, D. M., and Jacobs, G. K., 1981, A modified Redlich-Kwong equation for H_2O, CO_2, and H_2O-CO_2 mixtures at elevated temperatures and pressures: American Journal of Science, v. 281, p. 735–767.
Lanzirotti, A., and Hanson, G. N., 1996, Geochronology and geochemistry of multiple generations of monazite from the Wepawaug Schist, Connecticut, USA: Implications for monazite stability in metamorphic rocks: Contributions to Mineralogy and Petrology, v. 125, p. 332–340.
Lasaga, A. C., and Rye, D. M., 1993, Fluid flow and chemical reaction kinetics in metamorphic systems: American Journal of Science, v. 293, p. 361–404.
Lawson, C. L., and Hanson, R. J., 1974, Solving least squares problems: Englewood Cliffs, New Jersey, Prentice Hall, 340 p.
Léger, A., and Ferry, J. M., 1993, Fluid infiltration and regional metamorphism of the Waits River Formation, northeast Vermont, USA: Journal of Metamorphic Geology, v. 11, p. 3–29.
Manning, C. E., 1999, Solubility of corundum-kyanite in H_2O at 700C, 1 and 1.5 GPa: Evidence for high Al mobility in deep metasomatic environments: Geological Society of America Abstracts with Programs, v. 31, p. A-354.
——— 2001, Experimental studies of fluid-rock interaction at high pressure: The role of polymerization and depolymerization of solutes: Hot Springs, Virginia, 11th Annual V. M. Goldschmidt Conference.
Orville, P. M., 1969, A model for metamorphic differentiation origin of thin-layered amphibolites: American Journal of Science, v. 267, p. 64–86.
Palin, J. M., ms, 1992, Stable isotope studies of regional metamorphism in the Wepawaug Schist, Connecticut: Ph.D. thesis, Yale University, New Haven, 170 p.
Pan, Y., and Fleet, M. E., 1996, Rare earth element mobility during prograde granulite facies metamorphism: Significance of fluorine: Mineralogy and Petrology, v. 123, p. 251–262.
Pokrovskii, V. A., and Helgeson, H. C., 1995, Thermodynamic properties of aqueous species and the solubilities of minerals at high pressures and temperatures: the system Al_2O_3-H_2O-NaCl: American Journal of Science, v. 295, p. 1255–1342.
Press, W. H., Teukolsky, S. A., Vetterling, W. T., and Flannery, B. P., 1992, Numerical recipes in Fortran, the art of scientific computing, second edition: Cambridge, Cambridge University Press, 963 p.
Rubie, D. C., 1998, Disequilibrium during metamorphism: the role of nucleation kinetics, *in* Treloar, P. J., and O'Brien, P. J., editors, What drives metamorphism and metamorphic reactions?: Geological Society, London, Special Publications, v. 138, p. 199–214.

Rye, R. O., Schuiling, R. D., Rye, D. M., and Jansen, J. B. H., 1976, Carbon, hydrogen, and oxygen isotope studies of the regional metamorphic complex at Naxos, Greece: Geochimica et Cosmochimica Acta, v. 40, p. 1031–1049.

Shmulovich, K., Graham, C., and Yardley, B., 2001, Quartz, albite, and diopside solubilities in H_2O-NaCl and H_2O-CO_2 fluids at 0.5-0.9 GPa: Contributions to Mineralogy and Petrology, v. 141, p. 95–108.

Shock, E. L., Sassani, D. C., Willis, M., and Sverjensky, D. A., 1997, Inorganic species in geologic fluids: Correlations among standard molal thermodynamic properties of aqueous ions and hydroxide complexes: Geochimica et Cosmochimica Acta, v. 61, p. 907–950.

Sverjensky, D. A., 1987, Calculation of the thermodynamic properties of aqueous species and the solubilities of minerals in supercritical electrolyte solutions, *in* Carmichael, I. S. E., and Eugster, H. P., editors, Thermodynamic modeling of geological materials: Minerals, fluids, and melts: Mineralogical Society of America Reviews in Mineralogy, v. 17, p. 177–209.

Sverjensky, D. A., Hemley, J. J., and D'Angelo, W. M., 1991, Thermodynamic assessment of hydrothermal alkali feldspar-mica-aluminosilicate equilibria: Geochimica et Cosmochimica Acta, v. 55, p. 989–1004.

Tanner, P. W. G., and Miller, R. G., 1980, Geochemical evidence for loss of Na and K from Moinian calc-silicate pods during prograde metamorphism: Geological Magazine, v. 117, p. 267–275.

Thompson, A. B., 1975, Calc-silicate diffusion zones between marble and pelitic schist: Journal of Petrology, v. 16, p. 314–346.

Tracy, R. J., Rye, D. M., Hewitt, D. A., and Schiffries, C. M., 1983, Petrologic and stable-isotopic studies of fluid-rock interactions, south-central Connecticut: I. The role of infiltration in producing reaction assemblages in impure marbles: American Journal of Science, v. 283-A, p. 589–616.

van Haren, J. L. M., Ague, J. J., and Rye, D. M., 1996, Oxygen isotope record of fluid infiltration and mass transfer during regional metamorphism of pelitic schist, south-central Connecticut, USA: Geochimica et Cosmochimica Acta, v. 60, p. 3487–3504.

Vidale, R. J., 1969, Metasomatism in a chemical gradient and the formation of calc-silicate bands: American Journal of Science, v. 267, p. 857–874.

Vidale, R. J., and Hewitt, D. A., 1973, "Mobile" components in the formation of calc-silicate bands: American Mineralogist, v. 58, p. 991–997.

Walther, J. V., 1996, Fluid production and isograd reactions at contacts of carbonate-rich and carbonate-poor layers during progressive metamorphism: Journal of Metamorphic Geology, v. 14, p. 351–360.

Widmer, T., and Thompson, A. B., 2001, Local origin of high pressure vein material in eclogite facies rocks of the Zermatt-Saas zone, Switzerland: American Journal of Science, v. 301, 627–656.